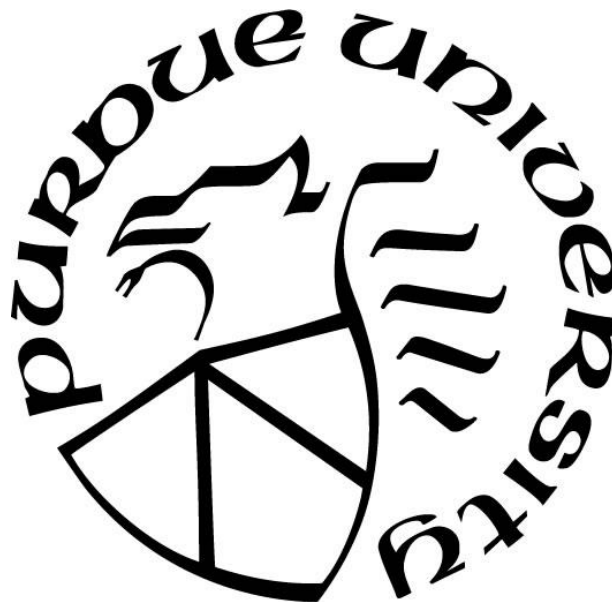# IMPROVEMENT OF STIFFNESS AND STRENGTH OF BACKFILL SOILS THROUGH OPTIMIZATION OF COMPACTION PROCEDURES AND SPECIFICATIONS

by

Shahedur Rahman

A Thesis

Submitted to the Faculty of Purdue University
In Partial Fulfillment of the Requirements for the degree of

Master of Science in Civil Engineering

Lyles School of Civil Engineering

West Lafayette, Indiana

December 2019

THE PURDUE UNIVERSITY GRADUATE SCHOOL
STATEMENT OF COMMITTEE APPROVAL

Dr. Monica Prezzi, Co-Chair

Lyles School of Civil Engineering

Dr. Rodrigo Salgado, Co-Chair

Lyles School of Civil Engineering

Dr. Peter Becker

Indiana Department of Transportation

Approved by:

Dr. Dulcy M. Abraham

Dedicated to my family

ACKNOWLEDGMENTS

First and foremost, praises and thanks to the God, the Almighty, for His showers of blessings throughout my research work to complete the research successfully.

I would like to express my sincere gratitude to my advisors Professor Dr. Monica Prezzi and Professor Dr. Rodrigo Salgado for giving me the opportunity to do research and providing invaluable guidance throughout this research. It was a great privilege and honor to work and study under their guidance. Besides my advisors, I would like to thank Dr. Peter Becker and Mr. Nayyar Zia Siddiki for their encouragement and insightful comments.

I am extremely grateful to my parents for their love, prayers, caring and sacrifices for educating and preparing me for my future. I am very much thankful to my wife for her love, understanding, prayers and continuing support to complete this research work.

Last but not the least, I would like to thank my fellow labmates and all the people at Purdue University who have supported me to complete the research work directly or indirectly.

TABLE OF CONTENTS

LIST OF TABLES

LIST OF FIGURES

ABSTRACT

Vibration compaction is the most effective way of compacting coarse-grained materials. The effects of vibration frequency and amplitude on the compaction density of different backfill materials (No. 4 natural sand, No. 24 stone sand and No. 5, No. 8, No. 43 aggregates), were studied in this research. The test materials were characterized based on the particle sizes and morphology parameters using digital image analysis technique. Small-scale laboratory compaction tests were carried out with variable frequency and amplitude of vibrations using vibratory hammer and vibratory table. The results show an increase in density with the increase in amplitude and frequency of vibration. However, the increase in density with the increase in amplitude of vibration is more pronounced for the coarse aggregates than for the sands. A comparison of the maximum dry densities of different test materials shows that the dry densities obtained after compaction using the vibratory hammer are greater than those obtained after compaction using the vibratory table at the highest amplitude and frequency of vibration available in both equipment. Large-scale vibratory roller compaction tests were performed in the field for No. 30 backfill soil to observe the effect of vibration frequency and number of passes on the compaction density. Accelerometer sensors were attached to the roller drum (Caterpillar, model CS56B) to measure the frequency of vibration for the two different vibration settings available to the roller. For this roller and soil tested, the results show that the higher vibration setting is more effective. Direct shear tests and direct interface shear tests were performed to study the impact of particle characteristics of the coarse-grained backfill materials on interface shear resistance. A unique relationship was found between the normalized surface roughness and the ratio of critical-state interface friction angle between sand-gravel mixture with steel to the internal critical-state friction angle of the sand-gravel mixture.

1. INTRODUCTION AND RESEARCH OBJECTIVES

1.1 Introduction

In order for the performance of transportation structures to be satisfactory over the long term, earthwork-related activities are carried out in the field to improve existing ground conditions. Backfill soils are used when the: (1) *in situ* soil at the construction site is too weak and unable to support the loads of the structure to be constructed over it and needs to be replaced by soil from another source or (2) existing ground needs to be raised up to a certain level before construction is undertaken (Indiana Department of Transportation 2018). Materials used in the construction of bridge approaches, mechanically stabilized earth walls, embankments and excavations for pipelines are called structural backfill materials. The strength and the stiffness of the backfill materials can be improved by reducing the void spaces between the particles, thus increasing the frictional interaction and interlocking of particles. Depending on the size of the particles of backfill soils, different methods are followed to improve their strength by compaction. Coarse-grained materials need confinement in order to be compacted effectively, and a combination of pressure and vibration is the most efficient way to produce reorientation of the particles into a denser arrangement (Denies et al. 2014). For these reasons, vibratory compaction is used for effective densification of coarse-grained backfill soils in the field.

The lift thickness, number of passes, frequency and amplitude of vibration are the factors that play an important role on the compaction of coarse-grained backfill soils. There are severe technical and economic consequences to an engineering project whenever ground improvement techniques are not properly selected and used in the field. Therefore, proper understanding of the impact of each factor on compaction is required for effective use of compaction methods. According to Massarsch and Fellenius (2002), compaction-related earthwork activities should specifically include: (1) selection and evaluation of the applicable compaction method(s); (2) design of the required compaction effort; (3) selection of the appropriate compaction equipment; (4) application of optimal compaction energy in terms of spacing, sequence, and duration; and (5) verification of the compaction results to conform to the design and specifications. Improper compaction reduces the durability of transportation structures and increases maintenance costs. Overuse of vibratory rollers to compact coarse-grained soil can lead to high construction costs. In

addition, over compaction by vibration can cause crushing of soil particles and segregation leading to nonuniformities in the compacted backfill soil. Accordingly, the main goal of this research was to study through laboratory and field compaction experiments the effects of amplitude and frequency of vibration on the compaction density of backfill materials of different gradations, morphology parameters and frictional characteristics that are often used by Indiana Department of Transportation (INDOT) in construction projects.

1.2   Research Objectives

To have safe and reliable road and embankment structures built using coarse-grained backfill materials, INDOT has developed specifications for compaction control in terms of number of passes, lift thickness and vibration frequency. For the compaction of coarse-grained backfill materials used in MSE wall construction, INDOT specifies a lift thickness of no more than 8 inches (before compaction). However, within a distance of 3 ft from the edge of an MSE wall, the lift thickness specified by INDOT is reduced to 5 inches (before compaction) due to the difficulties in compacting material near a structure. A vibratory roller with a minimum vibration of 2,000 vibrations per minute (vpm) is recommended by INDOT in order to achieve the specified 95% relative compaction. No specific number of passes is recommended by INDOT for structural backfill soils. The *in situ* density is assessed by performing Dynamic Cone Penetration (DCP) tests for sands, while Light Weight Deflectometer (LWD) tests are recommended for gravels.

Modern equipment used in earthwork construction have increased in size and weight over the years, and thus deliver greater energy levels to compact soils. For these reasons, there is a strong interest from both earthmoving contractors and INDOT officials in investigating the technical feasibility of reducing the number of passes by increasing the vibration amplitude and frequency used in a given pass. However, the effects on compaction density of using higher vibration amplitude and frequency need to be evaluated both in the laboratory and in the field before additional guidelines can be proposed.

The main objectives of this study were to evaluate the compaction density that could be achieved for coarse-grained backfill soils commonly used by INDOT when using different frequency and amplitude of vibrations in the laboratory and in the field. To accomplish these objectives, backfill materials of different gradations and particle characteristics commonly used by INDOT for subgrade and MSE wall construction were collected and tested. Laboratory

compaction densities were determined for the collected backfill materials for different vibration amplitudes and frequencies using a vibratory table and a vibratory hammer. The effects of particle characteristics on compaction density were also investigated. Direct shear tests and direct interface shear tests were performed to study the effects of particle characteristics of the coarse-grained backfill materials on internal and interface shear resistance. In addition, compaction was studied in the field using vibratory rollers with two vibration settings for every pass up to six roller passes during subgrade construction of two test sections of a ramp at the intersection of US 20 and IN 2 in Rolling Prairie, IN.

1.3   Section of this Thesis

This thesis has been divided into eight chapters. A literature review on compaction procedures, factors controlling compaction and specifications followed in the United States is detailed in Chapter 2. Chapter 3 describes the research methodology followed in this research work. Chapter 4 presents the backfill materials considered in this research work and the results of the grain size classification and particle morphology analyses. The results of small-scale compaction tests carried out in the laboratory using different equipment and vibration parameters are presented in Chapter 5. Chapter 6 describes the direct shear tests and direct interface shear tests carried out in the laboratory to determine the effect of particle characteristics of the coarse-grained backfill materials on interface shear resistance. The results of field compaction tests using vibratory rollers are presented in Chapter 7 demonstrating the effects of number of passes and vibration settings on the compaction density of the backfill materials. Chapter 8 presents the conclusions reached from this study, provides recommendations for implementation of the findings of this research, and highlights where further research is needed.

2. LITERATURE REVIEW

2.1 Factors Affecting Compaction Density

Mechanical compaction is a viable and economical method of soil improvement for coarse-grained soils that have inadequate strength or stiffness. Mechanical compaction refers to the densification of the soil by the application of mechanical energy. By the process of densification, the void space between the particles is reduced, leading to closer particle arrangements. In general, the denser the soil, the greater its shear strength is. The energy required to achieve the desired compaction density varies depending on the soil type, compaction water content, particle shape, and gradation. The factors affecting the compaction density of a soil are discussed in detail next.

2.1.1 Water content and soil type

Water acts as a lubricant between the soil particles to facilitate their sliding with respect to each other during compaction, resulting in higher density for a given compaction effort. At a certain compaction water content level, known as the optimum water content, the maximum dry density is achieved. However, adding more water beyond the optimum water content is no longer beneficial as the volume of voids taken up by the added water increases, reducing the dry density of the soil.

Different soil types behave differently with respect to maximum dry density and optimum water content. Johnson and Sallberg (1960) studied the effect of soil type and water content on the compaction dry density by performing Proctor compaction tests on different types of soils. The results are shown in Figure 2.1. A detailed description of the soil types shown in Figure 2.1 is presented in Table 2.1. As can be seen in Table 2.1, a well-graded sand with silt (classified as SW-SM according to the USCS classification system) has higher maximum dry density than a more uniform sand (classified as SP according to the USCS classification). For clayey soils, the maximum dry density tends to decrease as plasticity increases.
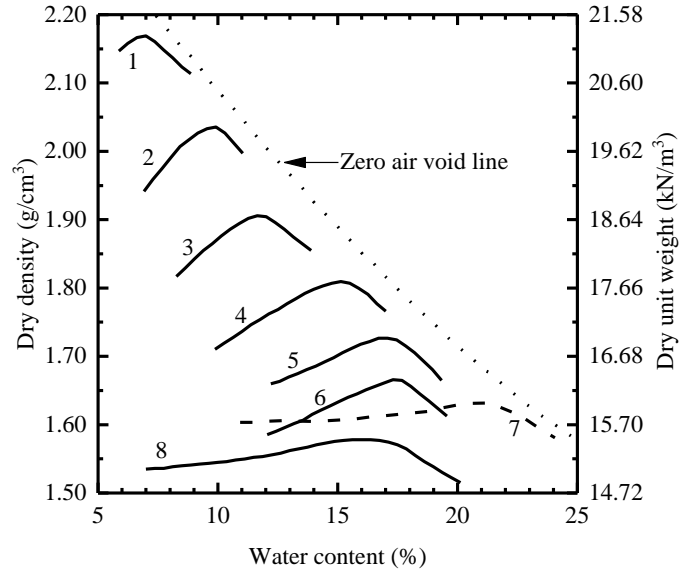
Figure 2.1 Water content vs dry density relationships for eight soils compacted according to the standard Proctor method (modified from Johnson and Sallberg, 1960))

Table 2.1 Soil texture and plasticity data (after Johnson and Sallberg, 1960)

Soil No.	Description and USCS symbol	Sand %	Silt %	Clay %	LL	PI
1	Well-graded sand with silt SW-SM	88	10	2	16	NP
2	Well-graded silt SM	72	15	13	16	NP
3	Clayey sand SC	73	9	18	22	4
4	Sandy lean clay CL	32	33	35	28	9
5	Lean silty clay CL	5	64	31	36	15
6	Loessial silt ML	5	85	10	26	2
7	Fat clay CH	6	22	72	67	40
8	Poorly graded sand SP	94	6	-	NP	-

2.1.2   Compaction energy

The density achieved during compaction depends on the amount of energy applied by the compaction process. The higher the compaction energy, the higher is the dry density and the lower is the optimum water content (Bowles 1996; Holtz et al. 2011). However, with the increase in compaction energy, particle crushing may also occur during compaction. If particle crushing occurs to a significant extent, it hampers the efforts to achieve the target compaction in the field.

18

The amount of particle crushing caused during compaction depends on the crushability characteristics of the particles and on the magnitude and nature of the compaction pressure applied (Wang et al. 2014). The main factors that affect particle crushability are gradation, mineralogy and morphology (Hagerty et al. 1993; Lade et al. 1996). Crushing of particles during compaction produce a different material from the one that existed originally. The partially crushed material has a different gradation, with an increase in the percentage of fines, slightly changed particle morphology, and consequently different maximum and minimum void ratios (Coop and Altuhafi 2011; Yamada and Sato 2005). Particle crushing is not the only possible outcome of excessive compaction effort. Particle segregation with compaction vibration is also possible. Field compaction of coarse-grained soils can cause segregation in two different ways. If the soil is being over-vibrated, fines will settle down towards the bottom of the compacted lift. If particle crushing occurs, finer material will result at the top of the compacted lift (USACE 1995). This may produce different degrees of compaction with depth in the compacted layer where a homogenous fill is desired to achieve uniform soil properties in the field. Overcompaction can lead to heaving for fine-grained soils.

The optimum water content required to reach the maximum density depends on the compaction energy. With an increase in compaction energy, the optimum water content is reduced and the maximum density achieved is increased, as observed in Figure 2.2. When excessive energy is applied by means of heavier equipment or increased number of passes, the water content of the soil exceeds the optimum water content determined for a compaction energy smaller than the applied one (Holtz et al. 2011). Since different equipment imparts different levels of energy, proper selection of compaction equipment and its application are necessary to achieve the desired density during compaction.
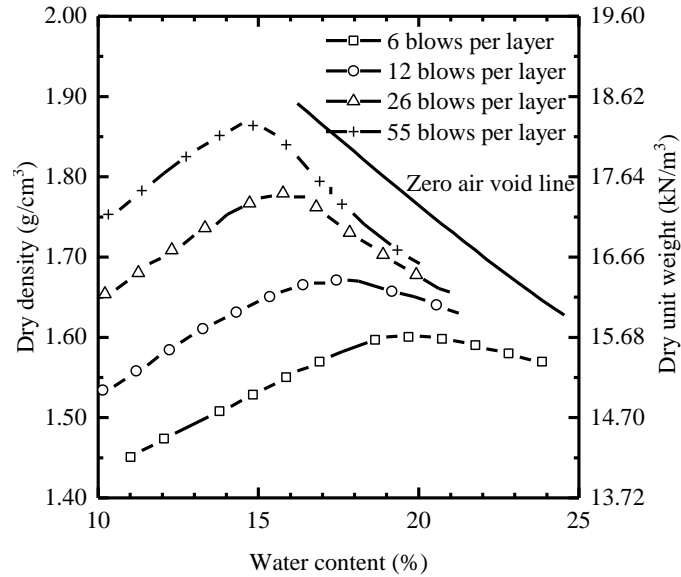
Figure 2.2 Dry density versus water content from modified Proctor compaction tests with variable blows per layer (modified from Holtz et al., 2011)

2.1.3 Grain size distribution and particle morphology

The grain size distribution and the morphology of particles of a soil influence its maximum and minimum densities and the corresponding void ratios (Altuhafi et al. 2016; Cho et al. 2006; Pike 1972; Dickin 1973; Youd 1973). The maximum void ratio is the void ratio of a soil corresponding to its loosest state attained with a stable fabric (non-collapsible), while the minimum void ratio is the void ratio corresponding to its densest state attained without particle crushing. Maximum and minimum void ratios are the limiting void ratios with respect to which the *in situ* relative density of a coarse-grained soil is determined.

Youd (1973) studied the effect of grain size distribution and particle morphology on the maximum and minimum void ratio of soils, as presented in Figure 2.3. The shape of the particles was quantified using a roundness parameter R, where roundness was defined as the ratio of the average radius of curvature of the corners of the particle to the radius of the maximum circle that can be inscribed to it (Wadell 1932). The smaller the roundness value of a particle, the more angular it is. The grain size distribution of a soil was quantified in terms of the coefficient of uniformity C_u. The coefficient of uniformity is the D_{60}/D_{10} ratio, where the D_{60} and D_{10} are the particle sizes obtained from the grain size distribution curve corresponding to 60% and 10% passing by weight. The smaller the coefficient uniformity, the more poorly graded or uniform the soil is. From Figure 2.3, it is observed that the maximum and minimum void ratios increase as the

20

particles become more angular or as the grain size distributions become more poorly graded or uniform.
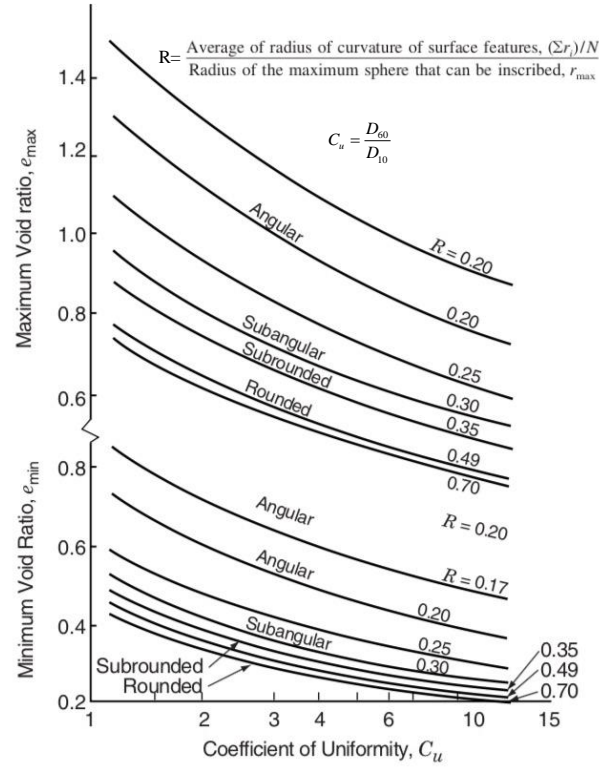
Figure 2.3 Maximum and minimum void ratio of sands as a function of roundness and the coefficient of uniformity (after Youd, 1973)

To isolate the effect of particle morphology from the grain size distribution on the limiting void ratios, Altuhafi et al. (2016) performed tests on various silica sands with uniform distributions and different particle morphology parameters. The relationship between the morphology parameters and the limiting void ratios for various natural silica sands observed by Altuhafi et al. (2016) is presented in Figure 2.4. The morphology of the particles was quantified in terms of sphericity S and aspect ratio AR. Sphericity was defined as the ratio of the projected perimeter of a circle having the same projected area as the particle to the perimeter of the particle (Mitchell and Soga 2005). The aspect ratio was defined as the ratio of the minimum Feret diameter to the maximum Feret diameter of a particle (Altuhafi et al. 2013). The smaller the sphericity or aspect ratio of a particle, the greater its angularity is. It is observed from Figure 2.4 that the maximum and minimum void ratios of silica sand increases as the sphericity and aspect ratio decrease. The

increase in limiting void ratios associated with increasing particle angularity is more significant for the maximum void ratios than for the minimum void ratios.
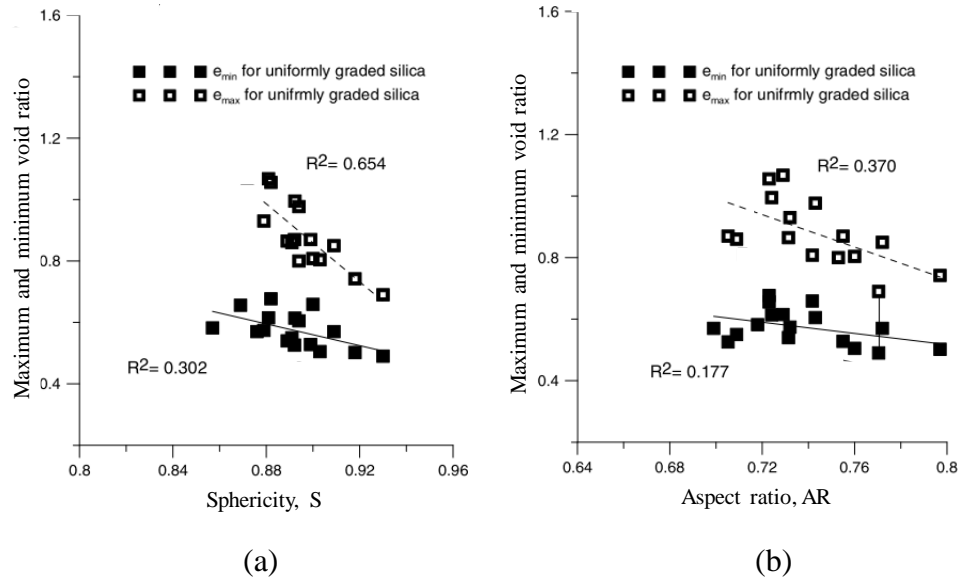
Figure 2.4 Maximum and minimum void ratio of natural sands with respect to the shape parameters (a) sphericity and (b) aspect ratio (after Altuhafi et al., 2016)

2.2 Compaction Equipment and Techniques

The selection of the compaction method depends primarily on the type of soil and the availability of equipment at the site (Holtz et al. 2011). Pounding, kneading, pressure, vibration, and dynamic compaction are the most common compaction methods used in the construction industry. Rollings and Rollings (1996) summarized the suitable compaction equipment for different types of soil, as shown in Table 2.2. It is observed from Table 2.2 that the use of vibratory rollers is recommended for compaction of sands and gravels, whereas sheepfoot rollers are used for compacting clays. The factors affecting the compaction of coarse-grained soils using vibratory rollers are discussed in the next section.

Table 2.2 Compaction method and type of compactor recommended by Rollings and Rollings (1996)

Soil	First choice	Second choice	Comment
Rock fill	Vibratory roller	Pneumatic roller	-
Plastic soil (CH, MH)	Sheepfoot or pad foot roller	Pneumatic roller	Thin lift usually needed
Low plasticity soils (CL, ML)	Sheepfoot or pad foot roller	Pneumatic vibratory roller	Water content often critical for silty soils
Plastic sands and gravels (GC, SC)	Vibratory, pneumatic roller	Pad foot roller	-
Silty sands and gravels (SM, GM)	Vibratory roller	Pneumatic, pad foot roller	Water content often critical
Clean sands (SW, SP)	Vibratory roller	Impact, pad foot roller	-

2.3 Controlling Parameters for Vibration Compaction in the Field

The most efficient method for compaction or densification of coarse-grained soils is vibration. The density of coarse-grained soils can be significantly increased if compaction is done by vibration in addition to compression (Selig and Yoo 1977). The mechanism through which compaction is achieved by vibration for coarse-grained soil particles can be explained in different ways. According to D'Appolonia et al. (1969), the particles reorient into a denser packing with each vibration cycle by the method of "free-fall" and "impact" in the presence of confinement. However, high confinement hinders the free-fall of particles and provides less efficient compaction density, while vibration without confinement causes chaotic motion of the particles and loosens the particles. Selig and Yoo (1977) and Wersäll et al. (2017) mentioned cyclic shear strain as the primary factor causing the rearrangement of the particles during vibration compaction. The amount of compaction achieved by vibration for any specific coarse-grained soil depends on the characteristics of the compactor and the compaction procedure. Holtz et al. (2011) summarized the characteristics of the rollers according to their mass, size, operating frequency and amplitude of vibration; the compaction process depends on the type of roller (frequency of vibration and towing speed), the number of passes of the roller, and lift thickness. The effects of type of vibration equipment and compaction procedures on the compaction density achieved in the field are discussed next.

2.3.1 Types of vibratory equipment

There are several types of compaction equipment available for vibratory compaction. They vary in size, mass and operating frequencies. In areas where large compactors cannot operate, small vibrating plates are used instead. Broms and Frossblad (1969) listed different types of vibratory compaction equipment suitable for different applications, as presented in Table 2.3.

Table 2.3 Types and applications of vibratory soil compactors (after Broms and Frossblad 1969)

Type of machine	Mass kg	Frequency Hz	Applications
Vibrating tampers:			
hand-guided	50-150	≈10	Street repair, fills behind bridge abutments, retaining and basement walls. Etc. Trench fills
Vibrating plate compactors:			
self-propelled, hand-guided	50-3000	12-80	Base and subbase compaction for streets, sidewalks, etc. Street repair. Fills behind bridge abutments, retaining and basement walls, etc. fills below floors. Trench fills
Multiple-type, mounted on tractors, etc.	200-300	30-70	Base and subbase compaction for highways
Crane mounted			Only limited use
Vibrating rollers:			
self-propelled, hand-guided	250-1500	40-80	Base. Subbase, and asphalt compaction for streets, sidewalks, parking areas, garage driveways, etc. Fills behind bridge abutments and retaining walls. Fills below floors. Trench fills
self-propelled, tandem-type	700-10000	30-80	Base. Subbase, and asphalt compaction for highways, streets, sidewalks, parking areas, garage driveways, etc. Fills below floors
self-propelled, rubber tires	4000-25000	20-40	Base. Subbase, and asphalt compaction for highways, streets, parking areas, airfield, etc. rock-fill dams. Fills (soil or rock) used as foundations for residentials and industrial buildings
Tractor-drawn	1500-15000	20-50	Base. Subbase, and asphalt compaction for highways, streets, parking areas, airfield, etc. Earth and rock-fill dams. Fills (soil or rock) used as foundations for residentials and industrial buildings. Deep compaction of natural deposits of sand

2.3.2 Frequency of vibration

The influence of vibration frequency on the compaction density has been studied by Mooney and Rinehart (2007), Selig and Yoo (1977) and Wersäll et al. (2017) among others. Figure 2.5 shows the density of soil as obtained for various frequency of vibration for different types of soils reported by Selig and Yoo (1977). The frequency at which maximum dry density is achieved is called the optimum frequency of vibration. The optimum frequency of vibration is a function of

the compactor-soil system and it changes as the density of the soil changes during the process of compaction (Holtz et al. 2011). However, Holtz et al. (2011) noted that the peaks for the dry density versus frequency curve for different soils are gentle, and that the use of compactors with a wide range of frequency is not necessary.
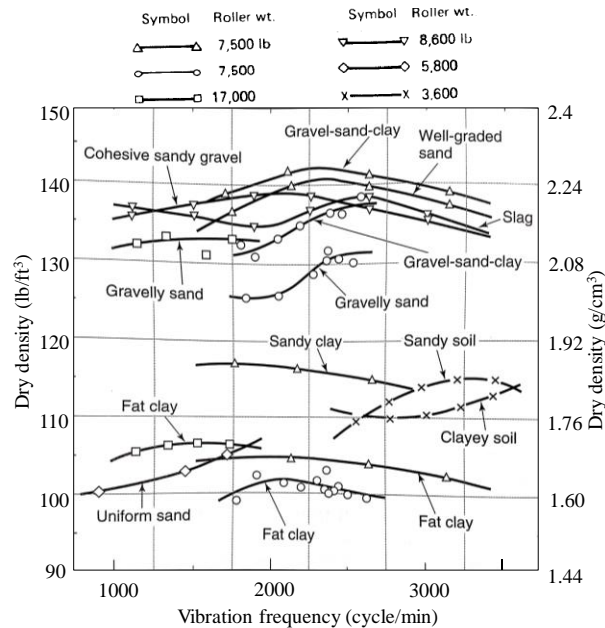
Figure 2.5 Variation of dry density with frequency of vibration by smooth-drum vibratory rollers
(after Selig and Yoo, 1977)

Small-scale laboratory compaction tests performed by Wersäll and Larsson (2013) on coarse-grained soils for variable frequency of vibration showed that maximum density can be achieved when the frequency of vibration is near the resonant frequency. Large-scale compaction tests were carried out by Wersäll et al. (2017) for well-graded gravel using a vibratory roller with variable frequency of vibration. Wersäll et al. (2017) observed that the increase in density with depth depends on the frequency of vibration, as presented in Figure 2.6.
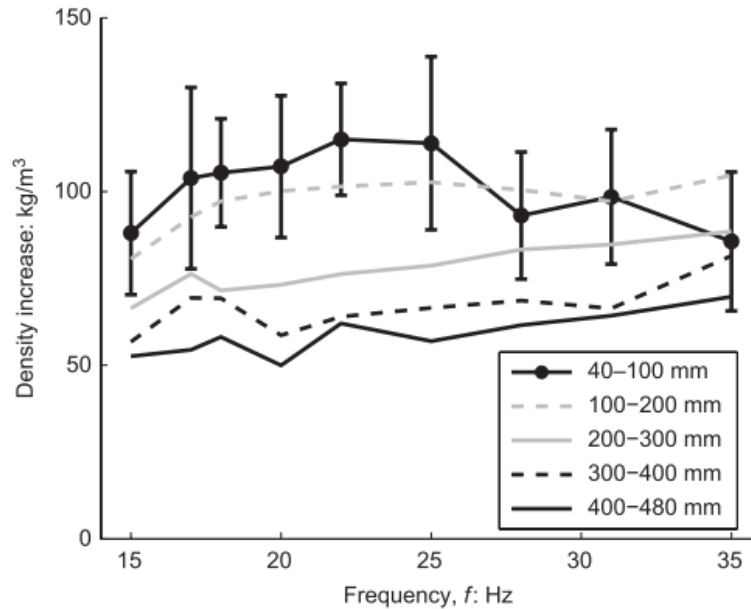
Figure 2.6 Increase in density in five layers as a function of frequency with the standard deviation of the sample in the top layer (after Wersäll et al., 2017)

2.3.3 Number of passes and towing speed

Selig and Yoo (1977) studied the effect of the number of passes and towing speed of a compactor on the compaction density of well-graded sand, as presented in Figure 2.7. The compaction density increases as the number of passes increases up to a certain point. For a given number of passes, density is increased with a decrease in the travel speed of the vibratory roller.
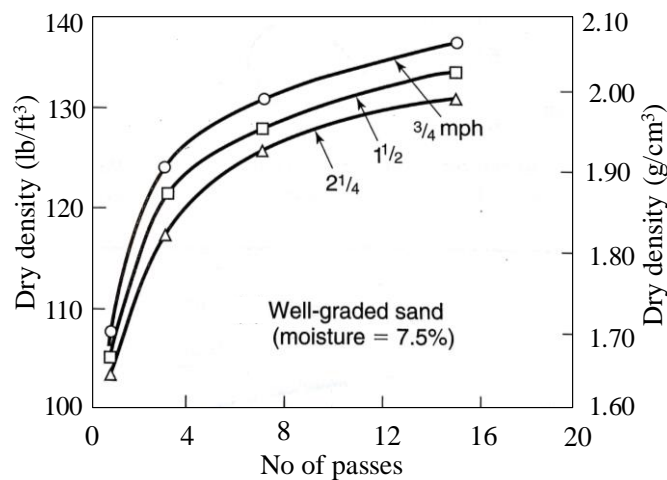
Figure 2.7 Effect of roller travel speed on amount of compaction with 7700 kg vibratory roller for well-graded sand (after Selig and Yoo, 1977)

2.3.4   Lift thickness

The effect of lift thickness on the compaction density was studied by D'Appolonia et al. (1969), and their findings are illustrated in Figure 2.8, as cited by Holtz et al. (2011). Compaction was carried out for northern Indiana dune sands using a 5,670 kg vibratory roller operating at a frequency of 27.5 Hz. It was observed that the soil reaches its maximum density for a given number of passes at about 45 cm depth. In addition, there was not a significant increase in density after 5 roller passes.
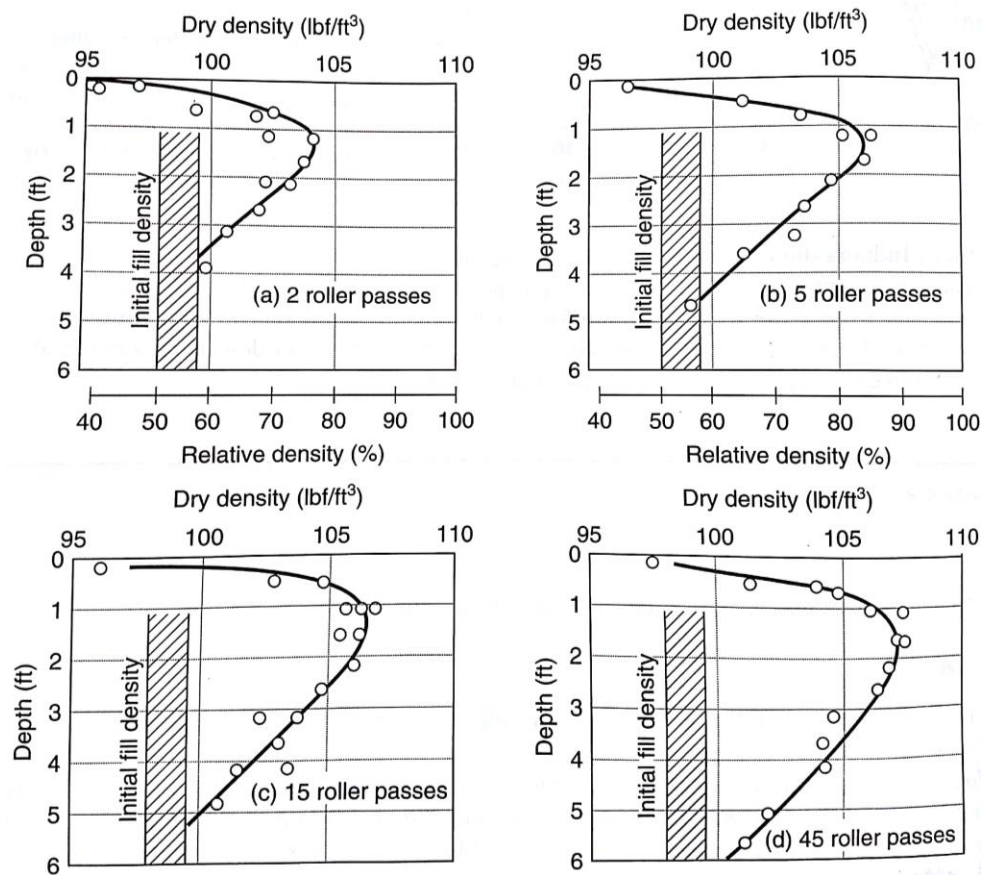
Figure 2.8 Density-depth relationship for a 5670 kg roller operating at 27.5 Hz for a 240 cm lift height for various number of passes (after D'Appolonia et al., 1969)

2.4   Compaction Specifications in the Unites States

Fratta and Kim (2015) and Hoppe (1999) summarized the compaction specifications by the Departments of Transportation of different states in the United States in terms of the lift thickness and relative compaction, as provided in Table 2.4.

27

Table 2.4 Compaction specifications followed by Departments of Transportation of different states in the Unites States (Fratta and Kim, 2015; Hoppe, 1999)

State	Loose lift thickness cm (in)	Relative compaction %	Remarks
Alabama	0.20 (8)	95	
Arizona	0.20 (8)	100	
California	0.20 (8)	95	For top 0.75 m
Connecticut	0.15 (6)	100	Compacted lift indicated
Delaware	0.20 (8)	95	
Florida	0.20 (8)	100	
Georgia	-	100	
Idaho	0.20 (8)	95	
Illinois	0.20 (8)	95	For top; remainder varies with embankment depth
Indiana	0.20 (8)	95	
Iowa	0.20 (8)	None	One roller pass per inch thickness
Kansas	0.20 (8)	90	
Kentucky	0.15 (6)	95	Compacted lift indicated, water +2% to -4% of optimum
Louisiana	0.30 (12)	95	
Maine	0.20 (8)	-	At or near optimum water
Maryland	0.15 (6)	97	For top 0.3 m, remainder is 92%
Massachusetts	0.15 (6)	95	
Michigan	0.23 (9)	95	
Minnesota	0.20 (8)	95	
Mississippi	0.20 (8)	-	
Missouri	0.20 (8)	95	
Montana	0.15 (6)	95	At or near optimum
Nebraska		95	
Nevada		95	
New Hampshire	0.30 (12)	98	
New Jersey	0.30 (12)	95	
North Dakota	0.15 (6)	-	
Ohio	0.15 (6)	-	
Oklahoma	0.15 (6)	95	
Oregon	0.20 (8)	95	For top 0.9 m; remainder is 90%
South Carolina	0.20 (8)	95	
South Dakota	0.20-0.30 (8-12)	97	0.2 m for embankment; 0.3 m for bridge and backfill

Table 2.4 (Continued)

State	Loose lift thickness cm (in)	Relative compaction %	Remarks
Texas	0.30 (12)	-	
Vermont	0.20 (8)	90	
Virginia	0.20 (8)	95	+ or -20% of optimum water
Washington	0.10 (4)	95	Top 0.6 m in 0.1 m lifts; remainder are 0.2 m lifts
Wisconsin	0.20 (8)	95	Top 1.8 m within 30 m of abutment; remainder is 90%
Wyoming	0.30 (12)	-	Use of reinforced geotextile layers

3. RESEARCH METHODOLOGY

Five different backfill soils commonly used by INDOT for the construction of MSE walls or road pavements were collected for this research work. The grain size distribution curves and the morphology parameters of the backfill soils were obtained to characterize the testing materials. The effects of vibration amplitude and frequency on the compaction density of the dry coarse-grained backfill soils were investigated by small-scale laboratory compaction tests performed using a vibratory table and a vibratory hammer. Soil samples were placed in molds of two sizes (0.1 ft^3 and 0.5 ft^3) before vibratory testing. The vibratory table used in this research has a fixed frequency of vibration of 60 Hz and variable amplitude of vibration ranging from 0.2 to 1.7 mm. On the other hand, the vibratory hammer has a fixed amplitude of vibration of 0.5 mm but variable hammer speeds (9 different vibration settings are possible, with the number of hammer blows per second ranging from 25 to 60). Accelerometer sensors were attached to both the vibratory table and hammer to measure the amplitude and frequency of vibration during compaction. A MATLAB code was used to analyze the measured accelerometer data to determine the amplitude and frequency of vibration during testing. The effect of water content on the dynamic compaction was investigated by performing standard and modified Proctor compaction tests in the laboratory. A comparison of the compaction densities that can be achieved for different backfill materials with different laboratory equipment with variable frequency and amplitude of vibration is presented. Critical-state friction angles and interface friction angles are important parameters used to determine the shear resistance of soils at the interface with structural elements. Direct shear tests were carried out for the collected backfill materials to determine their critical-state friction angles. The effect of gravel content and surface roughness on the interface friction angle was determined from direct interface shear tests performed for gravel-sand mixtures against smooth and rusted steel plates. Field tests were performed to investigate the effects of vibration frequency of a vibratory roller (Caterpillar, model No. CS56B) used for subgrade compaction of a ramp at the intersection of US 20 and IN 2 in Rolling Prairie, Indiana. The field compaction density of the subgrade was assessed based on DCP tests performed at two different sections of the ramp for 6-in compacted lift thickness, four passes of the roller and two different vibration settings (low vibration setting and high vibration setting).

3.1 Laboratory Compaction Tests Using a Vibratory Table

The dry unit weight of all the test materials compacted under variable amplitude and duration of vibration were determined with a vibratory table manufactured by ELE International. For this purpose, the amplitude of vibration of the vibratory table was varied using the voltage regulator of the equipment, while the frequency of vibration of the vibratory table was fixed at 60 Hz. Tests were also performed according to the ASTM D4253 (2016) standard (vibration frequency of 60 Hz and amplitude of 0.33 mm). Samples were prepared simply by placing the test materials with a scoop into molds of two sizes (volume=0.1 ft^3 and 0.5 ft^3) depending on their particle sizes. The large mold was used for compacting soils with a maximum particle size of up to 2 inches, whereas the small mold was used for compacting soils with a maximum particle size of up to 0.75 inch, as per the ASTM D4253 (2016) standard. The test materials were dried in the oven before testing. A surcharge of 14 kPa was applied on a steel disk placed on top of the samples. During compaction by vibration, the amplitudes of vibration for various voltage regulator readings of the vibratory table were measured for the table and mold using accelerometer sensors attached to them. Figure 3.1 shows the laboratory compaction test setup using a vibratory table.

(a)   (b)
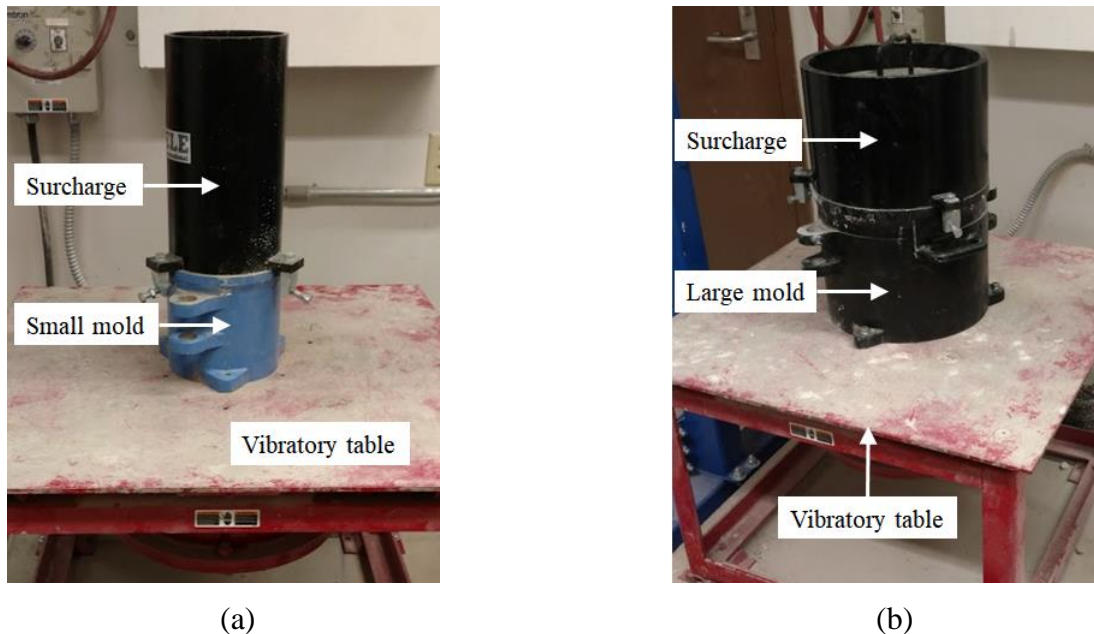
Figure 3.1 Laboratory compaction test setup using a vibratory table showing (a) small mold to test backfill soils with maximum particle size of up to 0.75 inch and (b) large mold to test backfill soils with maximum particle size of up to 2 inches

To study the effect of vibration time on compaction density, vibratory table compaction tests were carried out for various time intervals as well. The grain size distribution of the soil samples after testing were obtained at the end of each vibratory table compaction test; the grain size distribution curves before and after testing were compared to check whether particle crushing had occurred during vibration compaction. The dry unit weight γ_d (kN/m^3) of the test material after vibratory table compaction was calculated as the ratio of the dry weight of the soil W_s (kN) to the volume V_m of the mold (m^3). The dry unit weight γ_d was calculated as:

$$\gamma_d = \frac{W_s}{V_m}$$

(3.1)

3.2 Laboratory Compaction Tests Using a Vibratory Hammer

Laboratory compaction tests for four of the backfill soils (tests were not performed for the slag backfill material due to insufficient quantity for testing) were carried out using a vibratory hammer, according to the ASTM D7382 (2008) standard. The objective of the tests was to determine the dry unit weight of the test materials compacted under different vibration speeds of the hammer. The setup of the vibratory hammer equipment was manufactured by Humboldt Mfg. Co., while the vibratory hammer used in the equipment setup was manufactured by Bosch (vibratory hammer model No. 11264EVS). A tamper or circular base plate of 6 inches in diameter, which was connected to the vibrating hammer through a rod, applied vibration at the top of the soil surface inside the mold. A steady surcharge of 18.5 kPa was applied to the vibratory hammer to prevent it from bouncing up and down on the surface of the soil sample.

Two molds with volume equal to 0.1 ft^3 and 0.5 ft^3 were used in these experiments. The large mold was used for compacting soils with a maximum particle size of up to 2 inches, whereas the small mold was used for compacting soils with a maximum particle size of up to 0.75 inch, as per ASTM D7382 (2008). The test materials were dried in the oven before testing. The dry materials were placed inside the mold with a scoop and compacted in three layers. Figure 3.2 shows the maximum density test setup using a vibratory hammer equipment.

<div style="text-align:center">(a)   (b)</div>
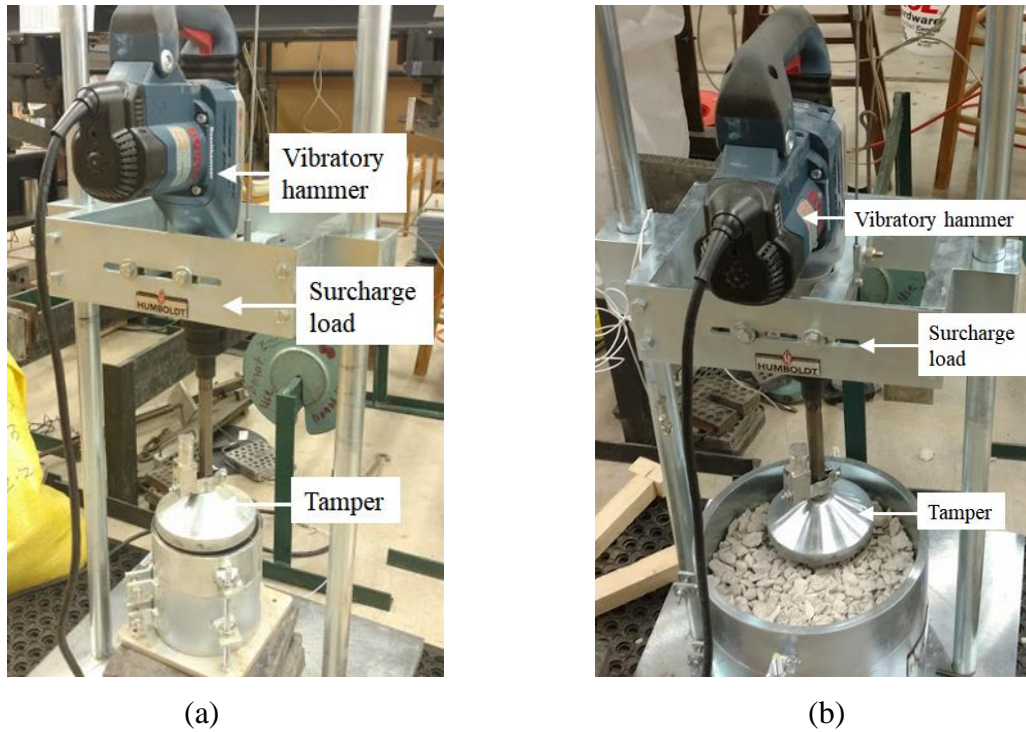
Figure 3.2 Laboratory compaction test setup using a vibratory hammer showing (a) small mold for testing backfill soils with the maximum particle size of 0.75 inches and (b) large mold for testing backfill soils with the maximum particle size of 2 inches

To compact the test soils in the large mold, the tamper was placed in sequence in eight different locations on the surface of each layer and vibrated by the hammer, as shown in Figure 3.3. The duration of vibration was one minute for each tamper position, following the ASTM D7382 (2008) standard. To compact the test soils in the small mold, the tamper was placed in a single location and vibrated by the hammer for one minute for each of the three layers. The vibratory hammer has a regulator to control the speed of vibration. After compaction with the vibratory hammer using various speeds of vibration, the dry unit weight and void ratio of the tested soils were calculated. Values of the dry unit weight were calculated from the volume of the mold and the weights of the compacted materials using Equation (3.1).
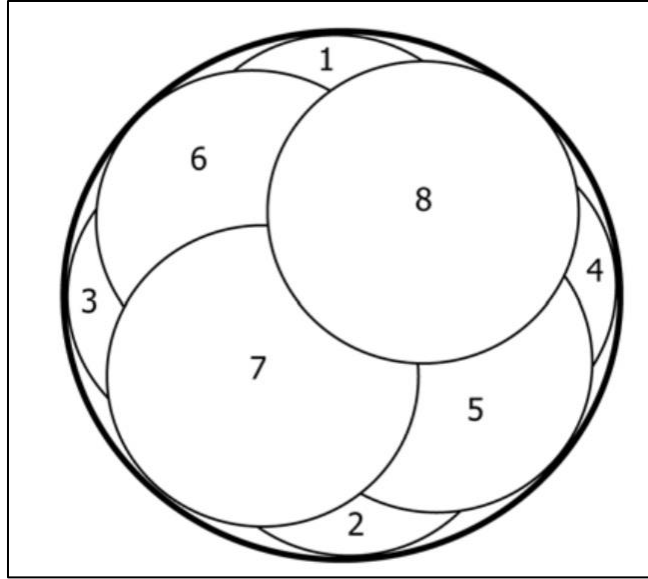
Figure 3.3 Sequence of tamper positions during compaction by the vibratory hammer for a large mold (after ASTM D7382, 2008)

3.3 Laboratory Compaction Tests Using a Proctor Hammer

Standard and modified Proctor compaction tests were carried out according to the ASTM D698 (2012) and ASTM D1557 (2012) standards, respectively, to determine the dry unit weights achieved at different water contents. A comparison of the test procedure prescribed in the standards and modified Proctor compaction tests is provided in Table 3.1.

Table 3.1 Comparison of standard and modified Proctor compaction test procedures

	Standard Proctor	Modified Proctor
Weight of hammer (lbf)	5.5	10
Drop height (in)	12	18
No. of layers	3	5
No. of blow per layer	25	25

3.4 Measurements During Vibratory Table and Hammer Compaction Tests Using Accelerometer

The amplitude and frequency of vibration of the compaction equipment were measured using accelerometers manufactured by PCB Piezotronics (model No. M350A14). The amplitude of vibration is a measure of the displacement of a point on a vibrating body from its equilibrium position. The number of times a complete motion cycle occurs during a period of one second is

the frequency of vibration, which is measured in hertz (Hz). The specifications of the accelerometers are listed in Table 3.2.

Table 3.2 Specifications of the accelerometers

Sensitivity (±15%)	1.0 mV/g
Measurement range	±5000 g pk
Frequency range (±10%)	0.4 to 7500 Hz
Weight	0.63 oz

The accelerometer data was collected by a signal acquisition system manufactured by National Instruments Corporation (NI). The signal acquisition module is a C series sound and vibration input module (model No. NI 9234), as shown in Figure 3.4, that has an in-built AC/DC coupling, IEPE open/short detection and IEPE signal conditioning. The input channels are capable of simultaneously measuring signals from four accelerometers. The signal acquisition module was connected to an NI Compact DAQ Chassis (model No. NI 9191) to transfer the measured accelerometer data to a computer (using an Ethernet cable) for processing and display. The NI Signal Express 2015 software was used to collect and display the data in a computer.

Figure 3.4 NI 9234 sound and vibration input module for collecting signal from accelerometer

To measure the vibration amplitude and frequency of the vibratory table during testing, two accelerometer sensors were attached to the test setup. One accelerometer was attached to the

top of the vibratory table, and the other one was attached to the mold. Figure 3.5 shows a schematic of the complete test setup for the compaction tests performed using the vibratory table. The attachment of the accelerometer sensors to the mold and the vibratory table is shown in Figure 3.6.
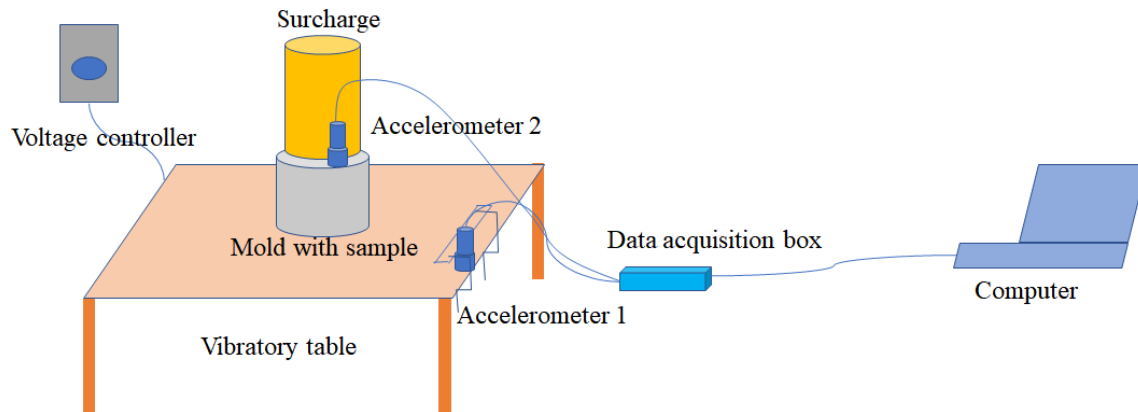
Figure 3.5 Schematic for the compaction test set up using the vibratory table

(a)   (b)
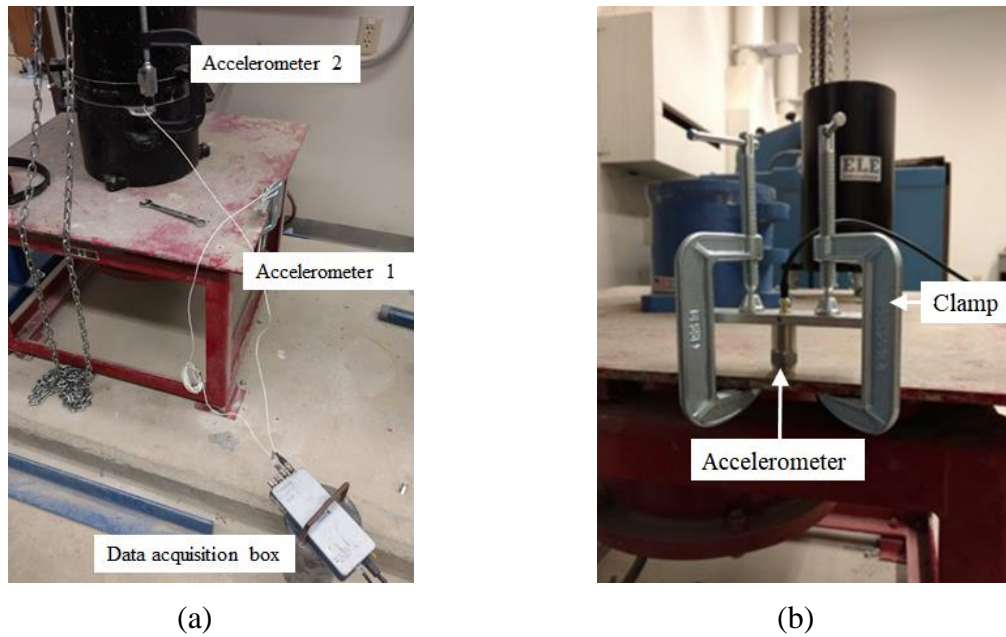
Figure 3.6 Attachment of the accelerometers to the mold and the vibratory table

To measure the amplitude and speed of vibration of the hammer during compaction, an accelerometer was attached to the vibratory hammer. A schematic of the complete test setup is shown in Figure 3.7. Figure 3.8 shows the accelerometer sensor attached to the tamping rod of the vibratory hammer.
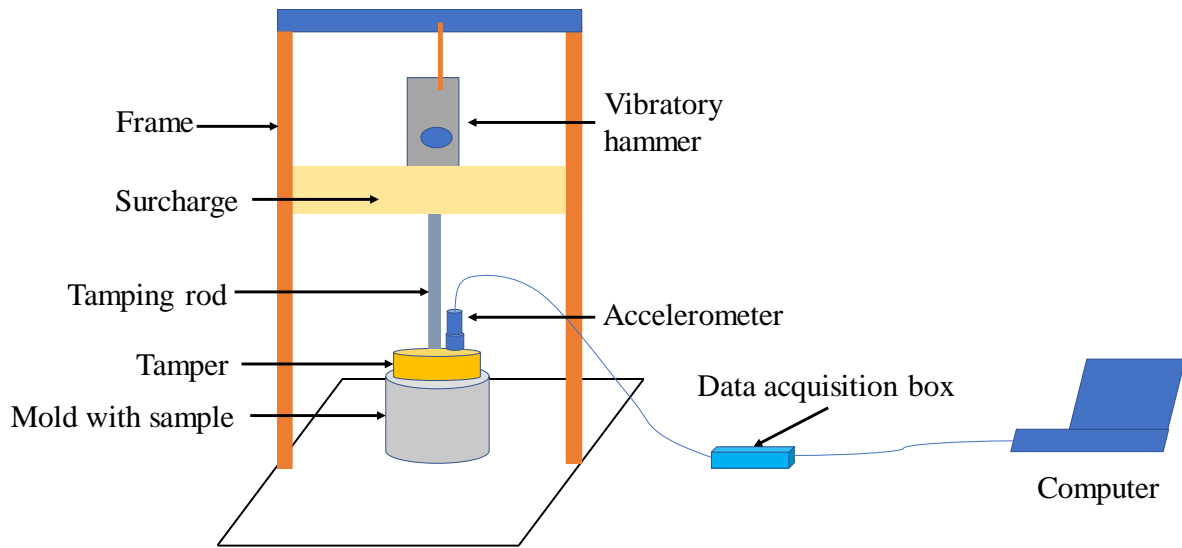
Figure 3.7 Schematic of the vibratory hammer test setup
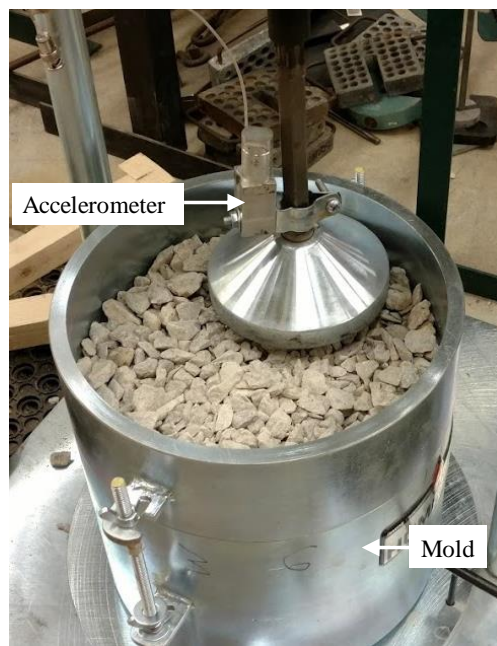
Figure 3.8 Attachment of the accelerometer sensor to the tamping rod of vibratory hammer

Any waveform generated from a vibration can be considered as a singular or a sum of a series of simple sinusoidal curves of different frequencies, amplitudes, and phases. Fourier analysis is used to deconstruct a vibration wave into its individual sine wave components and to determine vibration acceleration as a function of frequency. An accelerometer sensor collects acceleration of vibration as a function of time. A MATLAB code was used to analyze the acceleration data collected during the vibration compaction tests and to determine the corresponding frequencies by

Fourier transformation. High frequency noise (related to frequencies greater than the range of frequency of the vibration equipment; equal to 60 Hz for the vibratory table and 100 Hz for the vibratory hammer) with small magnitudes of accelerations were filtered out using the Butterworth filter function available in MATLAB. After removal of the noise frequency data, filtered acceleration versus time data plots were generated to obtain the dominant frequency. The displacement or amplitude of vibration was obtained by double integration of the filtered acceleration data. The steps followed to determine the frequency and amplitude of vibration from the accelerometer data are provided in Figure 3.9.

```
┌─────────────────────────────────┐
│     Collect  acceleration  data  │
└─────────────────────────────────┘
                │
                ▼
┌──────────────────────────────────────────┐
│  Obtain frequencies  by Fourier  transformation │
└──────────────────────────────────────────┘
                │
                ▼
┌────────────────────────────────────────────────┐
│  Apply  noise  cancellation  to obtain  dominant  frequency │
└────────────────────────────────────────────────┘
                │
                ▼
┌──────────────────────────────────────────────────┐
│  Generate  filtered  acceleration  data with  dominant  frequency │
└──────────────────────────────────────────────────┘
                │
                ▼
┌──────────────────────────────────────────────────┐
│  Determine  displacement  (amplitude)  by double  integration  of │
│            the filtered  acceleration  data              │
└──────────────────────────────────────────────────┘
```
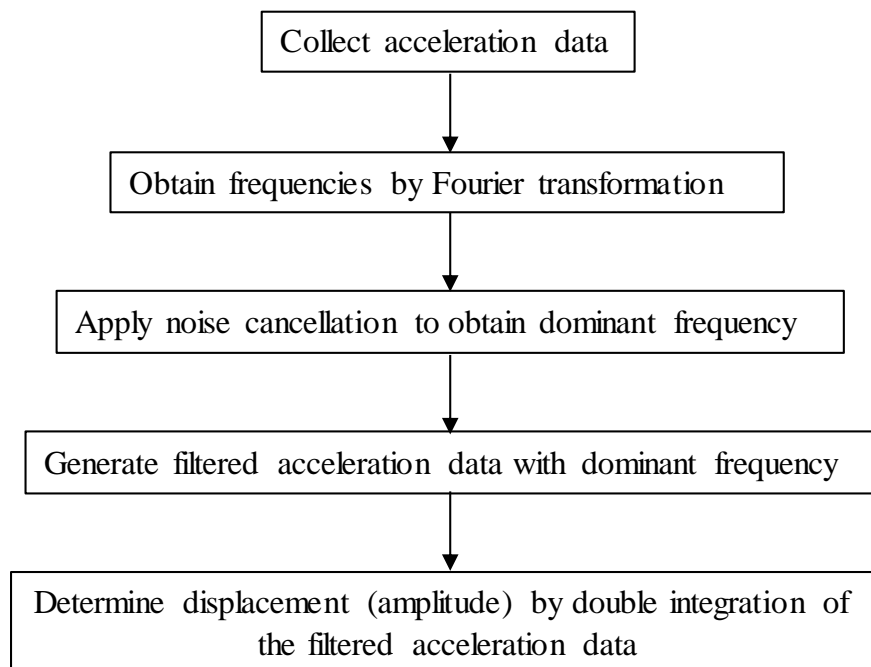
Figure 3.9 Steps to determine the frequency and amplitude of vibration using MATLAB code

Figure 3.10 shows a typical acceleration data that was obtained by an accelerometer attached to the vibratory table during vibration. This accelerometer data was analyzed using MATLAB to obtain acceleration magnitudes at different frequency of vibrations, as shown in Figure 3.11. It can be observed that there are small magnitudes of accelerations at high frequency of vibrations. The accelerations of small magnitude and high frequency are noise measured by the accelerometers during vibration. This noise needs to be filtered out to obtain the frequency of dominant vibration. It can be observed from Figure 3.12 that the dominant frequency of vibration is 60 Hz for the example acceleration vs. time data shown in Figure 3.10 obtained for the vibratory

table. The acceleration data obtained after noise cancellation is shown in Figure 3.13. The filtered acceleration data is then integrated twice to obtain the displacement or amplitude of vibration, as shown in Figure 3.14.
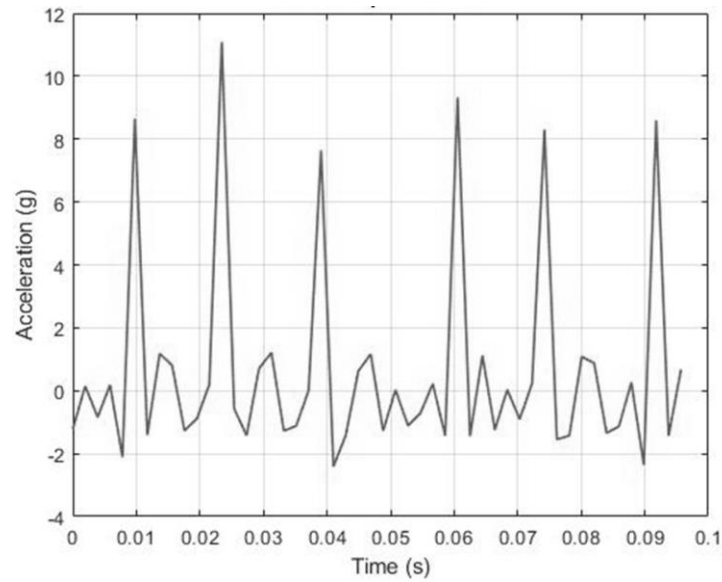
Figure 3.10 Example of raw acceleration versus time data from a vibratory table test (only a short period of time is shown for illustration)
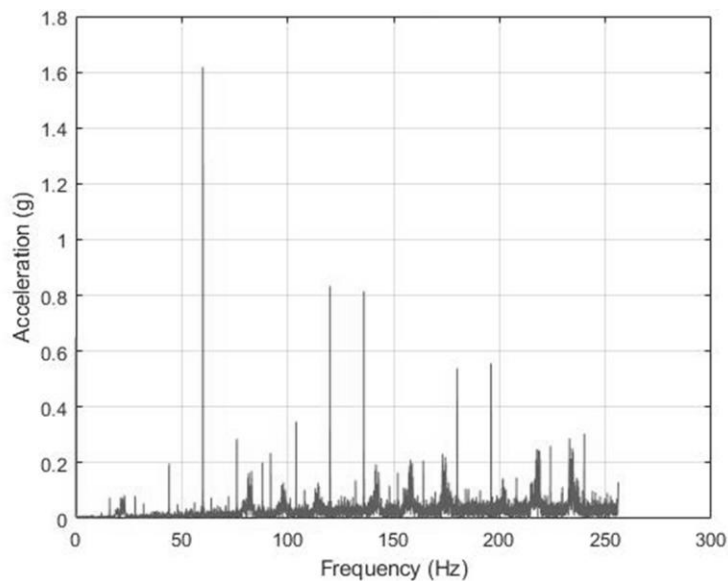
Figure 3.11 Frequency data obtained after Fourier transformation of the acceleration data
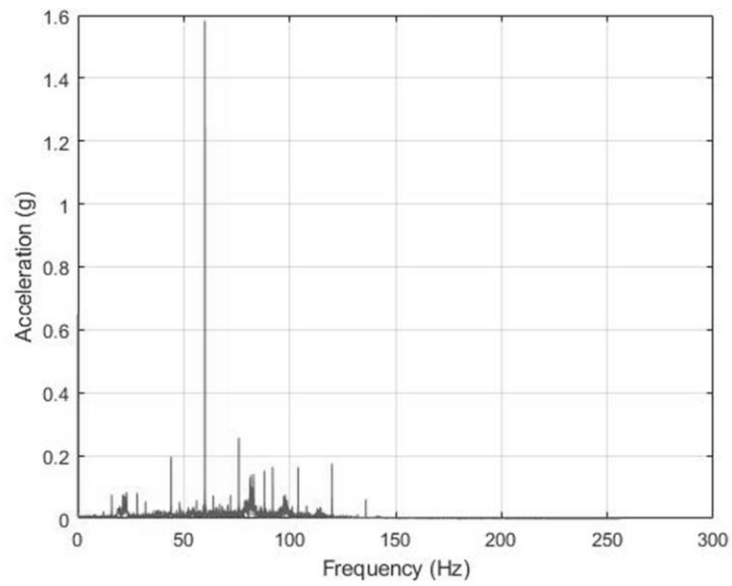
Figure 3.12 Acceleration versus frequency data after noise frequency cancellation
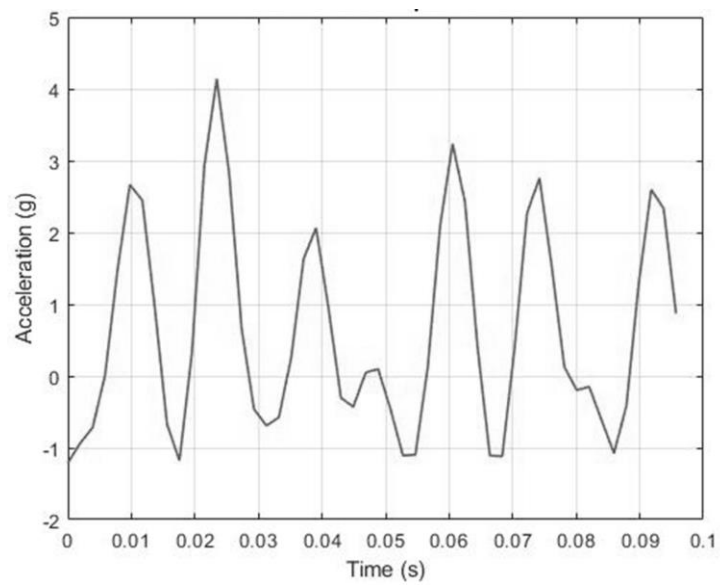
Figure 3.13 Filtered acceleration versus time data after noise frequency cancellation
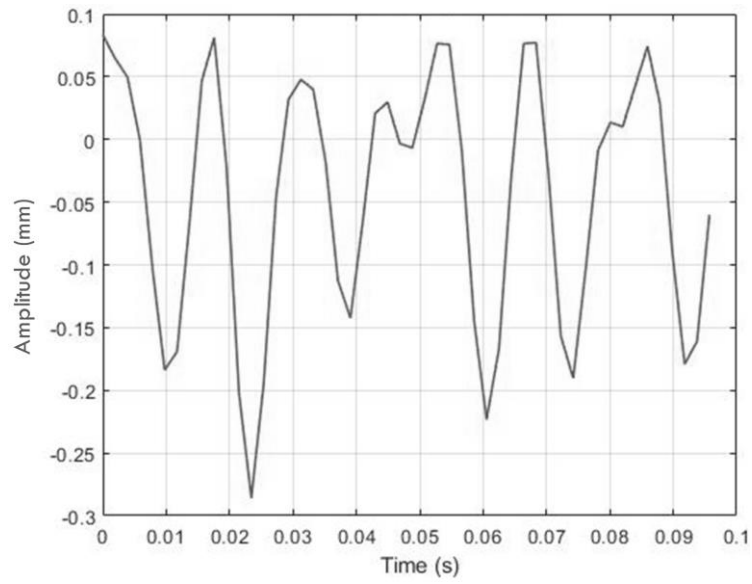
Figure 3.14 Amplitude of vibration (displacement) versus time after double integration of the filtered acceleration data

4. MATERIAL COLLECTION AND CHARACTERIZATION

4.1 Material Collection

Materials, commonly used for backfill purposes by INDOT, were collected for this research work. A total of five different backfill materials were collected. Two backfill materials had particle size less than 4.75 mm, which are referred as No. 4 natural sand and No. 24 stone sand according to the standard and specifications by the Indiana Department of Transportation (2018). The other three backfill materials had particle sizes greater than 4.75 mm; these are referred as No. 5, No. 8 and No. 43 aggregates according to the standard and specifications by the Indiana Department of Transportation (2018). No. 4 natural sand and No. 43 aggregates were collected from the construction site on I-65 in Lake county, Indiana. The No. 43 material is composed of air-cooled blast furnace slag aggregate Slag. All other backfill materials (No. 5, No. 8 and No. 24) were collected from a limestone quarry located in Delphi, Indiana, operated by US Aggregates. Limestone rocks are broken down in different sizes and sieved through specific size sieves at the quarry to produce aggregates with the grain size distributions specified by INDOT. Figure 4.1 and Figure 4.2 show the backfill materials collected for this research.

(a)   (b)   (c)
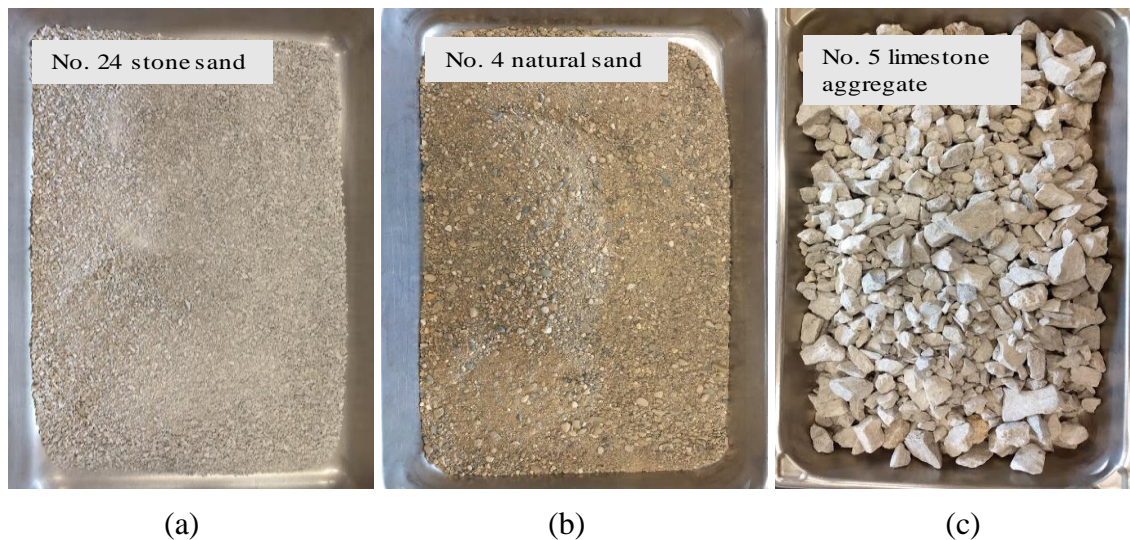
Figure 4.1 Collected backfill materials (a) No. 24 stone sand (b) No. 4 natural sand (c) No. 5 limestone aggregate

(a) (b)
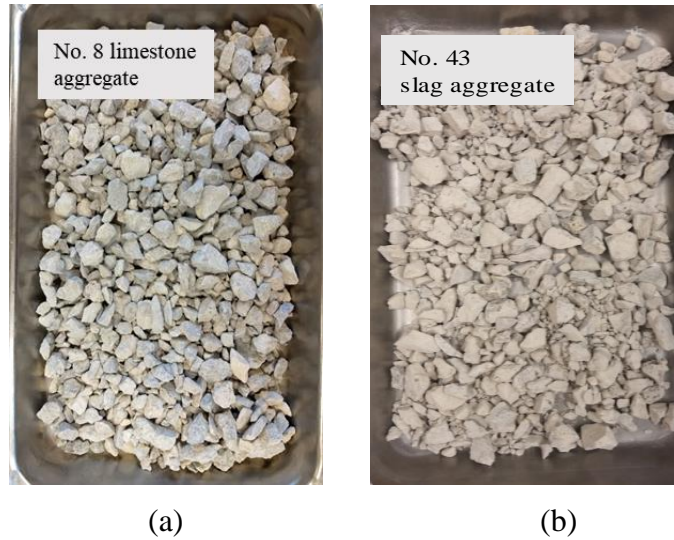
Figure 4.2 Collected backfill materials (a) No. 8 limestone aggregate (b) No. 43 slag materials

4.2   Grain Size Distribution and Soil Classification

The test materials were sieved through a set of sieves to determine their grain size distribution curves and to obtain their classifications according to the Unified Soil Classification System (USCS), as per ASTM D2487 (2017). Accordingly, a series of U.S. standard sieves with varying square openings were consecutively placed on top of each other to form a stack such that the sieve with the largest opening was placed at the top and the one with the smallest opening was placed at the bottom. The material passing through the sieve with the smallest opening (sieve #200) was collected on a pan placed under the stack of sieves. Soil classification depends on the determination of the percentage of particles passing through each U.S. standard sieve and the resulting grain distribution curve. Soil is first categorized as coarse or fine grained in terms of particle size. Coarse-grained soils have more than 50% of the particles greater than 75 μm, whereas, fine-grained soils have more than 50% of the particles smaller than 75 μm. According to the USCS soil classification, if more than 50% of the coarse fraction of particles are retained on sieve No. 4 (opening size=4.75 mm), the material is classified as gravel, otherwise it is classified as sand.

Grain size distribution curves are obtained by plotting particle size in the x axis (in log scale) versus the cumulative percentage of material passing through the corresponding sieve size in the y axis (normal scale). USCS uses two terms, coefficient of curvature and coefficient of uniformity, to determine whether a soil is well graded or poorly graded. According to ASTM D2487 (2017), the coefficient of uniformity C_u and the coefficient of curvature C_c are defined as:

$$C_u = \frac{D_{60}}{D_{10}} \tag{4.1}$$

$$C_c = \frac{\left(D_{30}\right)^2}{D_{60} \times D_{10}} \tag{4.2}$$

where D_{60}, D_{30} and D_{10} are the sieve sizes through which the percentage of particle passing through them are 60%, 30% and 10%, respectively. For a sand to be well-graded, C_u must be greater than 6 and C_c must be within 1 and 3. The criteria for well-graded gravel is that C_u must be greater than 4 and C_c must be within 1 and 3. The soil is considered poorly-graded if it does not fulfil the limiting criteria for C_u and C_c specified for well-graded soil. Figure 4.3 shows the grain size distribution curves for the test materials. A summary of the grain size distribution data is given in Table 4.1 along with the classification of the test materials according to the Unified Soil Classification System (USCS).
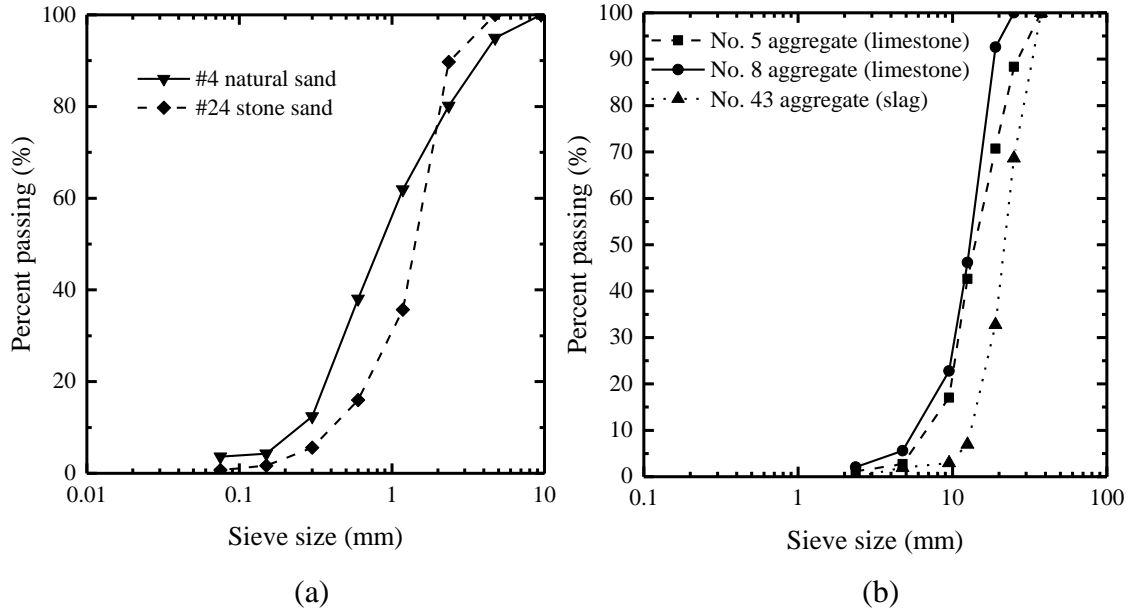
Figure 4.3 Grains size distribution curves for the test materials (a) No. 4 natural sand and No. 24 stone sand and (b) No. 5, No. 8 and No. 43 aggregates

Table 4.1 Grain size distribution test results and USCS classification for the test materials

Test materials	D_{10} (mm)	D_{30} (mm)	D_{50} (mm)	D_{60} (mm)	C_u	C_c	USCS
No. 4 natural sand	0.23	0.50	0.85	1.10	4.58	1.00	SP
No. 24 stone sand	0.40	0.90	1.30	1.60	4.00	1.26	SP
No. 5 limestone aggregate	6.50	10	13	17	2.62	0.90	GP
No. 8 limestone aggregate	5.50	10	12	14	2.55	1.30	GP
No. 43 slag aggregate	13	20	21	25	1.92	1.23	GP

4.3 Morphology Analyses

4.3.1 Morphology parameters of the test materials

Particle morphology parameters, which play an important role on the packing density and frictional resistance of soils, were determined for all the test materials in the geotechnical laboratory at Purdue University. There are many other important soil properties, such as the critical-state friction angle and particle crushing strength, that depend on particle characteristics as well (Altuhafi et al. 2013; Cho et al. 2006; Mitchell and Soga 2005). Among the numerous parameters that describe particle morphology, the most commonly used in geotechnical engineering are roundness, sphericity and aspect ratio. The morphology parameters of soil particles have historically been described using a standard chart against which individual soil particles were compared (Krumbein and Sloss 1951; Mitchell and Soga 2005). However, with the development of digital image analysis, software has often been used in the determination of particle morphology parameters from digital images since the entire process became more efficient and convenient (Zheng and Hryciw 2015). Different definitions of morphology parameters are followed in different methods of analyses and software applications. Due to the different definitions available in the literature for the various morphology parameters, accurate specification of the definitions used in determining them is necessary. The most commonly used morphology parameters, along with their interpretation are discussed next.

Roundness

Roundness is a measure of sharpness of the particle corners (Altuhafi et al. 2013). It was first introduced by Wadell (1932). Using two-dimensional images of particles, Wadell (1932) defined roundness as the ratio of the average radius of curvature of the corners of the projected outline of the particle to the radius of the maximum circle inscribed in the particle, as shown in Figure 4.4. This definition of roundness is still widely used by other researchers (Cho et al. 2006; Mitchell and Soga 2005; Zheng and Hryciw 2015). The roundness R_R proposed by Wadell (1932) is expressed as:

$$R_R = \frac{\sum\limits_{i=1}^{i=n} \dfrac{r_i}{n}}{R_I} \tag{4.3}$$

where r_i is the radius of individual corners of the particle, R_I is the radius of its maximum inscribed circle and n is the maximum number of particle corners.
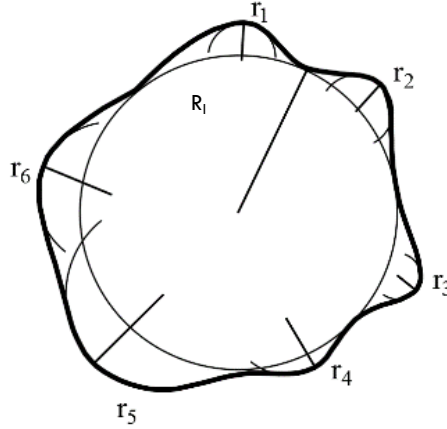
Figure 4.4 Roundness measurement according to Wadell (1932) for a 2D projected outline of a particle

The development of image analysis using computer software enabled the determination of roundness based on the projected area of a particle and the area of a circle with diameter equal to its major axis (Cox and Budhu 2008). The major axis is defined as the length of the longest axis of the ellipse best fitted on the 2D projected outline of the particle, as shown in Figure 4.5. The best fitting ellipse has the same area, orientation and centroid as the original particle (Ferreira and Rasband 2012). The roundness R_A is defined as the ratio of the particle's projected area A_s to the

area of a circle whose diameter is equal to the particle's major axis L_{major} of the best fitting ellipse (Cox and Budhu 2008; Ferreira and Rasband 2012) as:

$$R_A = \frac{4 \times A_s}{\pi \times L_{major}^2} = \frac{L_{minor}}{L_{major}} \tag{4.4}$$
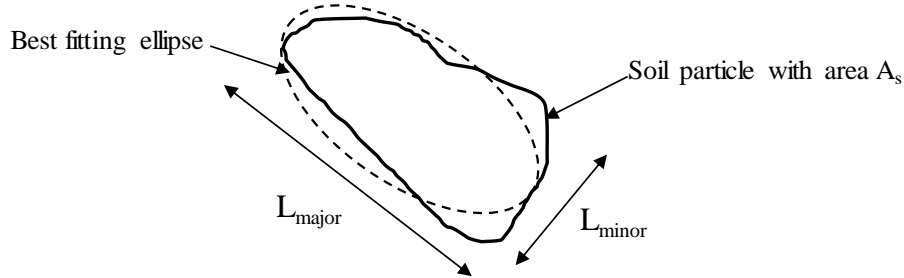
Figure 4.5 Major and minor axis of the ellipse best fitted to a 2D projected outline of a particle

Sphericity

Sphericity is a measure of the degree of similarity between the shape of a particle and a sphere (Altuhafi et al. 2013). Wadell (1932) first introduced the term sphericity as the ratio of the surface area of a sphere with the same volume as the particle to the actual surface area of the particle. Recognizing the practical difficulties in measuring the 3D surface areas of a particle, Wadell (1932) also proposed a practical definition of sphericity based on the 2D projected area of the particle. Wadell (1932) defined sphericity as the ratio of the diameter of a circle having an area equal to the largest projected area of the particle to the diameter of the smallest circle circumscribed to the particle's projected area.

To facilitate the determination of particle roundness and sphericity, Krumbein and Sloss (1951) provided a chart with reference images of particles that could be used for comparison (see Figure 4.6). The sphericity in the reference chart of Krumbein and Sloss (1951) is defined as the length-to-width ratio of the particle.
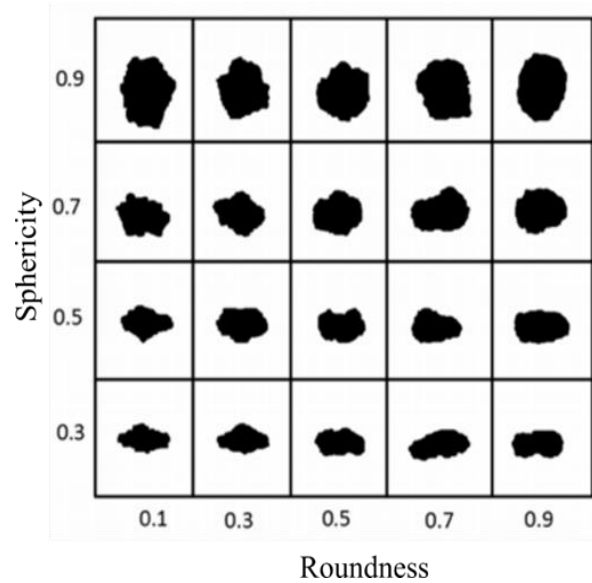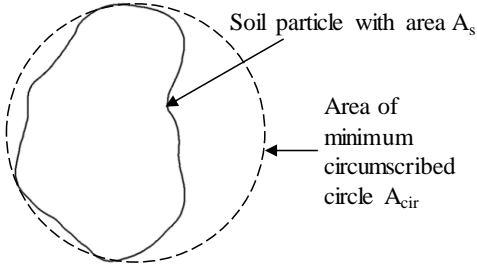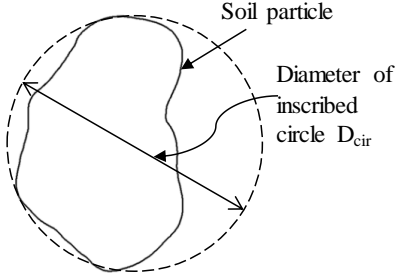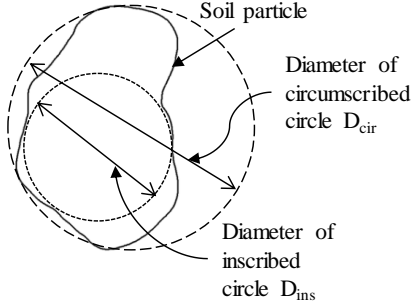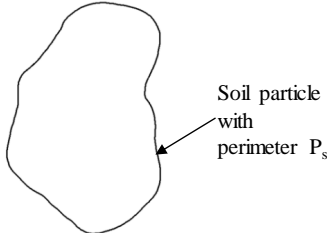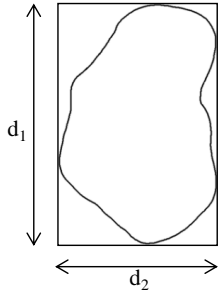
Figure 4.6 Roundness and sphericity chart (after Krumbein and Sloss, 1951)

Advances in optical image processing technologies has led to measurement of sphericity based on different parameters of a particle by different researchers. Mitchell and Soga (2005) and Zheng and Hryciw (2015) reviewed five of the most commonly used definitions of sphericity; these are summarized in Table 4.2.

Table 4.2 Commonly used sphericity equations

Sphericity name	Equation	Equation No.	Diagram
Area sphericity S_A	$S_A = \dfrac{A_s}{A_{cir}}$	(4.5)	Soil particle with area A_s; Area of minimum circumscribed circle A_{cir}
Diameter sphericity S_D	$S_D = \dfrac{D_c}{D_{cir}}$	(4.6)	Soil particle; Diameter of inscribed circle D_{cir}
Circle ratio sphericity S_C	$S_C = \dfrac{D_{ins}}{D_{cir}}$	(4.7)	Soil particle; Diameter of circumscribed circle D_{cir}; Diameter of inscribed circle D_{ins}
Perimeter sphericity S_P	$S_P = \dfrac{P_C}{P_S} = \dfrac{2\sqrt{\pi A_s}}{P_S}$	(4.8)	Soil particle with perimeter P_s
Width-to-length ratio sphericity S_{WL}	$S_{WL} = \dfrac{d_2}{d_1}$	(4.9)	d_1, d_2

In the sphericity definitions provided in Table 4.2, A_s is the projected area of a soil particle, A_{cir} is the area of the minimum circle circumscribing the particle, D_c is the diameter of a circle

having the same projected area as the particle, D_{cir} is the diameter of the minimum circumscribing circle, D_{ins} is the diameter of the largest inscribing circle, P_c is the perimeter of a circle having the same projected area as the particle, P_s is the perimeter of the particle, and d_1 and d_2 are the length and width of a particle, which are defined as the largest and smallest dimensions of a rectangle enclosing the particle; the selected rectangle is the rectangle with the largest possible dimension circumscribing the particle (Zheng and Hryciw 2015).

Aspect ratio and elongation ratio

The aspect ratio of a particle is a measure of how elongated the particle is. The aspect ratio can be quantified using the maximum and minimum Feret's diameter $D_{maxFeret}$ and $D_{min\ Feret}$. First, the orientation of the longest axis of the particle is determined. Two lines tangent to the particle are drawn with the same orientation as the longest particle axis. $D_{min\ Feret}$ is the perpendicular distance between these two parallel lines. Then, two parallel lines are drawn tangent to the two points farthest apart of the projected area of the particle. $D_{maxFeret}$ is the distance between these two parallel lines, as shown in Figure 4.7. The aspect ratio AR_{Feret} is calculated as the ratio of the $D_{min\ Feret}$ to the $D_{max\ Feret}$ of a particle (Altuhafi et al. 2013):

$$AR_{Feret} = \frac{D_{max\ Feret}}{D_{min\ Feret}} \tag{4.10}$$
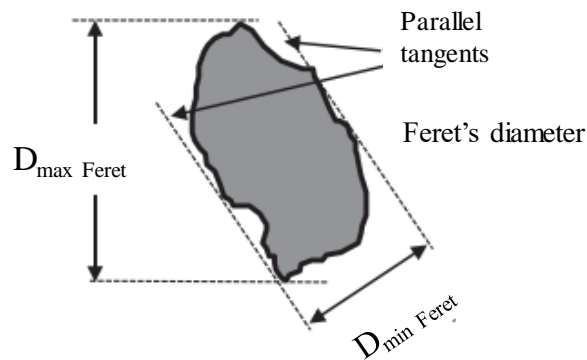
Figure 4.7 Schematic of Feret's diameter (Altuhafi et al. 2013)

According to Ferreira & Rasband (2012), the Aspect Ratio AR_{axis} is defined as the ratio of the major axis to the minor axis of the ellipse best fitted to the projected area of the particle:

$$AR_{axis} = \frac{L_{major}}{L_{minor}} \qquad (4.11)$$

where L_{major} and L_{minor} are the length of the major and minor axes of the best fitting ellipse to the particle area, as shown in Figure 4.5.

The reciprocal of the width-to-length ratio sphericity, as defined in Equation (4.9), is referred to as the elongation ratio (Zheng and Hryciw 2015):

$$ER_{wl} = \frac{1}{S_{WL}} = \frac{d_1}{d_2} \qquad (4.12)$$

where S_{WL} is the width-to-length ratio sphericity, and d_1 and d_2 are the length and width of the particle.

4.3.2   Procedure for particle morphology analyses

In this research, the particle morphology image analyses were carried out using computer software. Two methods were followed to analyze the images of the particles and to obtain the morphology parameters: (1) the digital image processing program called ImageJ, developed by National Institute of Health (NIH) (Ferreira and Rasband 2012), and (2) a MATLAB-based image analysis algorithm developed by Zheng and Hryciw (2015). First, each test material was sieved through the standard sieves and the particles retained in each sieve were collected in plastic bags, as shown in Figure 4.8. Then, images were taken of twenty-five randomly selected particles that were placed in an orderly fashion on top of a glass slide, as shown in Figure 4.10. The images of the particles retained on sieves #8, #16, #30 and #60 were used to carry out the morphology analyses for the No. 4 and No. 24 tests materials, while, for the No. 5, No. 8 and No. 43 aggregates, particles retained on sieve sizes of 25 mm, 19 mm, 12.5 mm, 9.5 mm and 4.75 mm were used instead.

Figure 4.8 Particles collected in plastic bags after sieving

High-resolution images of the particles were obtained using an 8.0-megapixel digital camera. In order to get high-resolution images of the particles with sizes smaller than 4.75 mm, the camera was attached to a microscope. The complete setup of the equipment used to take the images of the particles for morphology analyses consists of: 1) a microscope, 2) an 8.0 megapixel digital camera, 3) a light source, 4) a sample holder, 5) a computer with the AmScope software. Figure 4.9 shows the setup used for obtaining the digital images of the particles. The AmScope software, which controlled the digital camera, was used to visualize the images of the particles in the computer screen and to capture the images. A reference scale was placed next to the glass slide to be able to convert the particle image dimensions to the actual particle dimensions. Figure 4.11 shows images of some particles obtained using the microscope and the 8.0-megapixel digital camera. The morphology parameters for all the particles were obtained from the digital images using both the ImageJ software and the MATLAB code. The average of the morphology parameters was calculated for each specific size range considered for the test materials.
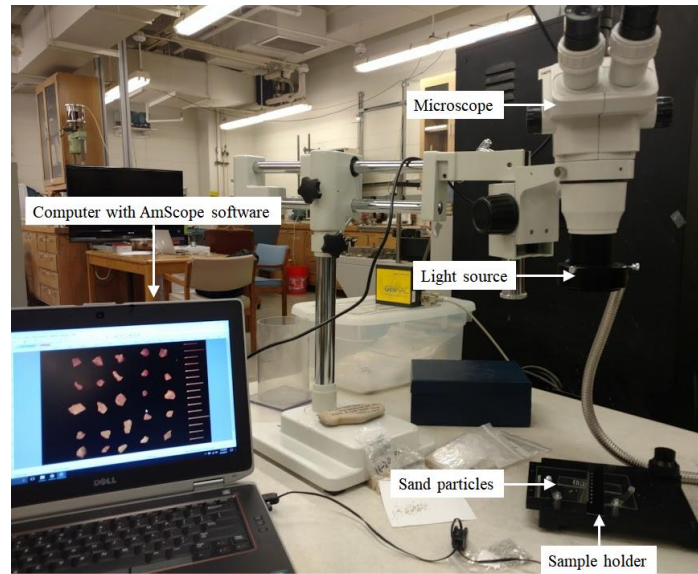
Figure 4.9 Experimental setup to obtain images of the particles
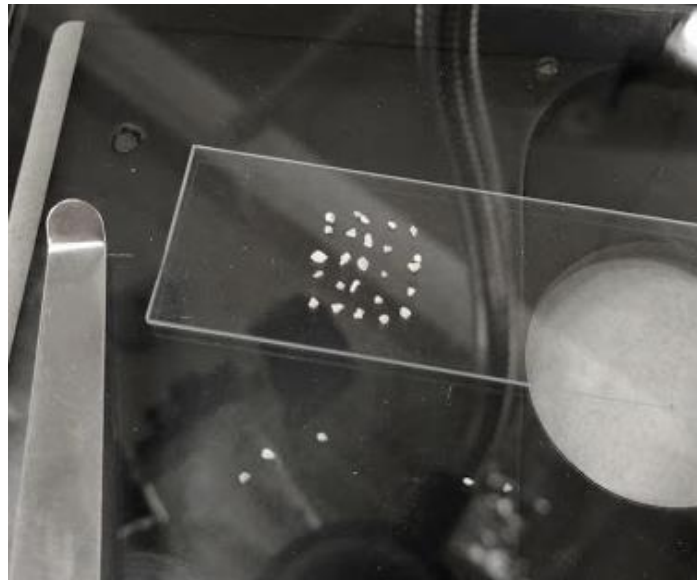
Figure 4.10 Arrangement of particles on a glass slide to capture images with the microscope and the 8.0-megapixel camera

<div align="center">(a)   (b)</div>
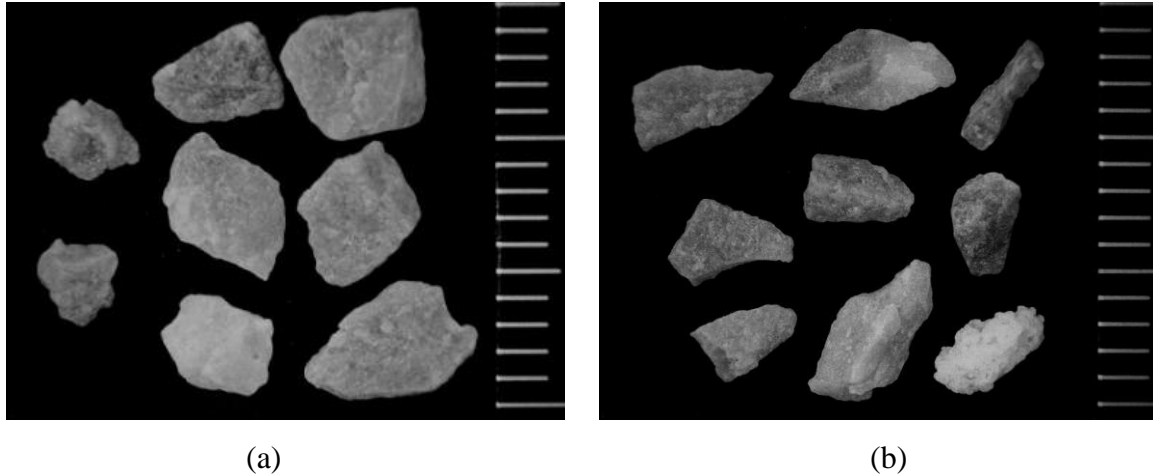
Figure 4.11 Images captured under the microscope using the 8.0 megapixel camera for the No. 24 stone sand with reference scale (the distance between each horizontal line is 1 mm) (a) particles passing the 4.75 mm sieve and retained in the 2.36 mm sieve (b) particles passing the 2.36 mm sieve and retained in the 1.18 mm sieve

4.3.3 Results of morphology analyses

As described previously, the morphology parameters of the particles of the test materials were determined using the ImageJ software and MATLAB code. Different definitions of the morphology parameters are used in these two image analyses software. The results obtained from both the methods are presented herein for comparison purposes.

The ImageJ software was used to analyze high-resolution images of the particles to determine length, width, projected area, perimeter, major and minor axis of the best fitting ellipse, and the Feret's diameters of the particles. These parameters were then used to calculate the morphology parameters roundness, sphericity and aspect ratio. Roundness was calculated using Equation (4.4), which is defined based on the projected area of a particle and the area of a circle whose diameter is equal to the major axis of the ellipse best fitted to the particle area. Sphericity was calculated using Equation (4.8), which is based on the projected perimeter of a particle and the perimeter of a circle with area equal to that of the particle. The aspect ratio was calculated using the ImageJ software; the aspect ratio is defined as the ratio of the major axis to the minor axis of the particle's best fitting ellipse (see Equation (4.11)). The elongation ratio, which is another parameter used to describe how elongated a particle is, can be calculated using Equation (4.10) and (4.11) since the ImageJ software gives as an output the length and width of the smallest possible rectangle enclosing a particle area as well as the Feret's diameters. In addition to

roundness, sphericity and aspect ratio, the ImageJ software provides as an output the circularity of a particle. Circularity C is defined as the square of the sphericity parameter (see Equation (4.9)) defined based on the projected area and perimeter of a particle. Results of the morphology analyses done using the ImageJ software for the test materials are shown in Figure 4.12 to Figure 4.19
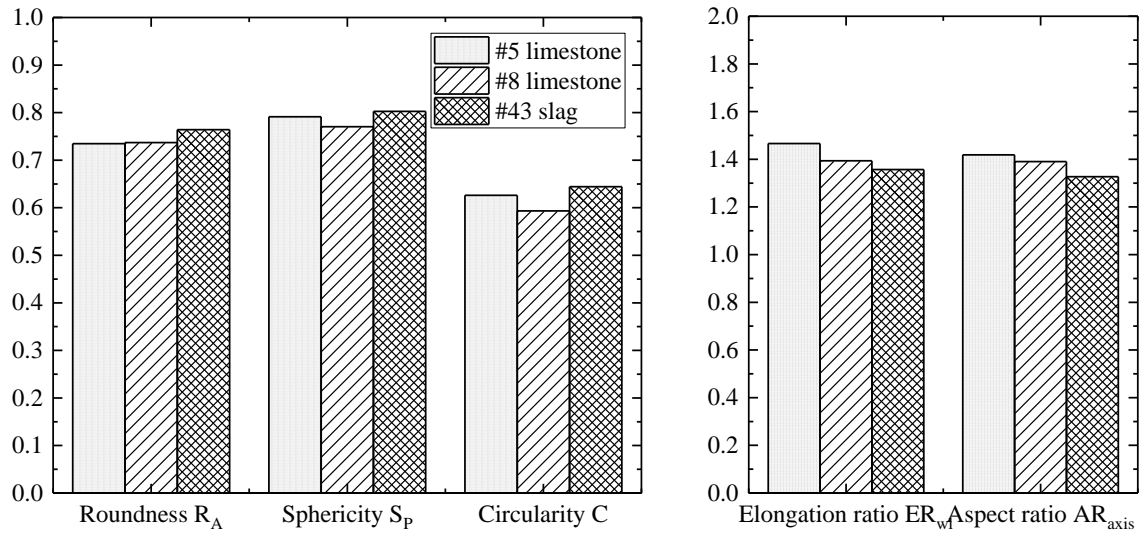
Figure 4.12 Results of morphology analyses of test aggregates using the ImageJ software for particles passing the 25 mm sieve and retained in the 19 mm sieve
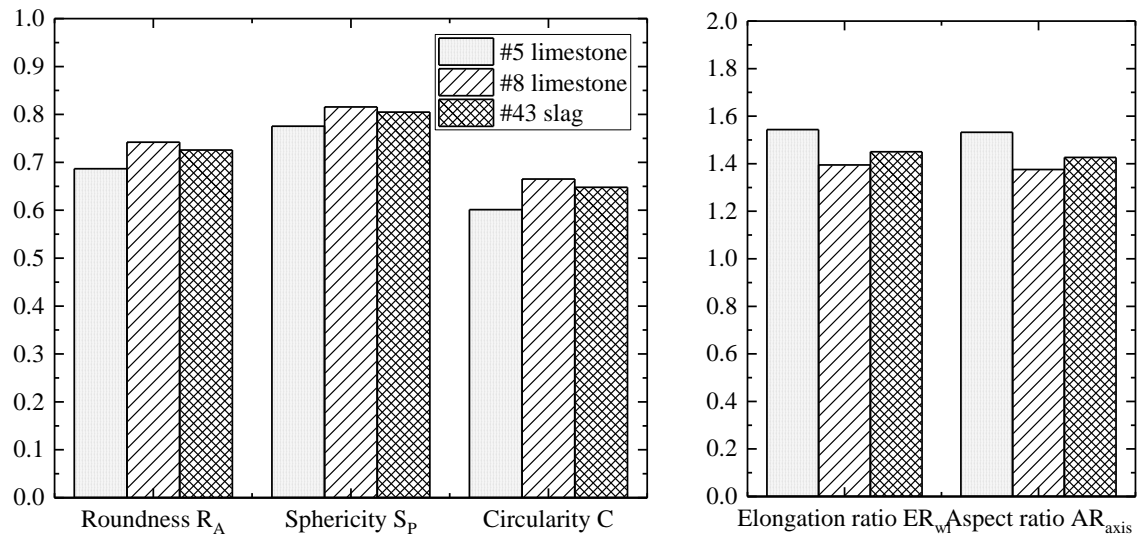
Figure 4.13 Results of morphology analyses of test aggregates using the ImageJ software for particles passing the 19 mm sieve and retained in the 12.5 mm sieve
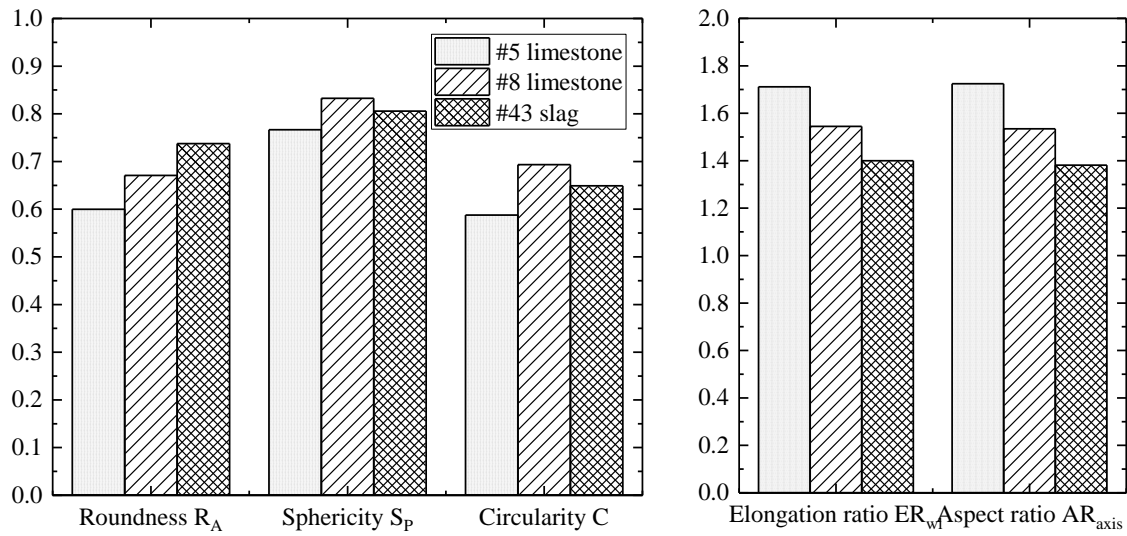
Figure 4.14 Results of morphology analyses of test aggregates using the ImageJ software for particles passing the 12.5 mm sieve and retained in the 9.5 mm sieve
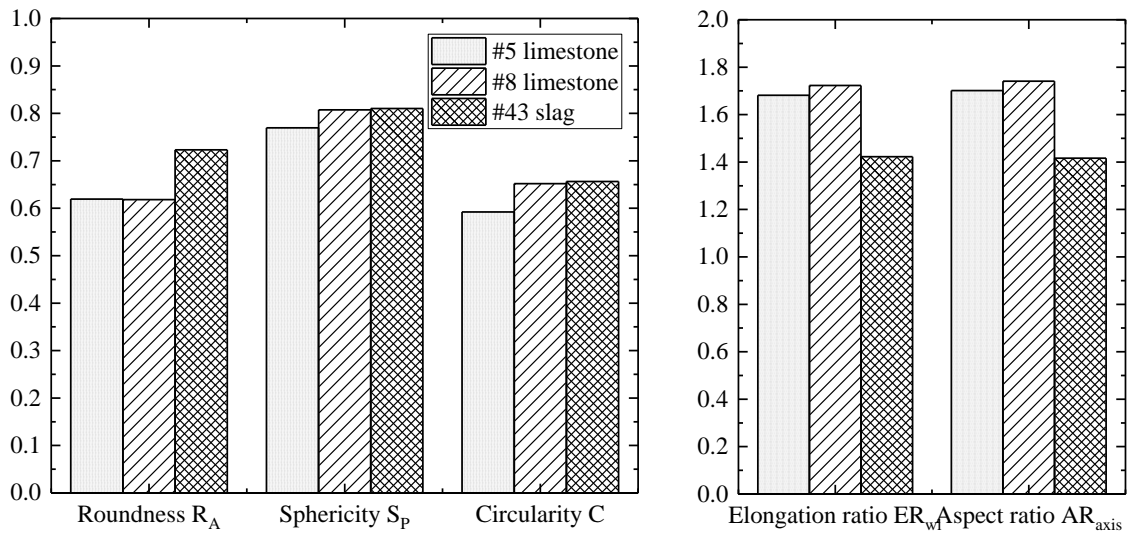
Figure 4.15 Results of morphology analyses of test aggregates using the ImageJ software for particles passing the 9.5 mm sieve and retained in the 4.75 mm sieve
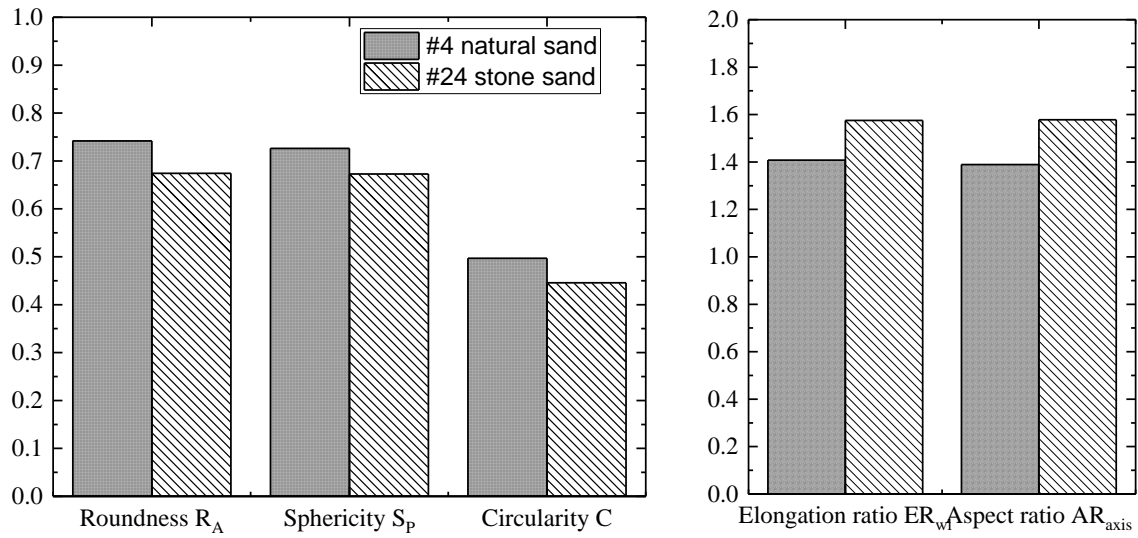
Figure 4.16 Results of morphology analyses of test sands using the ImageJ software for particles passing the 4.75 mm sieve and retained in the 2.36 mm sieve
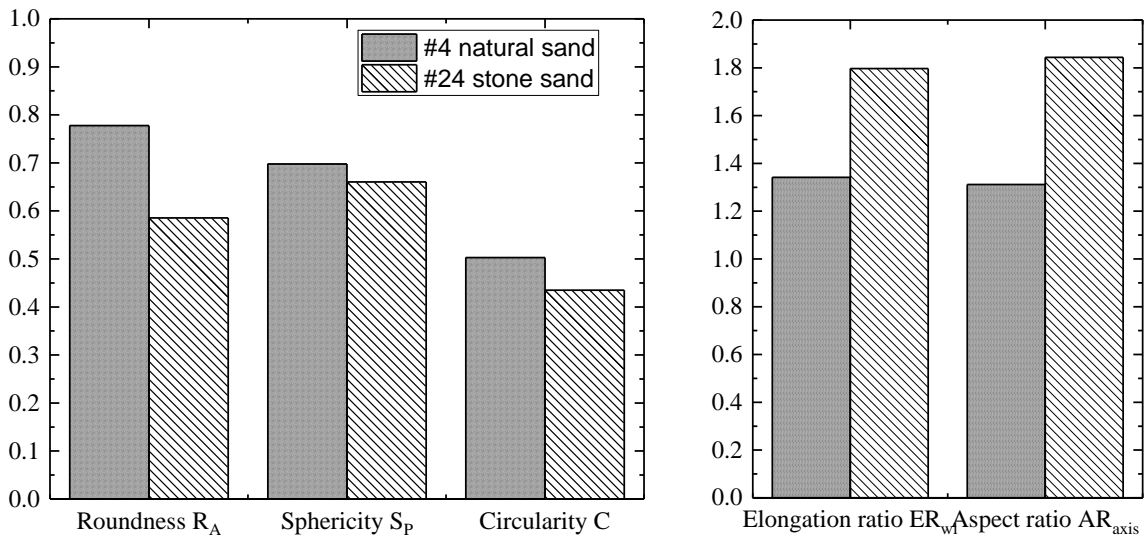
Figure 4.17 Results of morphology analyses of test sands using the ImageJ software for particles passing the 2.36 mm sieve and retained in the 1.18 mm sieve
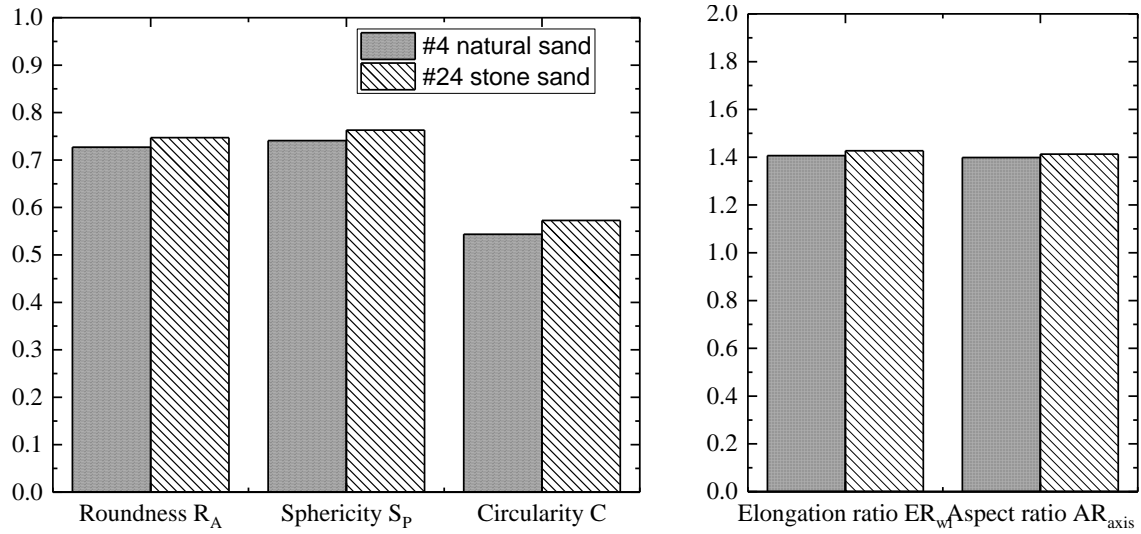
Figure 4.18 Results of morphology analyses of test sands using the ImageJ software for particles passing the 1.18 mm sieve and retained in the 0.6 mm sieve
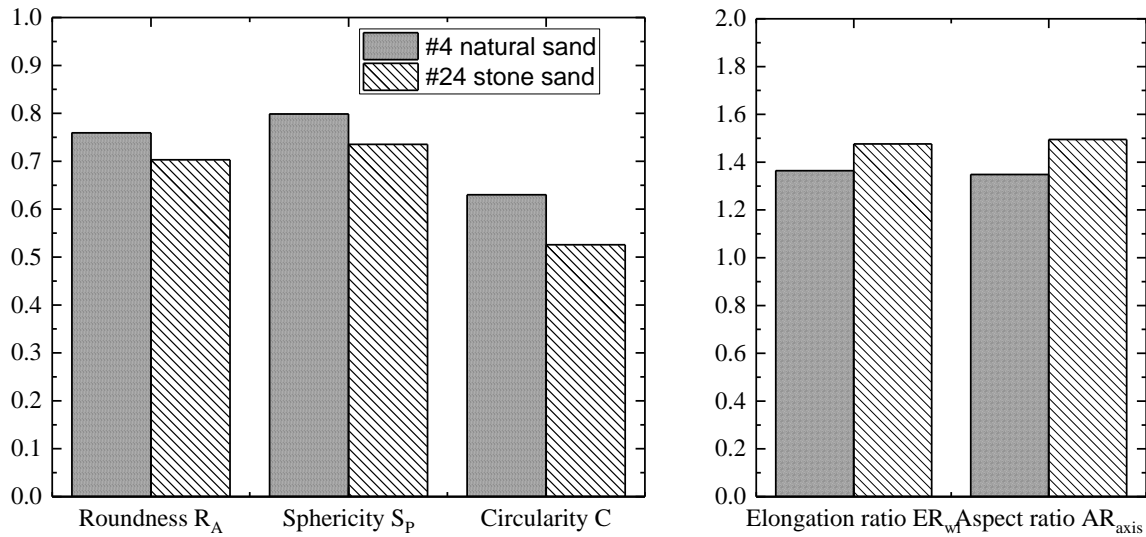
Figure 4.19 Results of morphology analyses of test sands using the ImageJ software for particles passing the 0.6 mm sieve and retained in the 0.25 mm sieve

The morphology parameters of the test materials were obtained using the MATLAB code developed by Zheng and Hryciw (2015). The MATLAB code provides values of the roundness and sphericity parameters as defined in Equations (4.3), (4.5), (4.6), (4.7), (4.8) and (4.9). The results of the morphology analyses using the MATLAB code developed by Zheng and Hryciw (2015) are shown in Figure 4.20 to Figure 4.23. Note that in these figures, R_R is the roundness

defined by Wadell (1932), S_A is the area sphericity, S_D is the diameter sphericity, S_C is the circle ratio sphericity, S_P is the perimeter sphericity and S_{WL} is the width-to-length ratio sphericity.

(a)   (b)
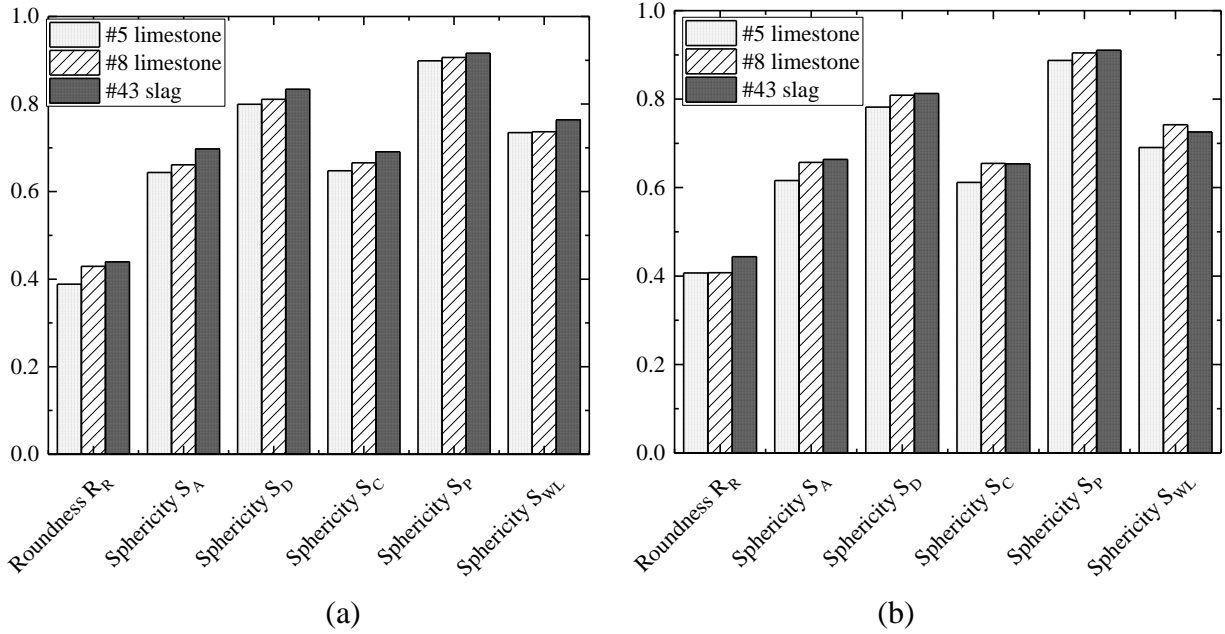
Figure 4.20 Results of morphology analyses of test aggregates using the MATLAB code for particles (a) passing the 25 mm sieve and retained in the 19 mm sieve and (b) passing the 19 mm sieve and retained in the 12.5 mm sieve
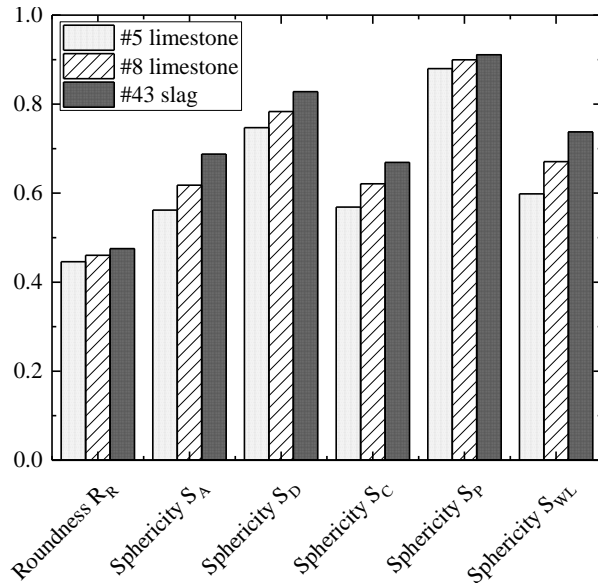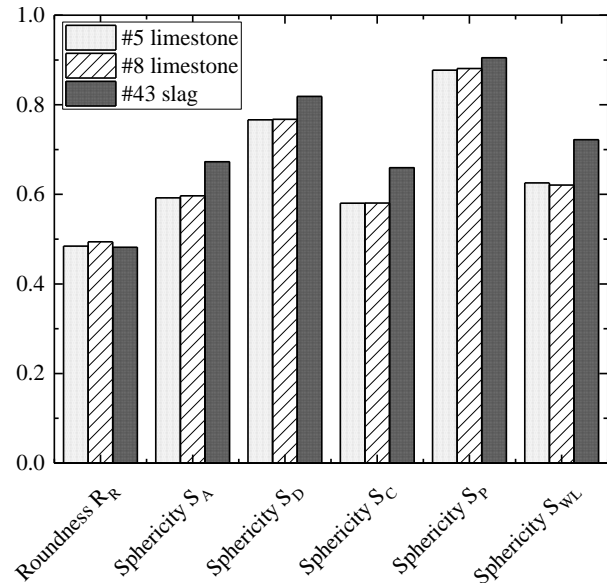
(a)   (b)

Figure 4.21 Results of morphology analyses of test aggregates using the MATLAB code for particles (a) passing the 12.5 mm sieve and retained in the 9.5 mm sieve and (b) passing the 9.5 mm sieve and retained in the 4.75 mm sieve
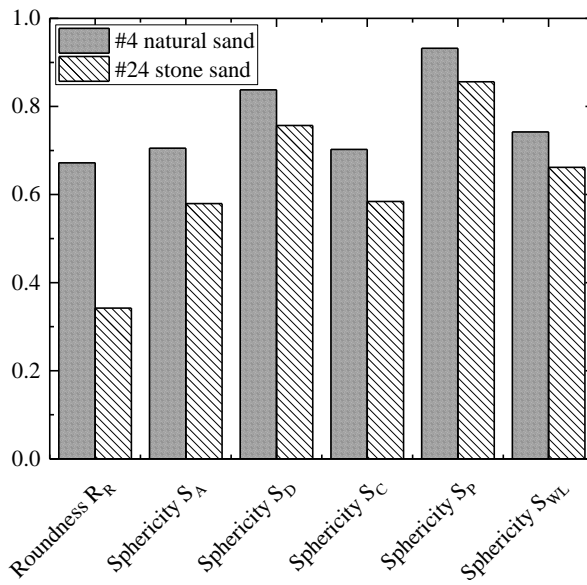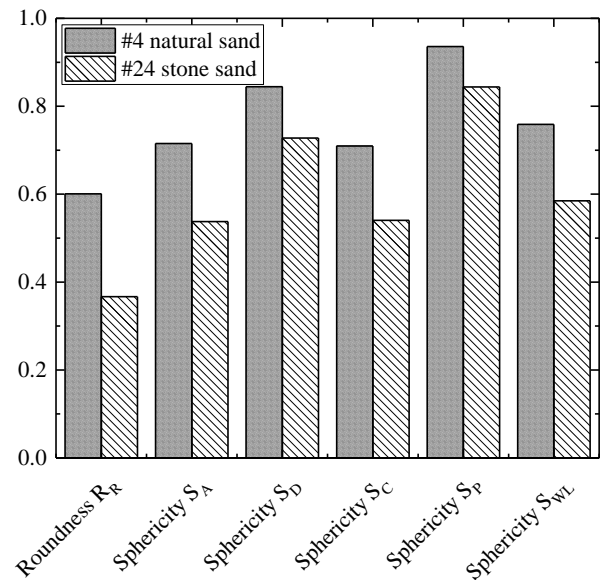
(a)   (b)

Figure 4.22 Results of morphology analyses of test sands using the MATLAB code for particles (a) passing the 4.75 mm sieve and retained in the 2.36 mm sieve and (b) passing the 2.36 mm sieve and retained in the 1.18 mm sieve
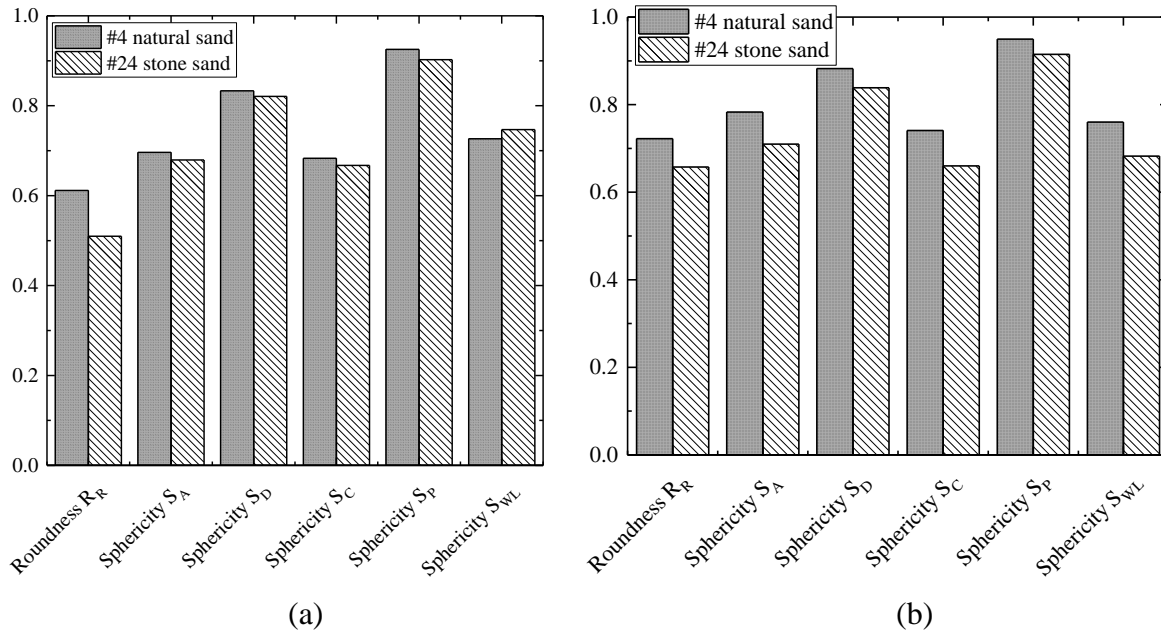
Figure 4.23 Results of morphology analyses of test sands using the MATLAB code for particles (a) passing the 1.18 mm sieve and retained in the 0.6 mm sieve and (b) passing the 0.6 mm sieve and retained in the 0.25 mm sieve

The test materials were also characterized based on the morphology parameters of the dominant particle size of each material. The dominant particle size was selected as the size range of the particles with maximum percentage by mass retained in a sieve. Table 4.3 shows the dominant particle size ranges of the test materials.

Table 4.3 Dominant particle size ranges of the test materials

Test materials	Dominant particle-size range
No. 24 stone sand	Passing 2.36 mm sieve and retained in 1.18 mm sieve
No. 4 natural sand	Passing 0.6 mm sieve and retained in 0.25 mm sieve
No. 5 limestone aggregate	Passing 19 mm sieve and retained in 12.5 mm sieve
No. 8 limestone aggregate	Passing 19 mm sieve and retained in 12.5 mm sieve
No. 43 slag aggregate	Passing 25 mm sieve and retained in 19 mm sieve

The morphology test results obtained from the two different image analyses software were compared for the dominant particle size range of the test materials. The roundness, sphericity and elongation ratio are the three most widely used morphology parameters. Hence, these three parameters were compared for the dominant particle sizes of the test materials. It should be noted that, out of the five different sphericity values obtained from the MATLAB code developed by

Zheng and Hryciw (2015), the sphericity parameter calculated from the perimeter of the particle (see Equation (4.9)) was used for comparison with the ImageJ results since ImageJ provides only the sphericity parameter based on this definition. The roundness parameter is calculated using two different equations in the ImageJ software (Equation (4.4)) and in the MATLAB code (Equation (4.3)). The elongation ratio in the MATLAB code by Zheng and Hryciw (2015) is obtained from the inverse of the length-to-width sphericity (see Equation (4.12)) of the particle. The comparison of the roundness, sphericity and elongation ratios from the analyses of the images of the particles by ImageJ software and the MATLAB code developed by Zheng and Hryciw (2015) are shown in, Figure 4.25, Figure 4.26 and Figure 4.26, respectively.
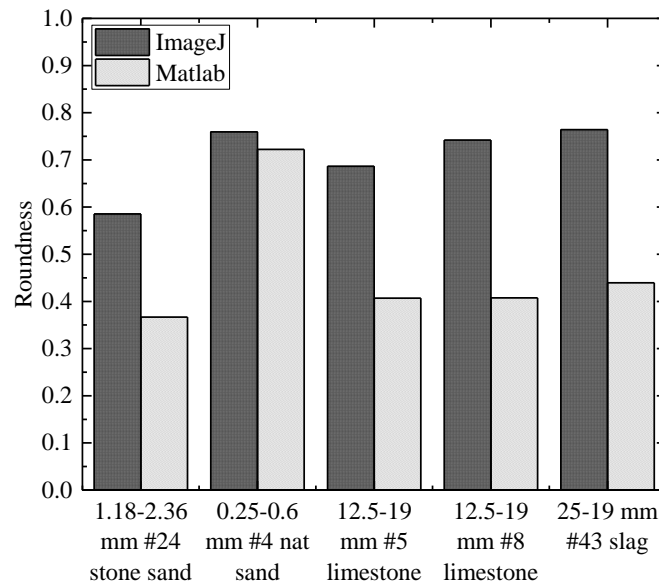
Figure 4.24 Comparison of roundness values determined by ImageJ and MATLAB code for the dominant particle sizes of the test materials (roundness calculated using Equation (4.3) in MATLAB code and Equation (4.4) in imageJ)
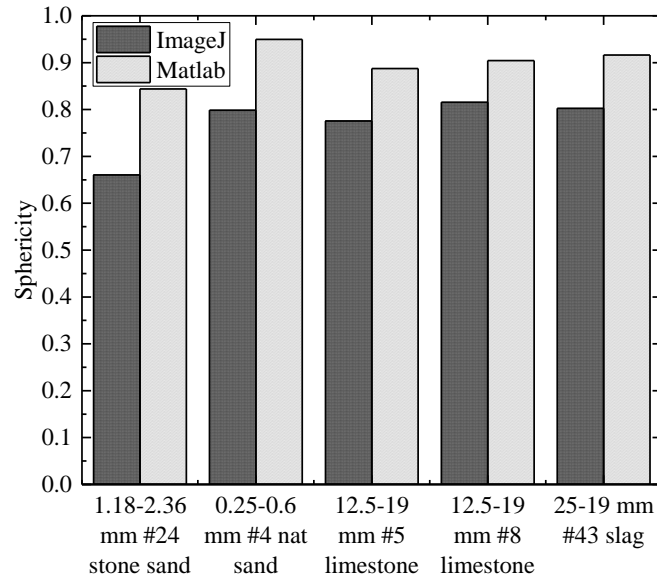
Figure 4.25 Comparison of sphericity values determined by ImageJ and MATLAB code for the dominant particle sizes of the test materials (sphericity calculated using Equation (4.9))
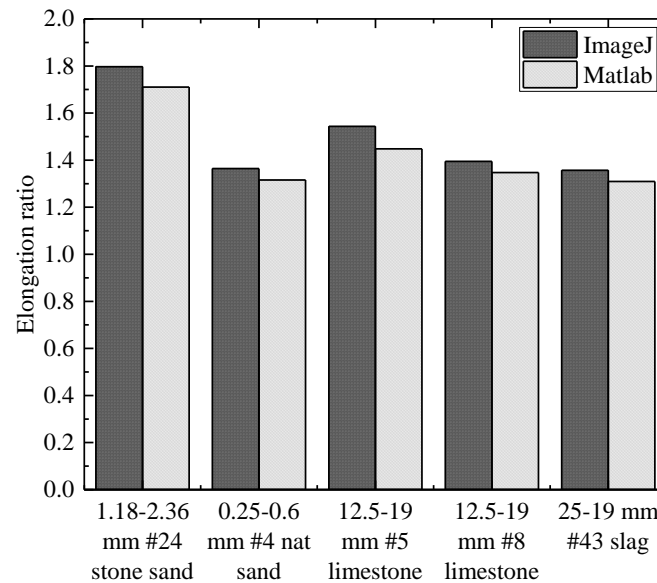
Figure 4.26 Comparison of elongation ratio values determined by ImageJ and MATLAB code for the dominant particle sizes of the test materials (elongation ratio calculated using Equation (4.10) in ImageJ and Equation (4.12) in MATLAB code)

From the comparison of the three morphology parameters obtained from the two different image analyses (see Figure 4.24, Figure 4.25 and Figure 4.26), it is observed that there are some differences in the values of the morphology parameters, especially for roundness and sphericity. Two different equations are used to calculate the roundness in the ImageJ software and the

MATLAB code. The MATLAB code uses the roundness definition introduced by Wadell (1932) (see Equation (4.3)); it is widely used by different researchers according to Zheng and Hryciw (2015). For this reason, the roundness values obtained using Equation (4.3) were used to characterize the test materials. It is observed that the roundness values of the dominant particle sizes for all the test materials varies between 0.37 and 0.44, except for No. 4 natural sand, for which the roundness value is 0.72. Figure 4.24 shows that the perimeter sphericity values obtained from the ImageJ software were always smaller than the values measured by the MATLAB code, even though both used the same equation (Equation (4.9)) to calculate the sphericity values.

According to Zheng and Hryciw (2015), the width-to-length ratio sphericity, as defined by Equation (4.9), is the most suitable sphericity definition among all the other definitions of sphericity used to characterize the shape of a particle based on sphericity. This width-to length-ratio sphericity is widely used by researchers, and most notably by the chart prepared by Krumbein and Sloss (1951), as presented in Figure 4.6. Out of all the sphericity definitions, the width-to-length ratio sphericity is simple, easy to determine from images, independent of roundness and has the largest range of values (between 0 to 1) compared with the other sphericity definitions (Zheng and Hryciw 2015). So, the width-to-length ratio sphericity was used to characterize the particles in this research. The MATLAB code provides the width-to-length ratio sphericity values as an output from the analyses of the images (this is not calculated by the ImageJ software; it only calculates the perimeter sphericity). Table 4.4 provides a summary of the average morphology parameters of the dominant particle size of the test materials. The tests aggregates have similar morphology parameters whereas the test sands are slightly different from each other. The No. 4 natural sand has higher roundness and sphericity compared to that of No. 24 stone sand. The higher the roundness value of a particle, the more rounded its corners are. Here, the higher the sphericity value, the more similar the dimensions of the particle with respect to length and width are.

Table 4.4 Summary of the morphological parameters of the test materials for the dominant particle sizes

Test materials	Dominant particle size range (mm)	Roundness R_R	Sphericity S_{WL}	Elongation ratio ER_{wl}
No. 24 stone sand	1.18 - 2.36	0.37	0.58	1.72
No. 4 natural sand	0.25 - 0.6	0.72	0.76	1.32
No. 5 limestone	12.5 - 19	0.41	0.69	1.45
No. 8 limestone	12.5 - 19	0.41	0.74	1.35
No. 43 slag	19 - 25	0.44	0.76	1.32

Note: Roundness and sphericity parameters were calculated with the MATLAB code developed by Zheng and Hryciw (2015)

Roundness is defined as the ratio of the average radius of curvature of the corners of the particle to the radius of the maximum circle that can be inscribed in the particle area (Wadell 1932)

Sphericity is defined as the width-to-length ratio of a particle

Elongation ratio is the inverse of the width-to-length ratio sphericity (Mitchell and Soga 2005)

5. SMALL-SCALE LABORATORY COMPACTION TEST RESULTS

5.1 Minimum Density

The minimum density of the test materials were determined following the ASTM D4254 (2016) standard. The objective of this test was to determine the maximum void ratio of the test materials. The materials were first dried in the oven and placed inside a mold following the standard procedure. The size of the mold used for this test depends on the size of the particles. For testing the coarse aggregates (No. 5, No. 8 and No. 43), the volume of the mold was 0.5 ft^3, while for the sands (No.4 and No.24), the volume of the mold was 0.1 ft^3. A metal scoop was used to fill the mold with coarse aggregates, according to the ASTM D4254 (2016) standard procedure. The aggregates were placed into the mold as loosely as possible by dropping them from the scoop positioned close to the sample surface inside the mold. To fill the mold with sand, the tube method was followed, in accordance with the ASTM D4254 (2016) standard. The tube was placed inside the mold and filled with sand. Then, the tube was raised quickly allowing the sand to fill up the mold.

Since the aggregates were placed inside the mold in as loose as possible state, a minimum amount of material was needed to fill up the volume of the standard mold. Hence, the dry density obtained under these conditions corresponded to the minimum possible density and maximum possible void ratio that the aggregates could achieve. The minimum unit weight $\gamma_{d,min}$ (kN/m^3) was calculated as the ratio of the weight of aggregate W_s (kN) to the volume V_m of the mold (m^3). The minimum dry unit weight γ_{dmin} is given by:

$$\gamma_{d,\min} = \frac{W_s}{V_m} \tag{5.1}$$

The maximum void ratio e_{max} is given by:

$$e_{\max} = \frac{G_s \gamma_w}{\gamma_{d,\min}} - 1 \tag{5.2}$$

where $\gamma_{d,,min}$ is the minimum unit weight of the aggregate (kN/m^3), G_s is the specific gravity and γ_w is the unit weight of water (kN/m^3). Table 5.1 provides the minimum density test results for the test materials.

Table 5.1 Minimum density test results

Test materials	Minimum unit weight (kN/m³)	Maximum void ratio
No. 24 stone sand	15.11	0.72
No. 4 natural sand	16.88	0.54
No. 5 limestone	13.61	0.91
No. 8 limestone	13.60	0.90
No. 43 slag	17.1	0.52

5.2   Vibratory Table Compaction Test Results

Accelerometer sensors were attached to the vibratory table and the mold. The vibration of the table was controlled by a voltage regulator. The analysis of the accelerometer sensor data shows that the frequency of vibration remained fixed to 60 Hz, but that the amplitude of vibration changed depending on the voltage regulator settings. It further shows that the amplitude of vibration of the table and the attached mold depend on the weight of the mold with the sample and the applied surcharge load on top of it (the surcharge stresses are the same for the two mold sizes but the loads are different). The vibration amplitude was measured for two different mold sizes (the mold size used depended on the particle sizes of the test materials) for various voltage regulator settings. Figure 5.1 shows the amplitude of vibration for different voltage regulator settings as measured by the accelerometers attached to the table and molds. It can be observed from these results that the amplitude of vibration of the table and the attached mold increase linearly with the increase in voltage setting. However, the amplitude of vibration of the molds and the table are slightly different from each other. This is due to the connection joints between the molds and the table. But it is the vibration of the mold that produces the rearrangement of the particles and compaction of the materials inside it. For this reason, for all test results where vibration amplitude is discussed in the context of the vibratory table test results, it is the vibration of the mold that is considered.
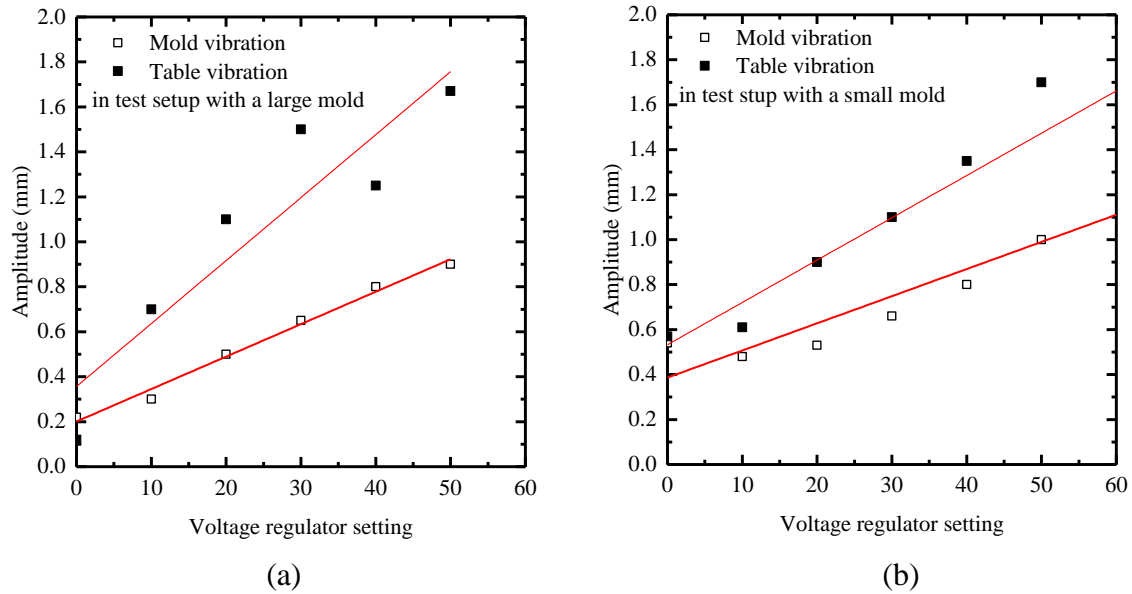
Figure 5.1 Amplitude of vibration of vibratory table and molds for different voltage regulator settings of the vibratory table (a) large mold with a surcharge load of 855 N and (b) small mold with a surcharge load of 255 N

Figure 5.2 shows the compacted dry density versus amplitude of vibration for different test materials. The frequency of vibration during the tests remained constant at 60 Hz and the duration of vibration was maintained at 8 minutes, as specified in the ASTM D4253 (2016) standard. In addition, a constant surcharge stress of 14 kPa was applied on top of the test materials, following the ASTM D4253 (2016) standard. As can be seen in Figure 5.2, the compacted dry density increases with increasing amplitude of vibration for all the test materials. However, the increase in density with the increase in amplitude of vibration is more pronounced for the coarse aggregates than for the sands. For example, with the increase in amplitude of vibration from 0.2 mm to 0.9 mm during compaction using the vibratory table, the density of No. 8 aggregate increases by 14%, whereas it increases by only 1.4% for No. 4 natural sand.
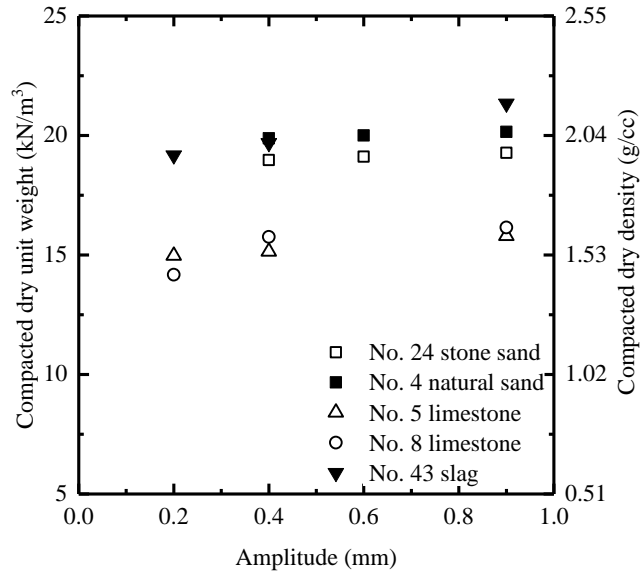
Figure 5.2 Effect of amplitude of vibration on the compaction dry densities of the test materials from vibratory table test

Figure 5.3 and Figure 5.4 show the effect of duration of vibration on the compaction density during compaction using the vibratory table at different amplitudes of vibrations for the test materials. The results show that the test materials reach an equilibrium density at 8 minutes of vibration. The grain size distribution curves of the test materials were obtained before and after compaction. Figure 5.5 shows that a small amount of crushing occurred for No. 24 stone sand during vibration at 0.9 mm of amplitude for 16 minutes. No crushing was observed for the other test materials, as seen in Figure 5.6.
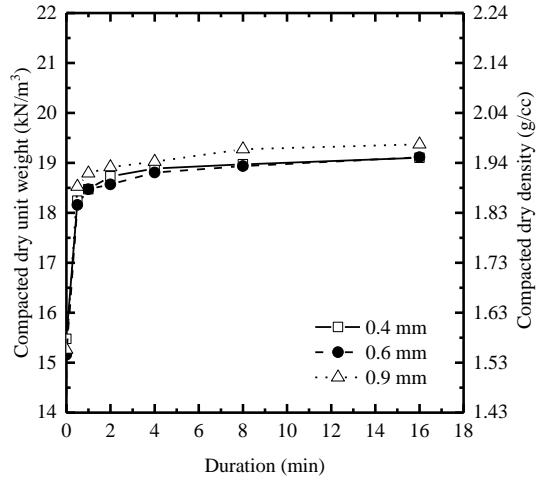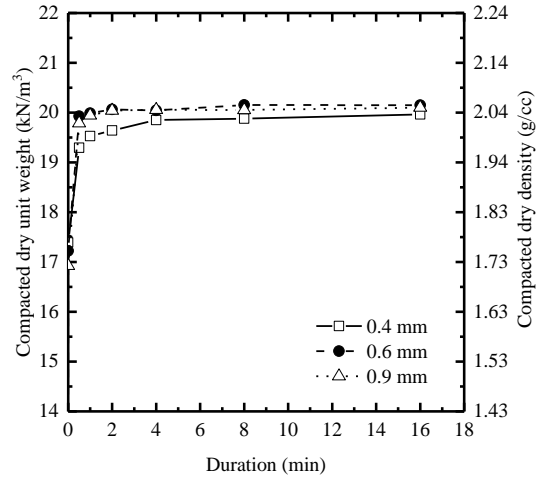
Figure 5.3 Effect of duration of vibration by vibratory table on the compaction density of (a) No. 24 stone sand and (b) No. 4 natural sand
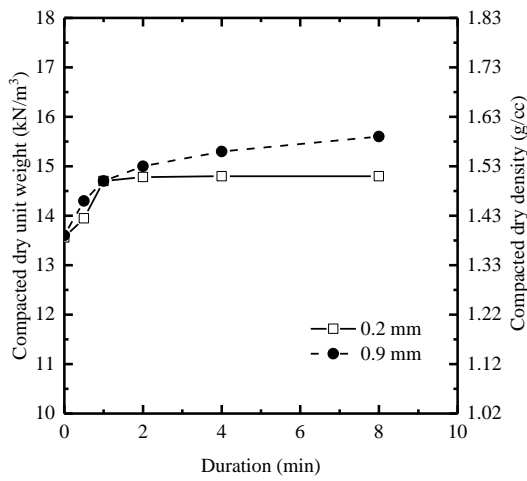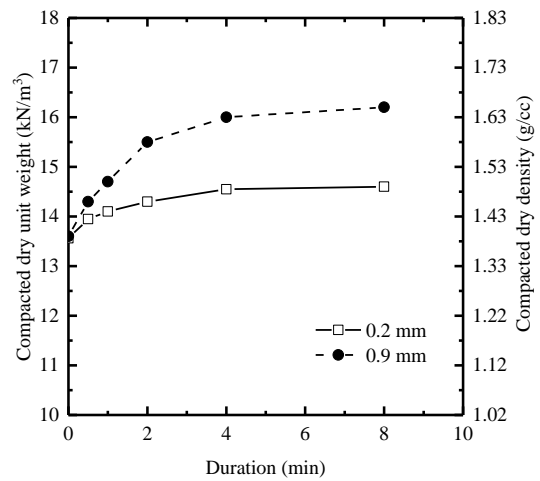
Figure 5.4 Effect of duration of vibration by vibratory table on the compaction density of (a) No. 5 limestone aggregate and (b) No. 8 limestone aggregate
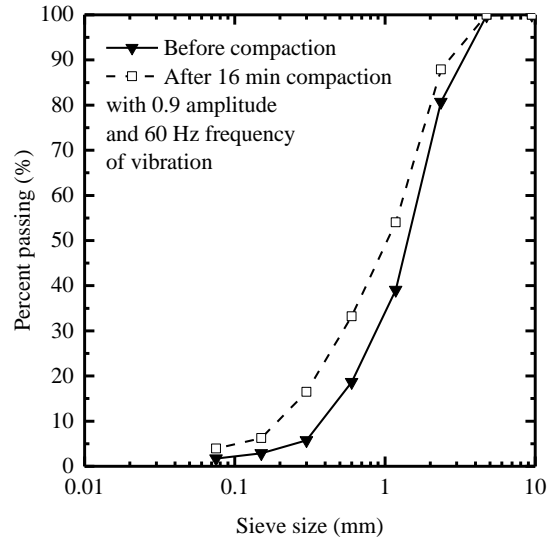
Figure 5.5 Grain size distribution curves for No. 24 stone before and after compaction by vibration at frequency of 60 Hz and amplitude of 0.9 mm using vibratory table
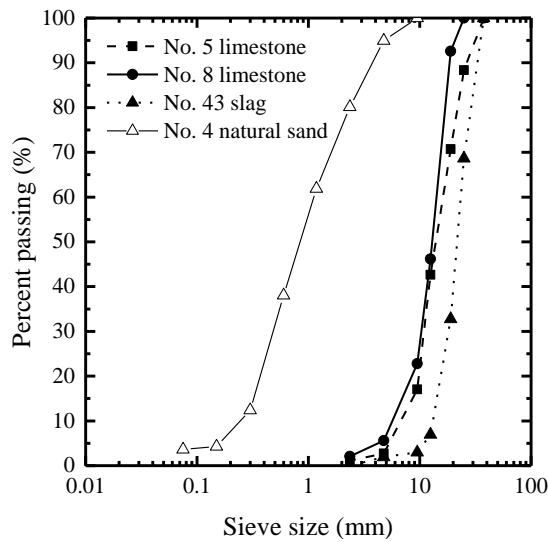
Figure 5.6 Grain size distribution curves for No. 5, No. 8, No 43 aggregates and No. 4 naturals sand before and after compaction by vibration at frequency of 60 Hz and amplitude of 0.9 mm using vibratory table (no changes in grain size distribution before and after compaction for these test materials)

5.3   Vibratory Hammer Compaction Test Results

The vibratory hammer applies vibration on top of the test sample to compact it inside the mold. A constant surcharge stress of 18.5 kPa was applied on the hammer to keep it in position during vibration for 1 min at each hammer position in the layer (there is one hammer position per layer for the small mold and eight hammer positions per layer for the large mold). The tests were

performed according to the ASTM D7382 (2008) standard. An accelerometer sensor was attached to the tamping rod of the vibratory hammer to measure the speed of vibration in terms of the number of hammer blows per second for different hammer settings. Analysis of the vibration data from the accelerometer sensor shows that with an increase in the hammer setting, the number of blows per second increases. However, the amplitude of vibration of the hammer remains constant at 0.5 mm. Figure 5.7 shows that the number of blows by the hammer increases from 25 blows per second to 60 blows per second when the hammer setting is changed from 1 to 9.
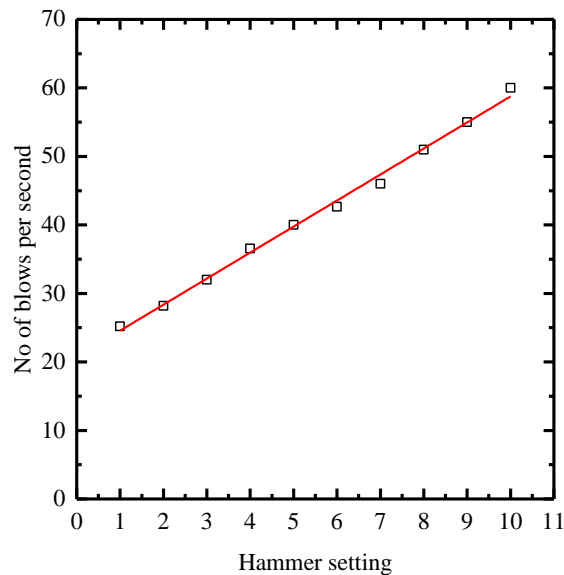
Figure 5.7 Vibration rate for different hammer settings of the vibratory hammer

Figure 5.8 shows the effect of hammer speed on the compaction density for all the test materials, except for No. 43 (slag material). The test results show that with an increase in the hammer blow rate, the compacted dry density increases for all the test materials. The density of the test materials increases by 3-7% for an increase in the hammer speed from 25 blows per second to 60 blows per second during compaction using the vibratory hammer.
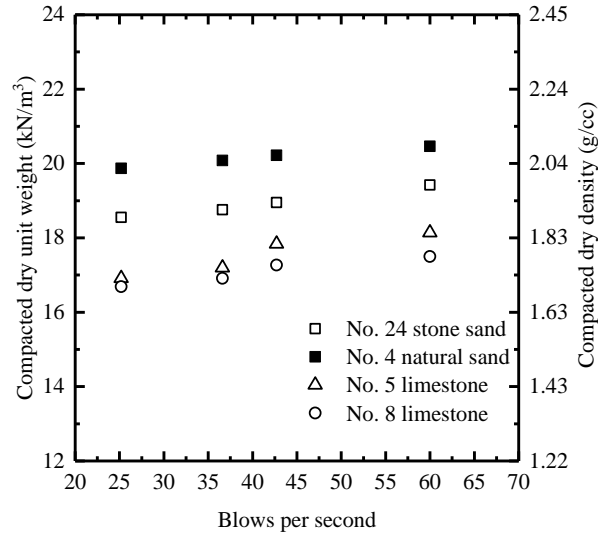
Figure 5.8 Effect of hammer speed on the compacted dry densities of the test materials from the vibratory hammer tests

5.4   Proctor Hammer Compaction Test Results

Proctor hammer compaction tests were carried out for No. 24 stone sand and No. 4 natural sand to determine the effect of water content on the compaction density. Two different methods of Proctor compaction were performed using the standard hammer and the modified hammer, according to the ASTM D698 (2012) and ASTM D1557 (2012) standards, respectively. Water was added to the test materials at various percentages before compaction. The dry density of the compacted materials was determined at the end of the test. Since both of the test materials were classified as poorly-graded sand, they had no affinity for water. Therefore, water started to bleed out of the sample when the water content was greater than 5%. In general, addition of water to the soil lubricates the particles, facilitating particle rearrangement into denser states. However, excess of water in the soil reduces the compacted dry density as the water takes up the void spaces between the particles. For a given compaction effort, either by the standard hammer or the modified hammer, addition of water did not increase the dry density of the test sands, as seen in Figure 5.9. Moreover, crushing of particles was observed for the No. 24 stone sand during compaction using the Proctor hammer for both the standard and modified Proctor methods, as seen in Figure 5.10. Compaction at water contents smaller than about 2% is beneficial for these materials.

73
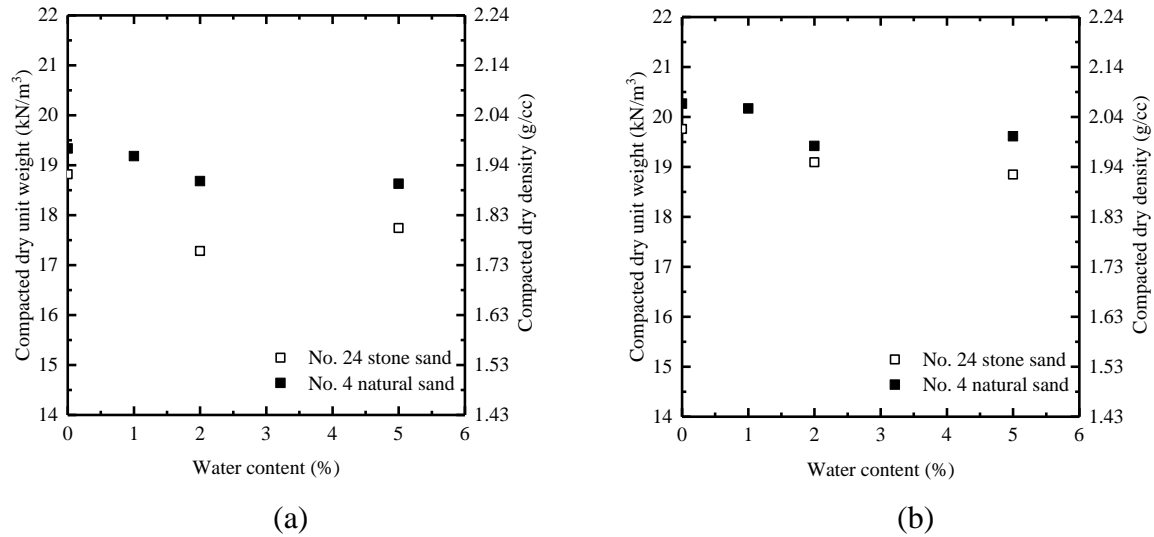
Figure 5.9 Effect of water content on the compaction dry density by (a) standard Proctor and (b) modified Proctor
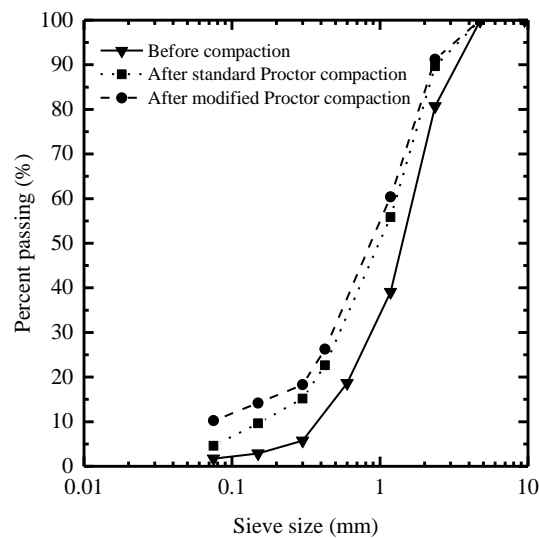
Figure 5.10 Grain size distribution curve for No. 24 stone before compaction and after compaction by Proctor method

5.5   Comparison of the Test Results

Table 5.2 shows the dry unit weights for the test materials after compaction using the vibratory table, vibratory hammer and Proctor hammer. The vibratory table was used to compact the test materials with a vibration amplitude of 0.9 mm and frequency of 60 Hz. The surcharge load, duration of vibration and the size of the molds used for testing were in accordance with the ASTM D4253 (2016) standard. The vibratory hammer was used to compact the test materials with

a vibration amplitude of 0.5 mm and hammer speed of 60 blows per second. The size of the mold, duration of compaction and the surcharge load used for testing were in accordance with the ASTM D7382 (2008) standard. The standard Proctor and modified Proctor tests were performed following the ASTM D698 (2012) and ASTM D1557 (2012) standards, respectively.

Table 5.2 Comparison of the dry unit weights of the test materials according to different compaction test methods

Test materials	Compacted dry unit weight (kN/m^3)			
	Vibratory table[a]	Vibratory hammer[b]	Standard Proctor	Modified Proctor
No. 24 stone sand	19.3	19.4	18.8	19.8
No. 4 natural sand	20.1	20.5	19.5	20.3
No. 5 aggregate	15.8	18.1	-	-
No. 8 aggregate	16.14	17.5	-	-

Note: All of the tests were performed at water content=0%
[a]vibratory table tests were performed with vibration amplitude of 0.9 mm and frequency of 60 Hz
[b]vibratory hammer tests were performed with vibration amplitude of 0.5 mm and hammer speed of 60 blows per second

It should be noted that the sieve analyses of the No. 24 stone sand after compaction by the standard and modified Proctor tests revealed that crushing of particles occurred during compaction. As a result of particle crushing during testing, a new material with different grain size distribution and particle morphology is produced. Based on the density results from the other methods of compaction, it can be observed that the vibratory hammer produces the maximum compaction density. Further analysis of the results shows that the test sands (No.4 and No. 24 sands) have comparable compaction densities when compacted using the vibratory table or vibratory hammer at the maximum amplitude and frequency of vibration available in both equipment, as shown in Figure 5.11. However, the coarse aggregates (No. 5 and No. 8 aggregates) have higher compaction unit weights when compacted using the vibratory hammer than when using the vibratory table at the maximum amplitude and frequency of vibration available in both equipment. For example, the difference between the unit weights of No. 4 natural sand compacted by the vibratory table and vibratory hammer is only 0.3 kN/m^3, whereas this difference for the No. 5 aggregate is 2.33 kN/m^3. The dry unit weight of No. 4 natural sand increases by 28.5% from its minimum unit weight

(determined according to ASTM D4254, 2016) when compacted using the vibratory hammer at maximum speed of vibration, whereas it increases by 27.5% from its minimum unit weight (determined according to ASTM D4254, 2016) when compacted using the vibratory table at maximum amplitude of vibration. For No. 5 aggregates, the dry unit weight increased by 33.3% from its minimum unit weight (determined according to ASTM D4254, 2016) when compacted using the vibratory hammer at the maximum hammer speed, whereas it increases by 16.1% from its minimum unit weight (determined according to ASTM D4254, 2016) when compacted using the vibratory table at the maximum amplitude.
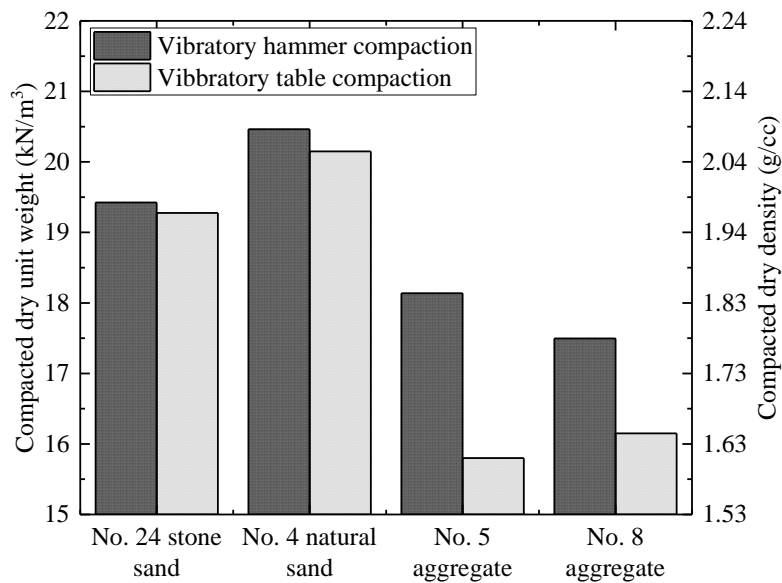
Figure 5.11 Comparison of compacted dry unit weights and densities obtained by vibratory hammer and vibratory table compaction of the test materials

The densities of the test materials achieved by compaction with the vibratory hammer and vibratory table were analyzed with respect to the physical properties of the particles. Figure 5.12 and Figure 5.15 show the compacted densities of the test materials with respect to the D_{50}, roundness, sphericity and elongation ratio. The test materials had similar morphology parameters. Thus, no direct correlations were obtained between the compacted density and the morphology parameters of the test materials.
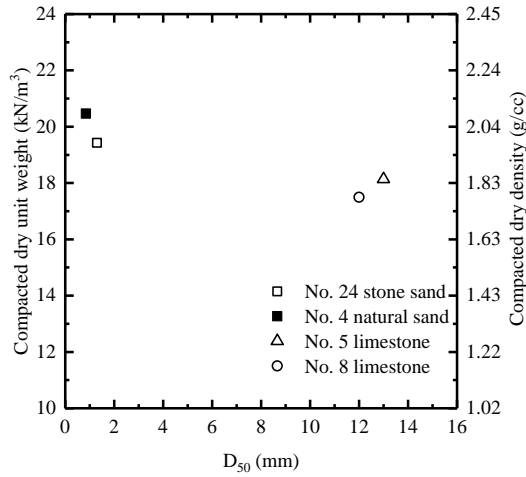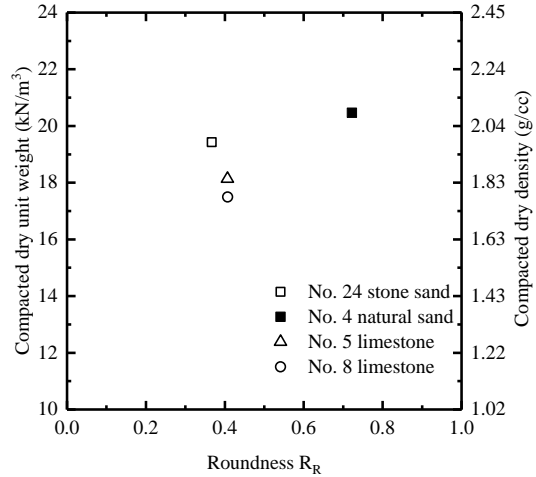
Figure 5.12 Compacted dry density versus (a) mean particle size D_{50} and (b) roundness of the test materials compacted by vibratory hammer at 0.5 mm amplitude and 60 blows per second hammer speed
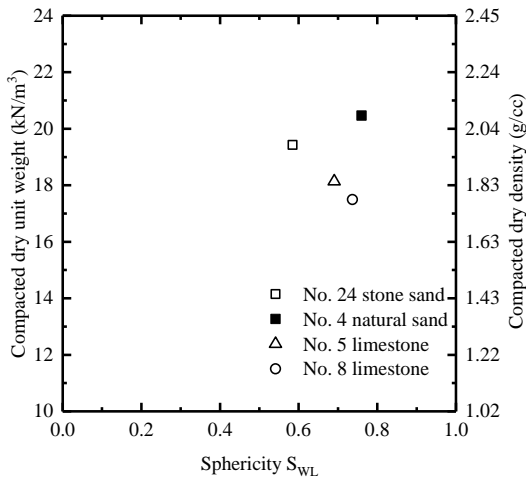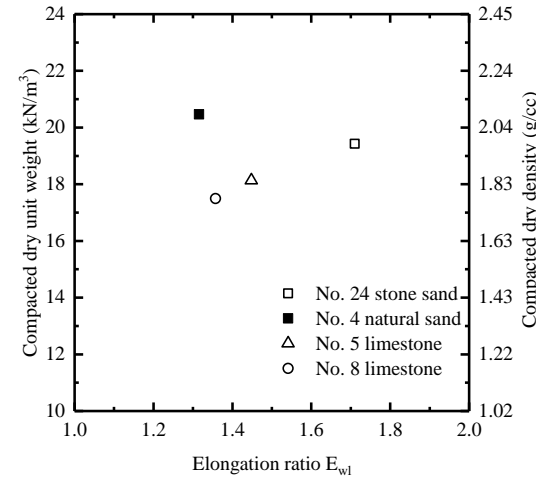
Figure 5.13 Compacted dry unit weight versus (a) sphericity and (b) elongation ratio of the test materials compacted by vibratory hammer at 0.5 mm amplitude and 60 blows per second hammer speed
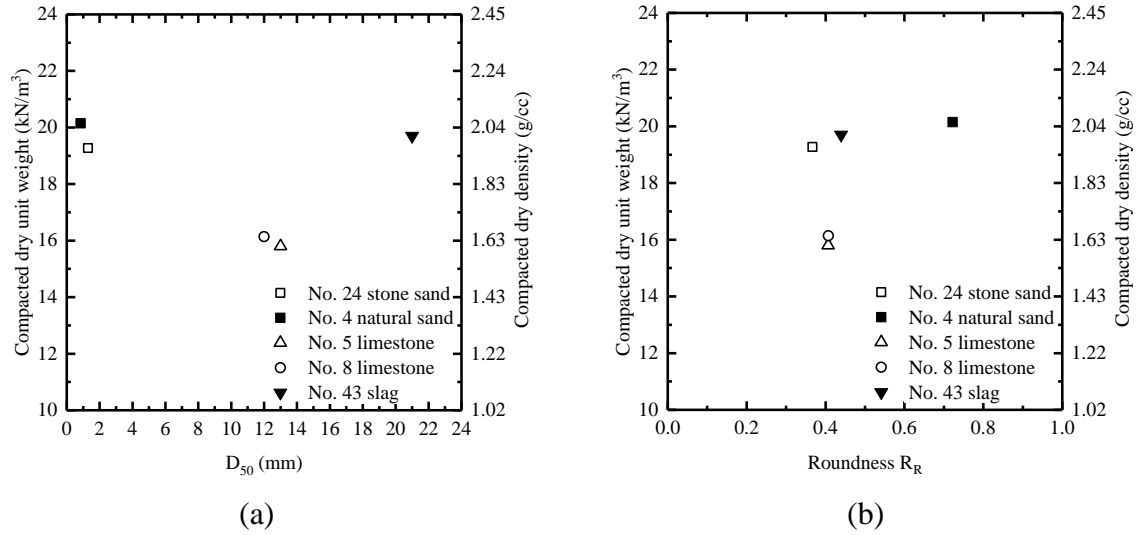
Figure 5.14 Compacted dry density versus (a) mean particle size D_{50} and (b) roundness of the test materials compacted by vibratory table at 0.9 mm amplitude and 60 Hz frequency of vibration
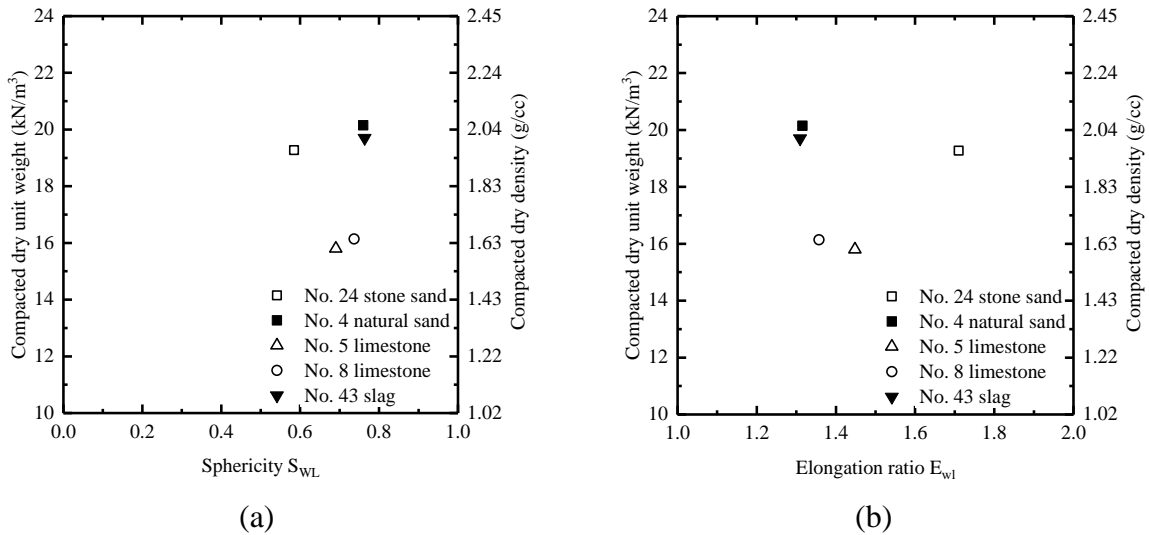
Figure 5.15 Compacted dry unit weight versus (a) sphericity and (b) elongation ratio of the test materials compacted by vibratory table at 0.9 mm amplitude and 60 Hz frequency of vibration

6. DIRECT SHEAR TESTS

Soil particles get rearranged to fill up the void spaces in between them during compaction by vibration. The ability to compact soil with a given effort and particle rearrangement during compaction depend on the morphology of the particles (Altuhafi et al. 2016; Cho et al. 2006), grain size distribution (Panayiotopoulos 1989; Youd 1972), water content (Holtz et al. 2011) and application of energy (Bowles 1996; Holtz et al. 2011). Soil resistance to change in density might be viewed as resistance to particle reorientation. According to Cruse et al. (1980), a significant portion of this resistance, particularly in coarse-grained soils, is due to friction between particles, which in turn is related to particle morphology and surface roughness. Cruse et al. (1980) studied the vibration energy required to compact sand particles of different surface roughnesses and concluded that compared to smooth particles, rough particles generate greater interparticle friction and interlocking, thus creating greater resistance to particle movement. Compaction or rearrangement of the particles near a geotechnical structure (for example, near an MSE wall) is also affected by the interface frictional resistance developing between the soil particles and the structure. The frictional resistance between soil and the surfaces of structural elements depends on the intrinsic properties of the soil particles and the roughness of the surface at the interface between these two materials; these resistances are represented by the critical-state friction angle (Salgado 2008) and the interface critical-state friction angle (Han et al. 2018). Particles with higher friction angles will require greater energy input to rearrange them into denser packing.

Direct shear testing is a standard testing method used to determine the critical-state friction angle of soils and the interface friction angle between soil and a surface. Interface direct shear tests were carried out for various gravel-sand mixtures and surface roughnesses to study the effects of gravel content and of surface roughness on the interface critical-state friction angle.

6.1   Test Materials

Direct shear tests were carried out to determine the internal friction angles of the materials commonly used by INDOT as structural backfill materials. They are No. 4 natural sand, No. 24 stone sand, No. 5 limestone and No. 8 limestone. The gradation and the morphological parameters of these materials were described in Chapter 4. To observe the effect of surface roughness and

mean particle size D_{50} on the interface friction angle, direct interface shear tests were performed for surfaces with different surface roughnesses for gravel-sand mixtures of various percentages. The gravel-sand mixtures were prepared by mixing Ohio gravel with Ohio sand. Ohio gravel and Ohio sand are referred to as OG and OS, respectively. The grain size distributions of the gravel-sand mixtures are presented in Figure 6.1. The gravel-sand mixtures are referred to by the initials of the Ohio gravel (OG) followed by the percentage by weight present in the mixture and the initials of the Ohio sand (OS) followed by the percentage by weight present in the mixture. For example, OG20+OS80 identifies a mixture containing 20% of Ohio gravel and 80% of Ohio sand. A total of seven mixtures with varying fractions of sand and gravel were prepared for direct interface shear tests with various surface roughnesses. A summary of the grain size distribution data of the different gravel-sand mixtures prepared for the direct interface shear tests is presented in Table 6.1.
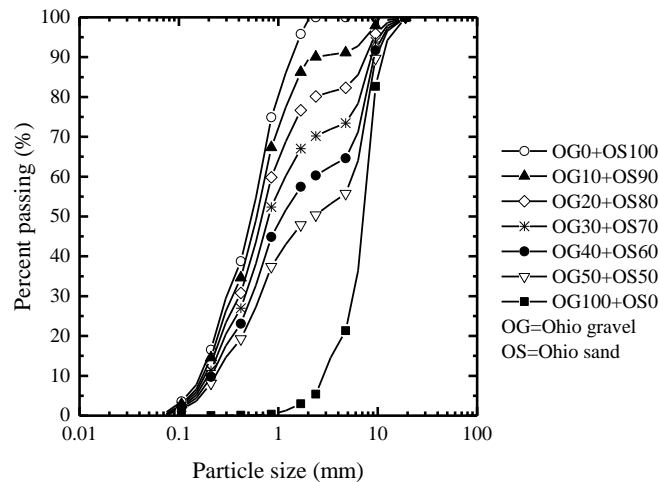
Figure 6.1 Grain size distributions of the test soils prepared for direct interface shear tests

80

Table 6.1 Properties of the test soils used for direct shear interface tests

Gravel-sand mixtures	D_{10} (mm)	D_{30} (mm)	D_{50} (mm)	D_{60} (mm)	C_u	C_c	Gravel fraction (%)	Sand fraction (%)
OG0+OS100	0.17	0.31	0.55	0.66	3.94	0.85	0	100
OG10+OS90	0.18	0.35	0.61	0.73	4.12	0.93	8.85	90.70
OG20+OS80	0.19	0.41	0.69	0.85	4.58	1.04	17.70	81.90
OG30+OS70	0.20	0.47	0.79	1.18	5.97	0.95	26.55	73.10
OG40+OS60	0.21	0.55	1.09	2.20	10.34	0.64	35.40	64.30
OG50+OS50	0.23	0.66	2.16	5.73	24.53	0.32	44.25	55.50
OG100+OS0	4.41	6.50	7.57	8.05	1.82	1.19	88.50	11.50

The morphology parameters of the particles of Ohio sand (OS) were obtained from Han et al. (2018). The morphology parameters of the particles of Ohio gravel (OG) were obtained from 2D image analyses following the procedure explained in Section 4.3. A summary of the morphology parameters of the sand and gravel particles is presented in Table 6.2. It is observed that the sand and gravel particles have similar sphericity, but the gravel particles are more rounded than the sand particles.

Table 6.2 Basic properties and morphology parameters of the test materials for the direct shear interface tests

Test material	Passing sieve size (mm)	Retaining sieve size (mm)	SiO_2 (%)	Al_2O_3 (%)	Fe_2O_3 (%)	TiO_2 (%)	Roundness[a] R_R	Sphericity[b] S_{WL}
OG	19	9.5	-	-	-	-	0.62	0.80
	9.5	4.75	-	-	-	-	0.56	0.75
OS	3.36	2	99.5	0.157	0.084	0.031	0.43	0.82
	2	1.19	99.5	0.157	0.084	0.031	0.44	0.77
	1.19	0.84	99.5	0.157	0.084	0.031	0.40	0.64
	0.84	0.42	99.5	0.157	0.084	0.031	0.39	0.75
	0.30	0.15	99.5	0.157	0.084	0.031	0.35	0.75

Note: Basic properties of the sand particles were collected from Han et al., (2018), roundness and sphericity parameters for the gravel particles were calculated using the MATLAB code developed by Zheng and Hryciw (2015)
[a]Roundness - defined as the ratio of the average radius of curvature of the corners of the particle to the radius of the maximum circle that can be inscribed (Wadell 1932)
[b]Sphericity - defined as the width-to-length ratio of a particle (Mitchell and Soga 2005)

6.2   Test Setup

A large-scale direct shear device manufactured by GeoComp Corporation (as shown in Figure 6.2) was used to perform the internal and interface direct shear tests. Tests were carried out following the ASTM D3080 (2011) standard. The direct shear apparatus consists of top and bottom square shear boxes, each with a side length of 305 mm and a height of 100 mm. Figure 6.3 shows the dimensions of the two shear boxes vertically stacked. The top shear box is maintained stationary during shearing, whereas the bottom shear box moves horizontally on a slide track at a specified speed controlled by a stepper motor. A load cell mounted between the bottom shear box and the stepper motor is used to measure the shear force. Vertical normal pressure is applied through a steel cap to the soil sample by a feedback-controlled actuator. A load cell attached between the steel cap and the actuator was used to measure the applied force. LVDTs were used to measure the vertical deformation of the soil sample and the shear displacement during shearing. Measurements of horizontal displacement, vertical displacement, normal force, and shear force were recorded using the ShearTrac System software.
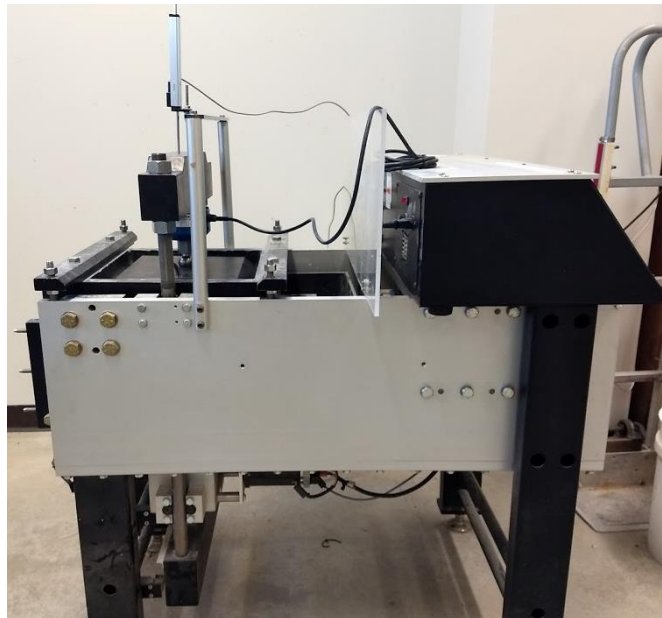
Figure 6.2 Large-scale direct shear machine manufactured by GeoComp
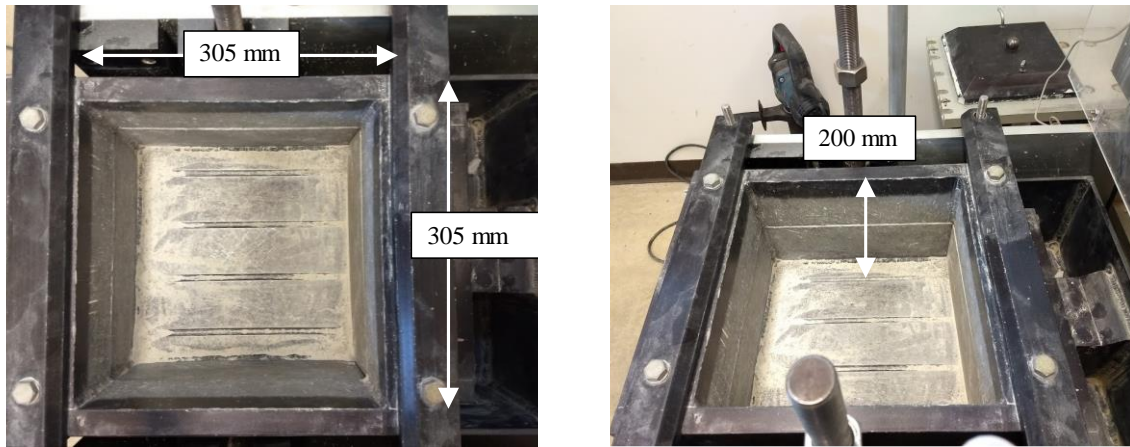
Figure 6.3 Direct shear box

The soil samples were prepared and tested in a dry condition. Due to the presence of a wide range of grain sizes in the test materials, sample preparation by dry pluviation would inevitably introduce particle segregation. Therefore, the samples were prepared by rapidly pouring well-mixed test materials in layers inside the shear box using a scoop, making sure that no segregation of particles occurred. This method of sample preparation of gravel-sand mixtures in large-scale direct shear testing was proposed by Simoni and Houlsby (2006).

For the interface shear tests, the bottom part of the shear box was fitted with a solid steel base, and a steel plate of the desired roughness was attached on top of it. Figure 6.4 shows the steel plate attached to the steel base that was fitted inside the bottom part of the shear box for interface shear testing. The top shear box was place on top of it, and the sample to be tested for determination interface shear testing was prepared on top of the steel plate inside the top shear box.
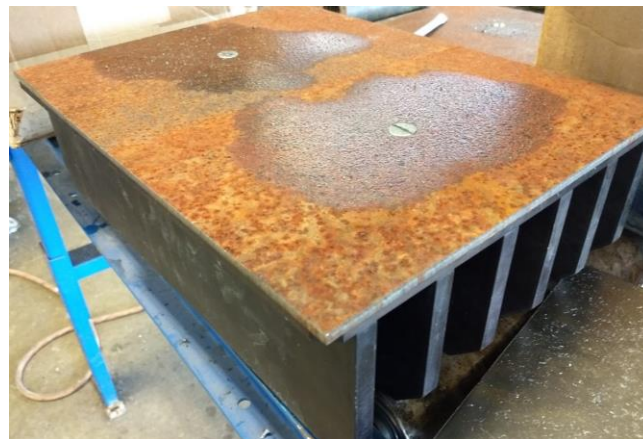
Figure 6.4 Attachment of rusted steel plate with the base for direct interface shear tests

After soil sample preparation, a normal stress was applied on top of the soil sample before shearing by displacing horizontally the bottom shear box. The top shear box was raised with respect to the bottom shear box to facilitate shear band formation between the two surfaces of the test materials. Simoni and Houlsby (2006) noted that a small gap may restrict the development of shear band, while a large opening causes stress reduction and material loss at the specimen edge. ASTM D3080 (2011) recommends a gap equal to the maximum particle size between the two boxes. However, considerable practical difficulties arise when applying such criterion to gravel materials because the required size of the opening would be more than a centimeter. Since systematic investigation of the effects of opening size with respect to grain size of test materials is outside the focus of this research, a fixed gap size of D_{50} was maintained for all test materials. During shearing of the test materials, no significant loss of materials was observed for the selected gap size. A constant shear displacement rate of 2 mm/min was maintained with the test samples sheared up to 38 mm.

6.3   Interface Roughness

In order to replicate the roughness of MSE wall panels, steel reinforcement bars or piles, steel plates of three different roughnesses were used for the direct interface shear tests. The steel plates selected for the tests were named as smooth, rusted and heavily rusted plates. A low-carbon steel plate without any rusting was selected as the smooth plate. A rusted steel plate was prepared by spraying a smooth steel plate with salt and hydrogen peroxide solution until the desired roughness was achieved. A heavily rusted steel plate, rusted under natural weather conditions, was collected from the backyard of the Bowen laboratory of Purdue University where scrap metal pieces are deposited in the yard and used for testing. Figure 6.5 shows the appearances of the smooth, rusted and heavily rusted steel surfaces used for the direct shear interface tests.
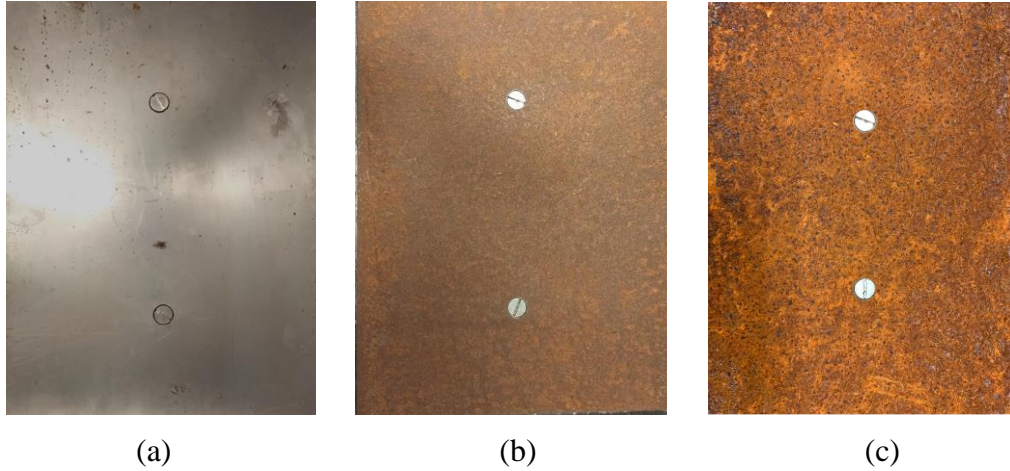
Figure 6.5 Interfaces used in the direct shear interface experiments (a) smooth steel surface, (b) rusted steel surface and (c) heavily rusted steel surface

The roughness values of the steel plates used for the direct shear interface tests were measured before testing. The most commonly used surface roughness parameters are the centerline average roughness R_a, the maximum peak-to-valley distance normal to the surface R_t, and the arithmetic mean of the highest peak-to-valley distance normal to the surface over a certain measuring length $R_{max,avg}$. Han et al. (2018) and Tovar-Valencia et al. (2017) summarized all of these three parameters used to quantify surface roughness of steel. The centerline average roughness R_a is defined as the average of the absolute values of the profile deviations z_i from the mean line of the roughness profile within a measurement length L, as explained in Figure 6.6. R_a is simply a surface property and thus independent of the size of the particles tested for interface shear resistance.

$$R_a = \frac{1}{n}\sum_{i=1}^{n}|z_i|$$

n = number of data points
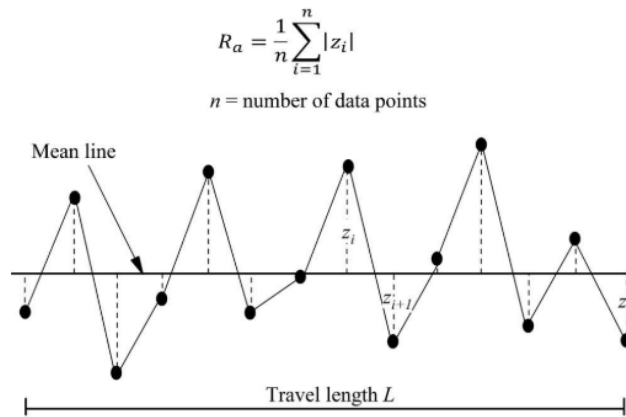
Figure 6.6 Centerline average roughness R_a (after Tovar-Valencia et al., 2017)

The R_t is the distance normal to the surface from the highest peak to the lowest valley within the entire measurement length L. The definition of R_t is explained in Figure 6.7. Another commonly used roughness parameter $R_{max,avg}$ was proposed by Uesugi and Kishida (1986). The calculation of $R_{max,avg}$ is illustrated in Figure 6.7. $R_{max,avg}$ is the arithmetic mean of all the highest peak-to-valley distance $R_{t,i}$ normal to the surface measured in an individual measuring length L_m equal to the D_{50} of the particle. When the $R_{max,avg}$ is normalized with respect to the particle size D_{50}, then it is called the normalized roughness R_n.
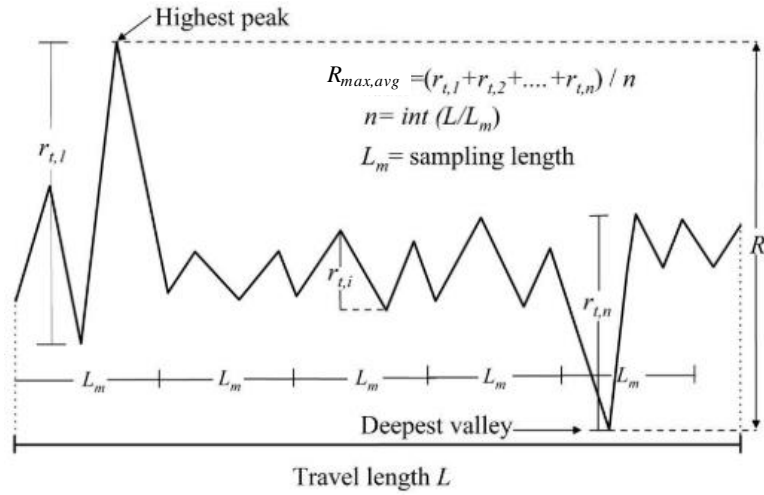
Figure 6.7 Definition of roughness parameters R_t and $R_{max,avg}$ (after Tovar-Valencia et al., 2017)

A modified roughness parameter $R^*_{max,avg}$ was proposed by Tovar-Valencia et al. (2017) which consists of taking the arithmetic mean of all the values of the highest peak-to-valley distances $R_{max,i}$ measured within a moving window [instead of using a segmented window, as proposed by Uesugi and Kishida (1986)]. The window size is equal to L_m, the moving step size Δx is the horizontal distance between two consecutive data points and n is the number of measurements. The definition of the normalized roughness R^*_n, according to the modified method developed by Tovar-Valencia et al. (2017), is illustrated in Figure 6.8.

$$R^*_n = \frac{R^*_{max,avg}}{L_m} = \frac{\sum_{i}^{n} R_{max,i}}{nL_m}$$

(Δx is the horizontal distance between two consecutive data points)
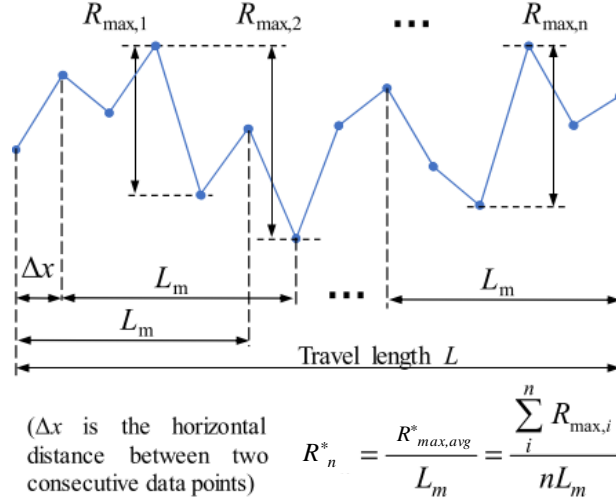
Figure 6.8 Definition of $R^*_{max,avg}$ and normalized roughness R^*_n (after Han et al., 2018)

A contact surface profilometer manufactured by Mitutoyo with model SJ-411 was used to measure the surface roughness of the steel plates (smooth, rusted and heavily rusted plates) used for direct interface shear tests. The measurement precision of the profilometer is 1×10^{-3} µm. The moving speed of the profilometer probe was set to 0.5 mm/s. Roughness measurements were performed for 20 mm length along the direction of shear at 12 different locations in each plate. Roughness measurements were carried out before and after the direct shear interface tests. Figure 6.9, Figure 6.10, and Figure 6.11 show the typical measured surface profiles for the three different plates selected for direct interface shear testing. The centerline average roughness of the smooth, rusted and heavily rusted steel plates are equal to about 1 µm, 10 µm and 20 µm, respectively. The values of $R^*_{max,avg}$ determined for all three steel plates according to the method proposed by Tovar-Valencia et al. (2017) are shown in Figure 6.12. Figure 6.13 shows the relationship between R^*_n and the particle size D_{50} for the three steel plates tested.
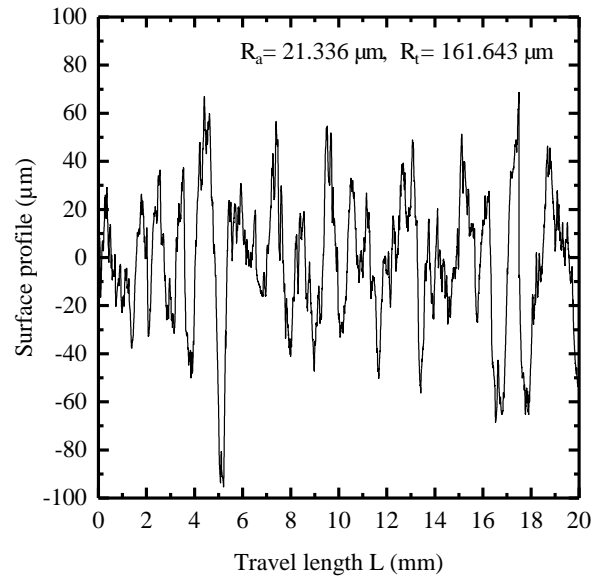
Figure 6.9 Typical surface roughness profile for the heavily-rusted steel plate
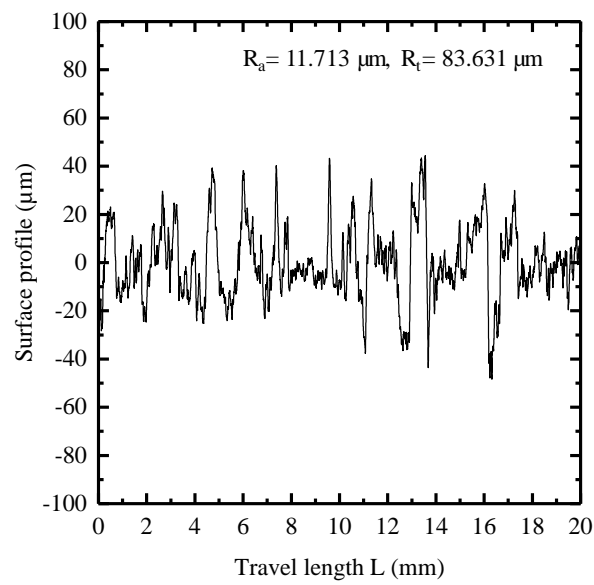
Figure 6.10 Typical surface roughness profile for the rusted steel plate
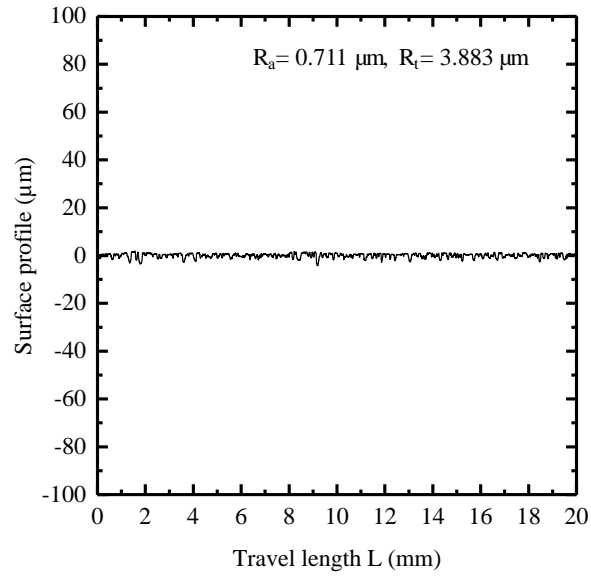
Figure 6.11 Typical surface roughness profile for the smooth steel plate
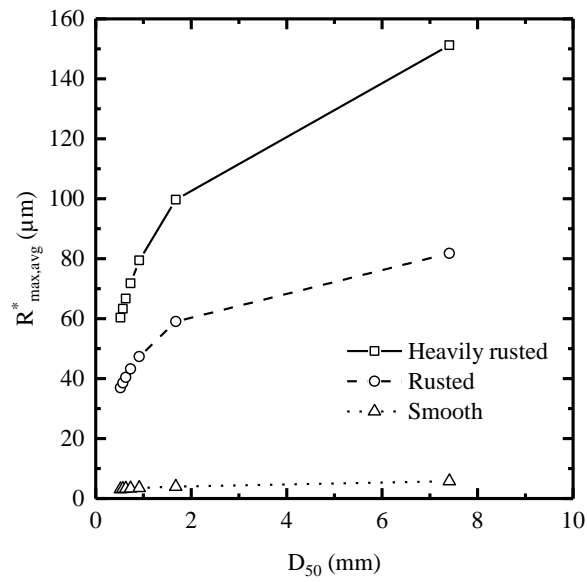
Figure 6.12 $R^*_{max,avg}$ values determined for the three testing plates considering $L_m = D_{50}$ of the test materials
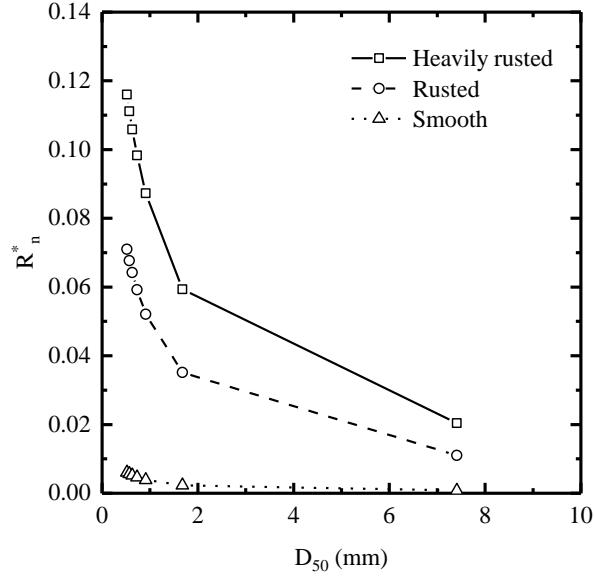
Figure 6.13 R^*_n vs. the particle size D_{50} for the steel plates used for the direct shear interface tests

6.4   Direct Shear Test Results

For each test material, two different vertical normal stresses were applied in the direct shear tests. The measured shear stresses at critical state were plotted against the corresponding normal stresses. The slope of the regression line with zero intercept for each set of data points was used to determine the critical-state friction angles of the test materials. This method of determining the critical-state friction angle from multiple direct shear test results is more reliable than from using a single test result since the influence of errors in any one test is minimized (Simoni and Houlsby 2006). Figure 6.14 and Figure 6.15 show the shear stress versus displacement plots and vertical displacement versus horizontal displacement for the direct shear tests performed with No. 4 natural sand and No. 24 stone sand. Shear stress versus displacement and vertical displacement versus horizontal displacement plots for No. 5 limestone and No. 8 limestone are shown in Figure 6.16 and Figure 6.17.
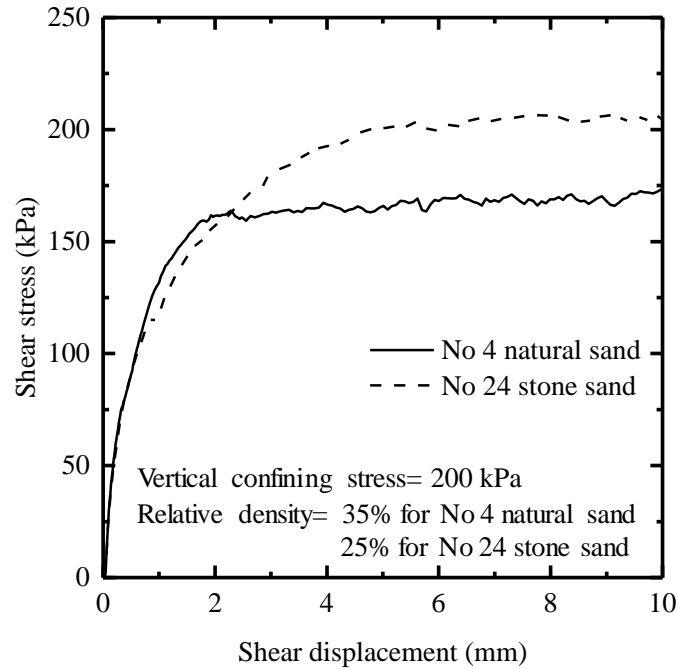
Figure 6.14 Shear stress versus shear displacement curves obtained from the direct shear tests for No. 4 natural sand and No. 24 stone sand
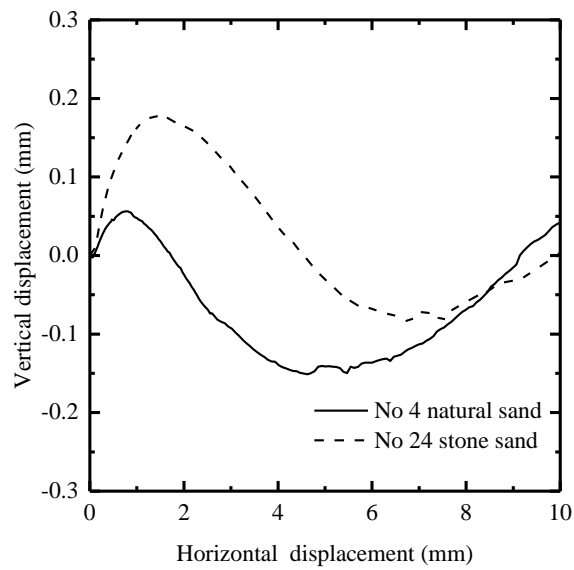
Figure 6.15 vertical displacement versus horizontal displacement curves obtained from the direct shear tests for No. 4 natural sand and No. 24 stone sand
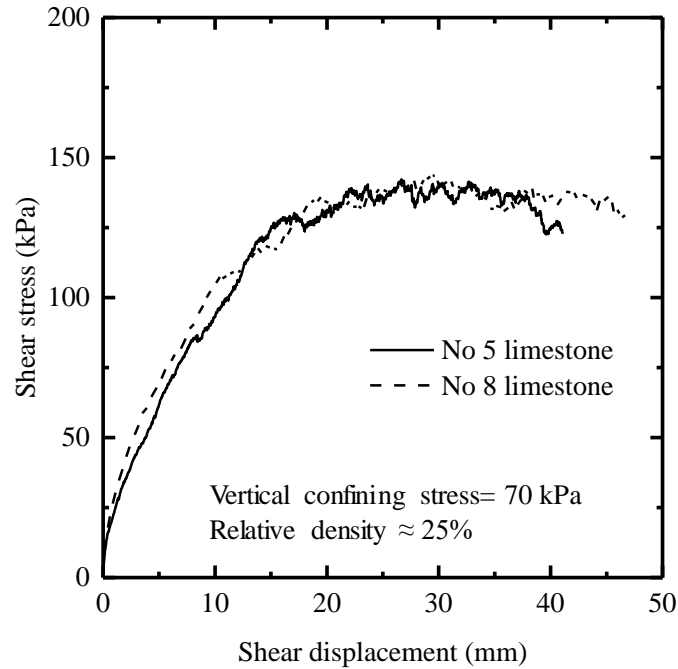
Figure 6.16 Shear stress versus shear displacement curves obtained from the direct shear tests for No. 5 limestone aggregate and No. 8 limestone aggregate
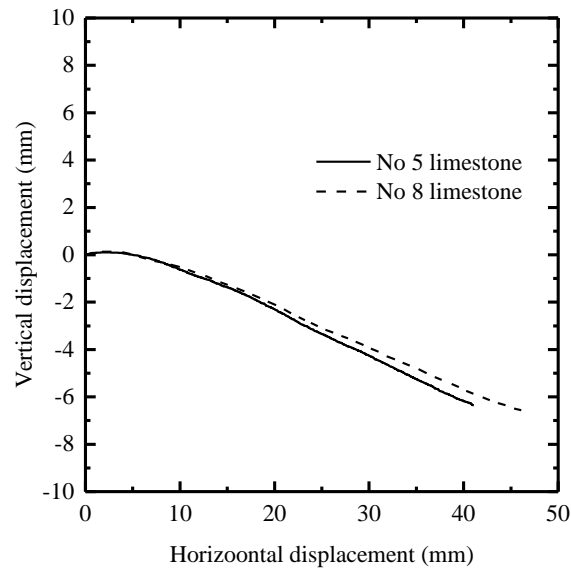
Figure 6.17 Vertical displacement versus horizontal displacement curves obtained from the direct shear tests for No. 5 limestone aggregate and No. 8 limestone aggregate

The summary of the direct shear test results for the backfill materials are shown in Table 6.3. It is observed that as the particle size increases, the critical-state friction angle increases. Figure 6.18 shows the critical-state friction angle versus D_{50} for the different backfill materials

tested in this research. The maximum unit weight, as determined by the vibratory hammer compaction tests, decreases with the increase in critical-state friction angle, as shown in Figure 6.19.

Table 6.3 Summary of the properties of the backfill materials and direct shear test results

Backfill material	D_{50} (mm)	R_R	S_{WL}	e_{max}	e_{min}	$\phi_{cs,DS}$ (degrees)
No. 24 stone sand	1.30	0.37	0.56	0.72	0.34	44.2
No. 4 natural sand	0.85	0.72	0.73	0.54	0.27	38.0
No. 5 limestone aggregate	13	0.41	0.65	0.91	0.44	62.9
No. 8 limestone aggregate	12	0.41	0.72	0.91	0.49	62.7

Note: R_R and S_{WL} are the roundness and sphericity parameters for the dominant particle size of the backfill materials determined using the MATLAB code developed by Zheng and Hryciw (2015). R_R is defined as the ratio of the average radius of curvature of the corners of the particle to the radius of the maximum circle that can be inscribed (Wadell 1932). S_{WL} is defined as the width-to-length ratio of the particle (Mitchell and Soga 2005).
e_{max}= maximum void ratio of the material determined following ASTM D4254 (2016), e_{min}= minimum void ratio of the material determined from the maximum compaction density using the vibratory hammer following ASTM D7382 (2008) and $\phi_{cs,DS}$ = critical-state friction angle obtained from direct shear test
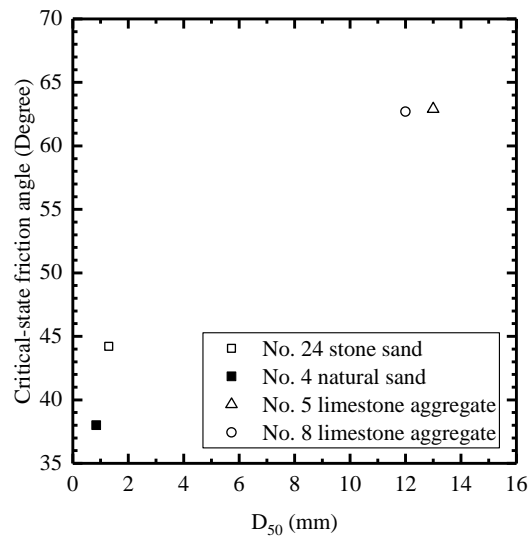
Figure 6.18 Critical-state friction angle versus D_{50} of the backfill materials
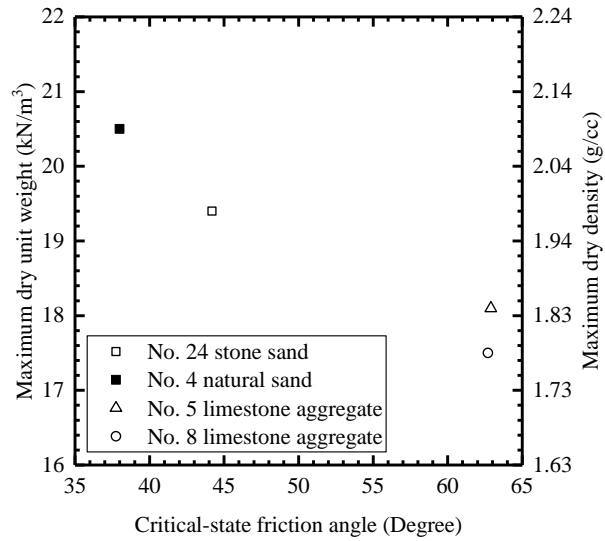
Figure 6.19 Maximum dry unit weight versus critical-state friction angle of the backfill materials

6.5　Direct Interface Shear Test Results for Gravel-Sand Mixtures

The results of the direct shear and interface tests for various gravel-sand mixtures were analyzed to determine the internal critical-state friction angles and the critical-state interface frictions angles for the tested surface roughnesses. A summary of the test results is shown in Table 6.4.

Table 6.4 Summary of the internal and interface direct shear test results for various gravel-sand mixtures

Gravel-sand mixture	D_{50} (mm)	$\phi_{cs,DS}$ (degrees)	Plate type	R_a (μm)	$R^*_{max,avg}$ (μm)	R^*_n	δ_{cs} (degrees)	$\delta_{cs}/\phi_{cs,DS}$
OG0+OS100	0.55	30.83	S	0.78	3.15	0.006	20.52	0.67
			R	9.66	33.52	0.061	26.83	0.87
			HR	22.51	62.30	0.113	29.99	0.97
OG10+OS90	0.61	31.72	S	0.78	3.23	0.006	22.39	0.71
			R	9.66	35.13	0.058	27.29	0.86
			HR	22.51	67.75	0.111	30.46	0.96
OG20+OS80	0.69	32.13	S	0.78	3.30	0.005	21.75	0.68
			R	11.54	41.75	0.061	27.96	0.87
			HR	19.13	67.17	0.097	29.18	0.91
OG30+OS70	0.79	33.75	S	1.15	6.92	0.009	24.01	0.71
			R	10.94	43.58	0.055	27.29	0.81
			HR	20.25	71.93	0.091	29.18	0.86
OG40+OS60	1.09	35.74	S	0.96	6.12	0.007	23.72	0.66
			R	9.02	43.26	0.040	26.63	0.75
			HR	17.28	73.40	0.067	27.63	0.78
OG50+OS50	2.16	36.51	S	0.96	7.43	0.004	22.61	0.62
			R	9.64	56.75	0.026	24.66	0.68
			HR	20.34	101.16	0.047	27.93	0.77
OG100+OS0	7.57	42.34	S	1.15	16.63	0.002	28.91	0.68
			R	9.82	74.99	0.010	30.14	0.71
			HR	17.22	113.58	0.015	28.96	0.68

Note: S= smooth steel plate, R= rusted steel plate and HR= heavily rusted steel plate, $\phi_{cs,DS}$ =critical-state friction angle obtained from direct shear tests, δ_{cs}=critical-state interface friction angle, $\delta_{cs}/\phi_{cs,DS}$ =critical-state friction angle ratio

The mean particle size D_{50} of the sand-gravel mixtures increases with increasing gravel content in the mixture. From the direct shear tests, it was observed that the critical-state friction angle increases as the D_{50} of the sand-gravel mixture increases, as shown in Figure 6.20. The mean particle size in the sand-gravel mixtures increases from 0.55 to 7.57 mm with an increase in gravel content in the mixture from 0% to 100%; with the increase in the mean particle size in the mixture, the critical-state friction angle of the sand-gravel mixture increases from 30.8 degrees to 42.3 degrees. Similar observation of the dependency of the critical-state friction angle on particle size was reported by Simoni & Houlsby (2006).
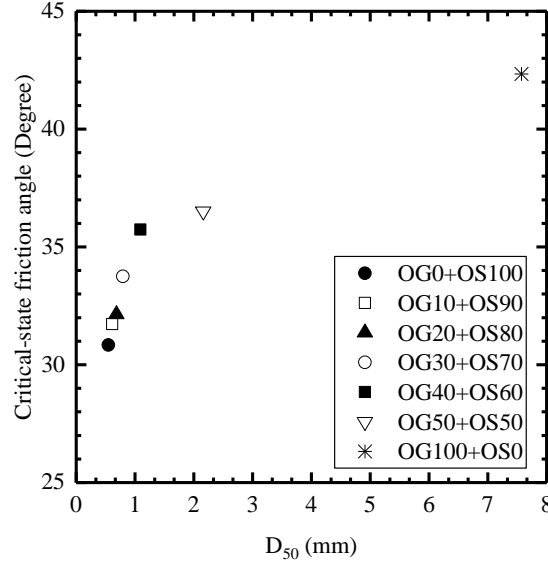
Figure 6.20 Critical-state friction angle versus D_{50} for various gravel-sand mixtures

The interface friction angles for the gravel-sand mixtures were plotted against the centerline average roughness R_a in Figure 6.21. An increasing trend of the interface friction angle with increasing surface roughness R_a was observed. The effect of particle size on the interface friction angle can be eliminated by normalizing the steel plate surface roughness with respect to the mean particle size and the interface friction angle with respect to the critical-state friction angle for each sand-gravel mixture. Figure 6.22 shows that when the critical-state friction angle ratio $\delta_{cs}/\phi_{cs,DS}$ is plotted against the normalized surface roughness R^*_n, a clear trend of increasing $\delta_{cs}/\phi_{cs,DS}$ with increasing R^*_n was found that is independent of the mean particle size. From Figure 6.22, it is observed that the $\delta_{cs}/\phi_{cs,DS}$ increased from 0.65 to a value slightly less than 1 for the range of R^*_n (0.006 to 0.11) of the rusted steel plates and the sand-gravel mixtures. Similar studies were conducted by Han et al. (2018) reporting on the effect of R^*_n on $\delta_{cs}/\phi_{cs,DS}$. The study was limited to Ohio sands of different gradations with mean particle sizes up to 1.5 mm. A comparison of $\delta_{cs}/\phi_{cs,DS}$ vs R^*_n results for Ohio sands of different gradations from Han et al. (2018) with Ohio sand-gravel mixtures is shown in Figure 6.23. It is observed that for materials with varying gradations and mean particle sizes, a similar increasing trend in $\delta_{cs}/\phi_{cs,DS}$ with respect to R^*_n is also observed. Figure 6.23 also shows that $\delta_{cs}/\phi_{cs,DS}$ would approach 1 only with further increase in R^*_n. The dependency of $\delta_{cs}/\phi_{cs,DS}$ on the R^*_n, irrespective of the soil grain size distributions with varying particle sizes, implies that the interface friction angle δ_{cs} of any sand, gravel or sand gravel mixtures could be obtained from Figure 6.23 if the surface roughness profile, D_{50} and ϕ_{cs} are known.

Further testing is required on natural and reconstituted soils with different characteristics to confirm these observations.
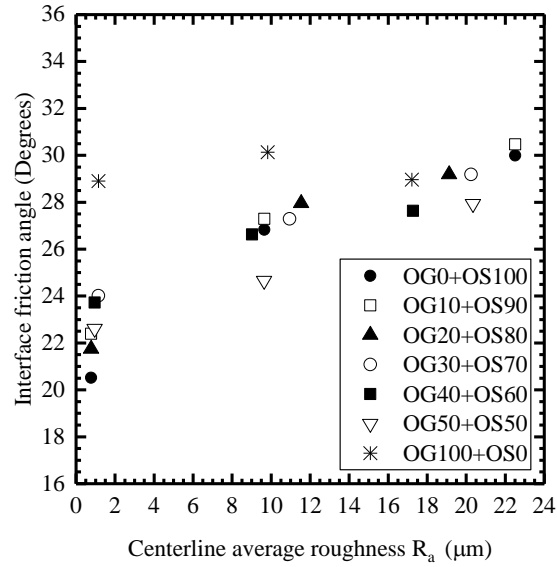
Figure 6.21 Interface friction angle at critical-state δ_{cs} versus centerline average roughness R_a
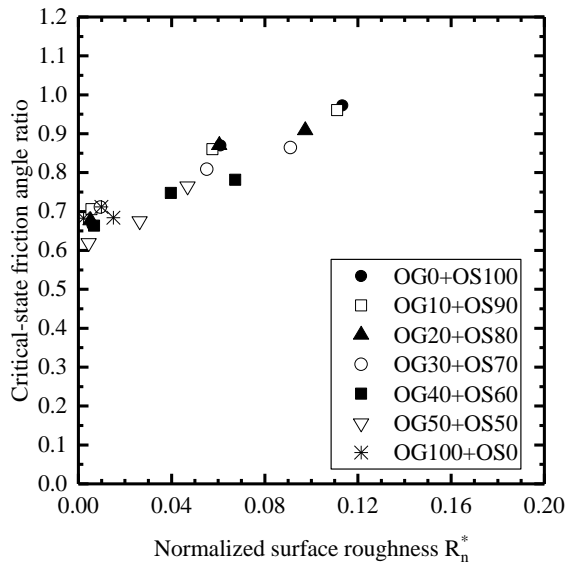
Figure 6.22 Critical-state friction angle ratio $\delta_{cs}/\phi_{cs,DS}$ versus normalized surface roughness R^*_n
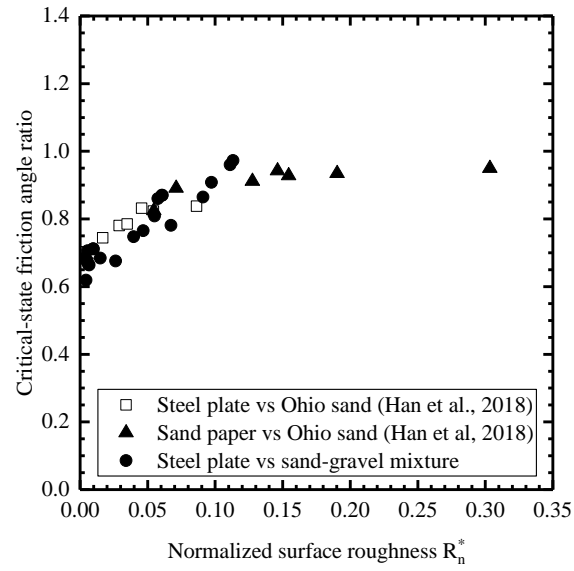
Figure 6.23 Critical-state friction angle ratio $\delta_{cs}/\phi_{cs,DS}$ versus normalized surface roughness R^*_n for materials of different gradations and mean particle sizes

7. FIELD TESTING

Vibratory rollers are used in the field to compact coarse-grained backfill soils. Vibratory rollers have multiple vibration settings that produce different frequencies of vibration. The compaction density achieved in the field by compacting a specific backfill soil depends on the selected vibratory roller vibration setting, the lift thickness and the number of passes. Figure 7.1. presents the methodology followed in the field to determine the optimum vibration frequency and number of passes required to achieve a target relative compaction.
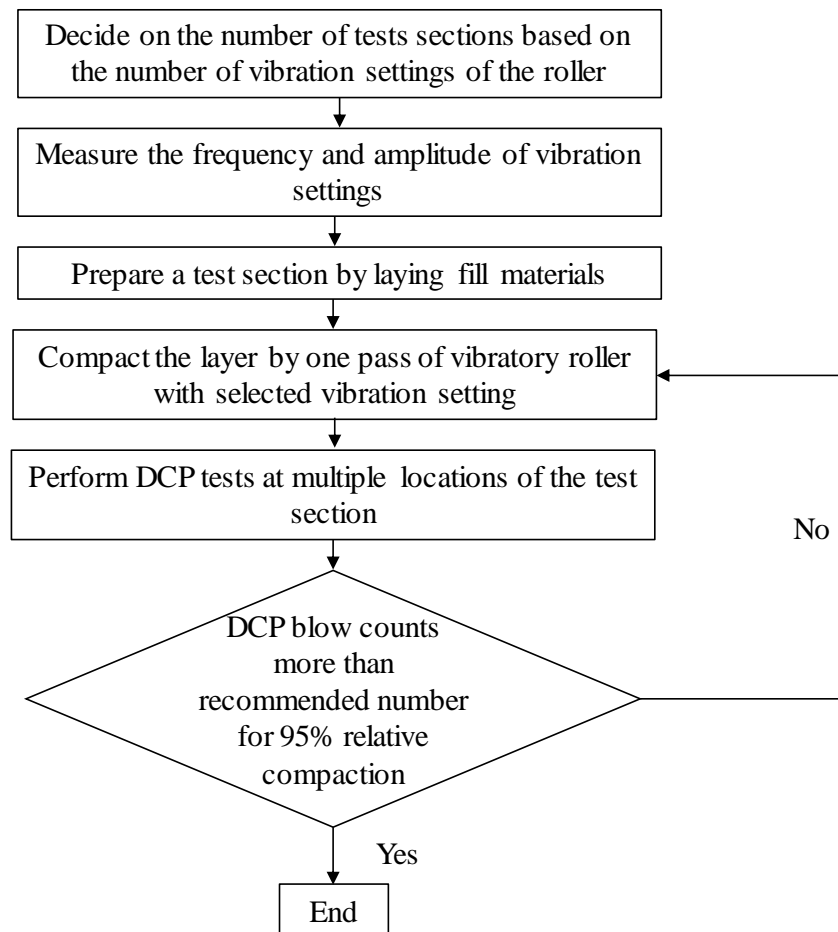
Figure 7.1 Steps to determine optimum vibration and number of passes to achieve desired relative compaction in the field

7.1　Vibration Measurements of Vibratory Roller

Vibration frequency and amplitude of two vibratory rollers were measured using accelerometer sensors for this research work. One of the vibratory rollers, manufactured by Bomag with model number 211D-3 (as shown in Figure 7.2), was used for the construction of I-65 near Lake county, Indiana. The vibratory roller has weight of 10,400 kg with drum diameter of 1.5 m and drum width of 2.13 m. The roller has two vibration settings (low and high) that produces two different frequency of vibrations. The other vibratory roller used in this research work was manufactured by Caterpillar (model number CS56B), as shown in Figure 7.3. This roller was used to compact subgrade soil for a ramp at the intersection of US 20 and IN 2 in Rolling Prairie, Indiana. It has two vibration settings (low and high) as well with two different frequency of vibrations. The weight of the roller is 24,887 lb. It has drum width and diameter of 7 ft and 5 ft, respectively.

Figure 7.2 Bomag 211D-3 used for subgrade soil compaction

Figure 7.3 Caterpillar CS56B vibratory roller used for subgrade soil compaction

An accelerometer sensor was attached to the roller drums to measure the vibration frequency and amplitude. A data acquisition system connected with the sensor transferred the data to a computer for display and analysis. Details of the accelerometer sensor data collection and analysis are provided in Section 3.4. The frequency of vibration for the roller manufactured by Bomag at low setting was 27 Hz, while the frequency of vibration at high setting was 34 Hz. From the analyses of the accelerometer sensor attached to the vibratory roller manufactured by Caterpillar, it was observed that the frequency of vibration produced at low setting was 25 Hz, while the frequency of vibration at high setting was 32 Hz. For both vibratory rollers, the amplitude of vibration was measured in the field as well with the accelerometer sensor. It was observed that the amplitude of vibration varies depending on the density or stiffness of the compacted soil. The vibration settings of the equipment can only control the frequency of vibration of the drum. The amplitude of vibration of the roller manufactured by Bomag was measured to be 1.3 mm vibrated over No. 43 slag aggregates compacted at 95% relative compaction. In the case of the vibratory roller manufactured by Caterpillar, the amplitude of vibration was measured to be 2.4 mm vibrated over No. 30 sand compacted at 95% relative compaction.

7.2   DCP Tests for Relative Compaction Assessment

The Dynamic Cone Penetrometer (DCP) is a simple device commonly used by INDOT to assess the strength and stiffness of soils compacted *in-situ* (Ganju et al. 2018; Indiana Department of Transportation 2018). It is inexpensive, easy to perform and the results are repeatable. These factors have made it a popular method of quality control of subgrade compaction amongst various state agencies. A schematic of the DCP device is shown in Figure 7.4.
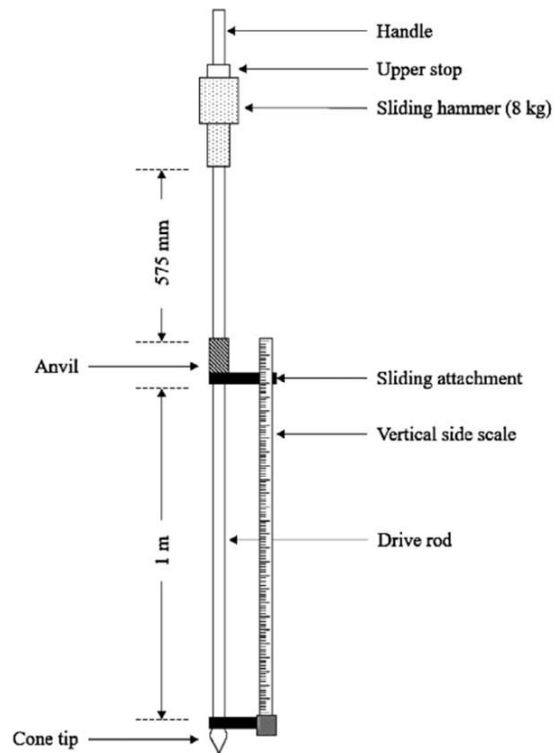
Figure 7.4 A schematic of a DCP device (after Ganju et al. 2018)

Ganju et al. (2018) and Salgado and Yoon (2003) conducted research using the DCP device to establish correlations between the DCP blow counts and the relative compaction of different types of soils. INDOT specifies the required number of blows for 95% relative compaction of different types of structural backfill materials. Table 7.1 summarizes the minimum number of blows for 12-inch penetration by the DCP to achieve 95% or 100% relative compaction of structural backfill materials according to INDOT.

Table 7.1 DCP blow count requirements for compaction quality check for different structural backfill materials according to Indiana Department of Transportation (2018)

Backfill materials	Acceptable minimum DCP value for 12 in. for 95% compaction	Acceptable minimum DCP value for 12 in. for 100% compaction
No. 30	6	9
No. 4	7	10
½ inch	11	14
1 inch	16	19

A construction site was selected where compaction of subgrade backfill soil was underway using a vibratory roller. The site is located in Rolling Prairie, IN, where a ramp for the intersection of US 20 and IN 2 was being constructed using No. 30 backfill soil as a subgrade soil. A vibratory roller manufactured by Caterpillar (Model number CS56B) was used to compact the soil by vibration (see Figure 7.3). The vibratory roller has two vibration settings (low and high) that apply two different frequency of vibrations. The frequency and amplitude of vibration of the roller for two vibration settings were measured using an accelerometer sensor. The frequency of vibration produced at low setting was 25 Hz, while the frequency of vibration at high setting was 32 Hz. The amplitude of vibration was measured to be 2.4 mm for both settings, vibrated on top of No. 30 sand compacted at 95% relative compaction. Two test sections were prepared to determine the required number of passes to achieve the desired relative compaction of the soil for each vibration setting. Figure 7.5 shows the construction site where the two test sections were prepared for the field compaction tests.

Figure 7.5 Subgrade compaction for No. 30 backfill soil using vibratory compactor for the construction of ramp at US 20 and IN 2 intersection at Rolling Prairie, IN

Each test section had a width of 2 m and a length of 15 m. No. 30 sand was laid down in a layer with loose thickness of 12 inches. Two test sections were compacted using the vibratory roller with two different vibration settings (low and high). Multiple passes were carried out to compact the backfill soil. A constant travel speed of the roller was maintained during each pass. A backward static pass was carried out to move the roller to the initial position after every vibratory pass. DCP tests were carried out after every vibratory pass for four different locations in the test section. Figure 7.6 shows a schematic of a test section with the locations of the DCP tests. Vibration passes were carried out until the required number of blow counts were achieved for 95% relative compaction by the DCP tests in all locations of the test section. Based on Table 7.1, for 95% relative compaction of No. 30 backfill soil, the minimum required number of blow counts for 12-inch penetration of DCP is 6.
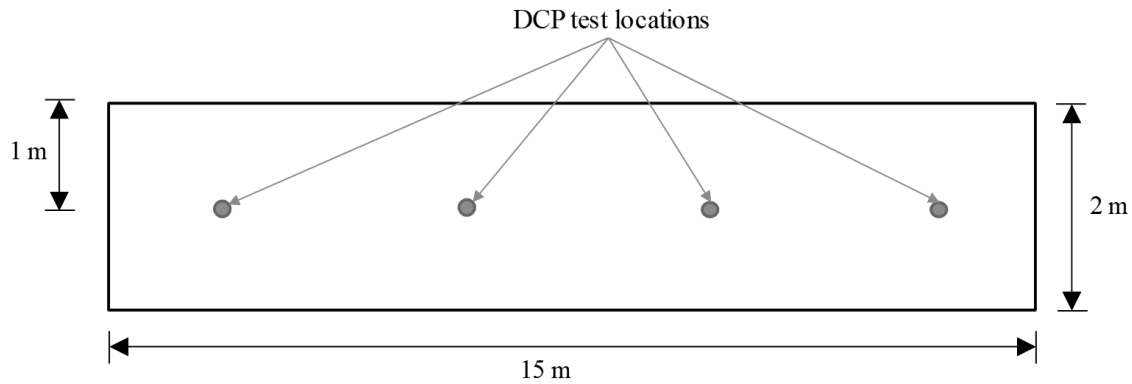
Figure 7.6 Schematic of a test section for field testing showing the dimensions of the test area and DCP test locations (not in scale)

DCP test results for 12 inch penetration for both test sections are shown in Figure 7.7 and Figure 7.8. The results show that three vibratory passes with a static roller pass in between each vibratory pass were required to achieve 95% relative compaction of No. 30 backfill soil by both low and high vibration settings of the roller. However, compaction with high vibration setting produces more uniform stiffness than compaction with low vibration setting of the roller. But the high vibration setting of the roller has higher operating cost and causes more wearing of the equipment. Similar compaction tests can be carried out in the field for different backfill materials.

Vibratory pass No.	Location 1	Location 2	Location 3	Location 4
1	4	2	5	3
2	6	5	6	5
3	8	7	7	7
4	8	7	7	8

Legend
6 and above
4 to 5
2 to 3

Figure 7.7 DCP blow counts at different locations after every vibratory pass by the roller in low vibration setting

Vibratory pass No.	Location 1	Location 2	Location 3	Location 4
1	7	6	6	5
2	8	6	6	5
3	8	7	6	6
4	9	8	7	7

Legend
6 and above
4 to 5
2 to 3

Figure 7.8 DCP blow counts at different locations after every vibratory pass by the roller using the high vibration setting

8. CONCLUSIONS AND RECOMMENDATIONS

Vibration compaction is the most effective way of compacting coarse-grained materials. The effect of vibration frequency and amplitude on the compaction density of different backfill materials were studied in this research work. Small-scale laboratory compaction tests were carried out for No. 4 natural sand, No. 24 stone sand and No. 5, No. 8, No. 43 aggregates. Large-scale vibratory roller compaction tests were performed in the field for No. 30 backfill soil. A methodology was developed to measure the frequency and amplitude of vibration using accelerometer sensors. The accelerometers were attached to the vibrating equipment to collect acceleration data during compaction. A MATLAB code was used to analyze the accelerometer data collected in the laboratory and field tests to determine the frequency and amplitude of vibration.

Small-scale laboratory compaction tests were carried out using a vibratory hammer and a vibratory table. The vibratory table was manufactured by ELE and has a fixed frequency of vibration of 60 Hz and variable amplitude ranging from 0.2 mm to 0.9 mm. The setup of the vibratory hammer equipment was manufactured by Humboldt Mfg. Co., while the vibratory hammer used in the equipment setup was manufactured by Bosch (model No. 11264EVS). The vibratory hammer has a fixed amplitude of 0.5 mm and variable hammer speed ranging from 25 to 60 blows per second. The effect of vibration amplitude on the compaction density was determined from the tests using the vibratory table, while the effect of vibration speed or frequency of vibration on the compaction density was determined from the compaction tests using the vibratory hammer. The laboratory compaction tests using the vibratory table show that the compaction density increases with increasing amplitude of vibration. The increase in density with the increase in amplitude of vibration is more pronounced for the coarse aggregates than for the sands. For example, with the increase in amplitude of vibration from 0.2 mm to 0.9 mm during compaction using the vibratory table, the density of No. 8 aggregate increases by 14%, whereas it increases by only 1.4% for No. 4 natural sand. Increasing the hammer speed during compaction using the vibratory hammer increases the compaction density of the materials. The test results show that the density of different test materials increases by 3-7% for an increase in the hammer speed from 25 blows per second to 60 blows per second for compaction using the vibratory hammer.

A comparison of the maximum dry densities of different test materials shows that the dry densities obtained after compaction using the vibratory hammer is more than that obtained after compaction using the vibratory table at the highest amplitude and frequency of vibration available in both equipment. However, the compacted dry densities of the test sands (No. 4 and No. 24 sands) obtained from both equipment are comparable to each other, while the dry densities of the aggregates (No. 5 and No. 8 aggregates) compacted by the vibratory hammer are 8 to 15% higher than those obtained by compaction with the vibratory table. During compaction using the vibratory table at 0.9 amplitude of vibration, particle crushing was observed for No. 24 stone sand, producing a completely different material with different grain size distribution and particle morphology. No crushing was observed for the test materials while compacting using the vibratory hammer. The vibratory hammer is a more efficient method of compacting the coarse aggregates.

The effect of water content on the compaction density was studied for No. 4 natural sand and No. 24 stone sand using the standard Proctor hammer and the modified Proctor hammer tests. Water contents less than 2% were observed to be beneficial to achieve the maximum dry density of these test materials. While using the standard Proctor and the modified Proctor, crushing of No. 24 stone sand was observed during compaction

The morphology parameters (roundness and sphericity) were studied using digital image analysis techniques for the particles of the collected backfill materials. The images of the particles were analyzed using the ImageJ software and a MATLAB code developed by Zheng & Hryciw (2015). The test materials were characterized based on the morphology parameters of the dominant particle size of each material. The dominant particle size was selected as the size range of the particles with maximum percentage by mass retained in a sieve. The roundness values (which show how rounded the corners of the particles are) of the dominant particle sizes for all the test materials varied between 0.37 and 0.44, except for No. 4 natural sand, for which the roundness value was 0.72. The width-to-length ratio sphericity values of the dominant particle sizes of the test materials varied from 0.69 to 0.76, except for No. 24 stone for which it was 0.58. Because of the similarities of the morphology parameters of the test materials, no conclusions were reached on its effect on the compaction densities.

The critical-state friction angle, which is an indicator of the shear strength of soil at large displacements was determined from direct shear tests. The results of the direct shear tests performed with the test materials show that with increasing mean particle size, the critical-state

friction angle of the materials increases. The critical-state friction angle of No. 4 natural sand and No. 24 stone sand are 38.0 and 44.2 degrees, respectively. The critical-state friction angle of No. 5 and No. 8 aggregates are 62.9 and 62.7 degrees, respectively. To understand the effect of surface roughness on the interface critical-state friction angle, direct shear interface tests were also performed for different mixtures of gravel with sand against smooth and rusted steel plates. The interface critical-state friction angle normalized by the critical-state friction angle of the sand-gravel mixtures increases with increasing surface roughness normalized by the mean particle size. For a range of normalized surface roughness of 0.006 to 0.11, the interface critical-state friction angle ratio increases linearly from 0.65 to a value slightly less than 1.

The effect of vibration frequency and number of passes on the compaction density was studied in the field for a vibratory roller manufactured by Caterpillar (Model CS56B). Accelerometer sensors were attached to the roller drum to measure the frequency and amplitude of vibration for two different vibration settings available to the roller. The frequency of vibration of the roller was measured to be 25 and 32 Hz at two different vibration settings. The amplitude of vibration was measured to be 2.4 mm vibrated over No. 30 sand compacted at 95% relative compaction. A test pad was prepared to compact a layer of No. 30 backfill soil with two vibration settings and multiple number of roller passes. DCP tests were performed after each pass to check if the 95% relative compaction had been achieved. For the given roller and soil tested, the results show that the higher vibration setting produces more uniform compaction density. However, a greater number of tests are required with different backfill materials to establish the effect of roller passes on the 95% relative compaction of backfill materials for variable vibration settings.

Optimum use of vibration frequency during compaction by vibratory rollers can reduce the operation time and in turn reduce the cost of construction. The vibratory rollers used in this research work (Caterpillar model CS56B and Bomag model 211D-3) had only two vibration settings with two different frequency values. The contractors had to select either of these two vibration settings to compact the backfill soils. The frequency of the high and low vibration settings was slightly different for the two different models of vibratory rollers considered in this research work. For this reason, the required number of passes required to reach the desired relative compaction needs to be investigated for different vibratory rollers commonly used by the contractors.

With the recent adoption of mechanistic empirical pavement design method, use of strength or stiffness-based compaction quality control instead of density-based compaction quality control has become more popular in pavement construction. Lightweight deflectometer (LWD) tests are carried out for this purpose during compaction of aggregates. Further studies need to be conducted in establishing reliable correlations between *in-situ* field compaction density and stiffness values.

REFERENCES

Altuhafi, F. N., Coop, M. R., and Georgiannou, V. N. (2016). "Effect of Particle Shape on the Mechanical Behavior of Natural Sands." *Journal of Geotechnical and Geoenvironmental Engineering*, 142(12), 04016071.

Altuhafi, F., O'Sullivan, C., and Cavarretta, I. (2013). "Analysis of an image-based method to quantify the size and shape of sand particles." *Journal of Geotechnical and Geoenvironmental Engineering*, 139(AUGUST), 1290–1307.

ASTM D1557. (2012). "Standard Test Methods for Laboratory Compaction Characteristics of Soil Using Modified Effort."

ASTM D2487. (2017). "Standard Practice for Classification of Soils for Engineering Purposes (Unified Soil Classification System)." *ASTM International*.

ASTM D3080. (2011). "Standard Test Method for Direct Shear Test of Soils Under Consolidated Drained Conditions." *ASTM international*, 1–9.

ASTM D4253. (2016). "Standard Test Methods for Maximum Index Density and Unit Weight of Soils Using a Vibratory Table." *ASTM international*.

ASTM D4254. (2016). "Standard Test Methods for Minimum Index Density and Unit Weight of Soils and Calculation of Relative Density." *ASTM international*.

ASTM D698. (2012). "Standard Test Methods for Laboratory Compaction of Soil Using Standard Effort." *ASTM International*.

ASTM D7382. (2008). "Standard test methods for determination of maximum dry unit weight and water content range for effective compaction of granular soils using a vibrating hammer." *ASTM International*.

Bowles, J. E. (1996). *Foundation analysis and design*. McGraw-Hill.

Broms, B. B., and Frossblad, L. (1969). "Vibratory Compaction of Cohesionless Soils." *Proceedings of the Specialty Session No. 2 on Soil Dynamics of 7th International Conference on Soil Mechanics and Foundation Engineering*, Mexico City, 101–118.

Cho, A. G., Dodds, J., and Santamarina, J. C. (2006). "Particle Shape Effects on Packing Density, Stiffness and Strength – Natural and Crushed Sands." *Journal of Geotechnical and Geoenvironmental Engineering*, 132(May), 591–602.

Coop, M. R., and Altuhafi, F. N. (2011). "Changes to particle characteristics associated with the compression of sands." *Géotechnique*, 61(6), 459–471.

Cox, M. R., and Budhu, M. (2008). "A practical approach to grain shape quantification." *Engineering Geology*, 96(1–2), 1–16.

Cruse, R. M., Cassel, D. K., and Averette, F. G. (1980). "Effect of Particle Surface Roughness on Densification of Coarse-Textured Soil1." *Soil Science Society of America Journal*, 44(4), 692.

D'Appolonia, D. J., Whitman, R. V, and D'Appolonia, E. (1969). "Sand Compaction with Vibratory Rollers." *Journal of Soil Mechanics & Foundations Div*, 95(1), 263–284.

Denies, N., Canou, J., Roux, J.-N., and Holeyman, A. (2014). "Vibrocompaction properties of dry sand." *Canadian Geotechnical Journal*, NRC Research Press, 51(4), 409–419.

Dickin, E. A. (1973). "Influence of Grain Shape and Size upon the Limiting Porosities of Sands." *ASTM Special Technical Publications*, (523).

Ferreira, T., and Rasband, W. (2012). "ImageJ User Guide IJ 1.46r."

Fratta, D., and Kim, K. (2015). *Effective depth of soil compaction in relation to applied compactive energy*.

Ganju, E., Kim, H., Prezzi, M., Salgado, R., and Siddiki, N. Z. (2018). "Quality assurance and quality control of subgrade compaction using the dynamic cone penetrometer." *International Journal of Pavement Engineering*, Taylor & Francis, 19(11), 966–975.

Hagerty, M. M., Hite, D. R., Ullrich, C. R., and Hagerty, D. J. (1993). "One-Dimensional High-Pressure Compression of Granular Media." *Journal of Geotechnical Engineering*, 119(1), 1–18.

Han, F., Ganju, E., Salgado, R., and Prezzi, M. (2018). "Effects of Interface Roughness, Particle Geometry, and Gradation on the Sand–Steel Interface Friction Angle." *Journal of Geotechnical and Geoenvironmental Engineering*, 144(12), 04018096.

Holtz, R. D., Kovacs, W. D., and Sheahan, T. C. (2011). *An introduction to geotechnical engineering*. Pearson.

Hoppe, E. J. (1999). *Guidelines for the use, design, and construction of bridge approach slabs*. Charlottesville, Virginia.

Indiana Department of Transportation. (2018). *Standard and Specifications*.

Johnson, A. W., and Sallberg, J. R. (1960). "Factors that influence field compaction of soils." *Highway Research Board Bulletin*, (272).

Krumbein, W., and Sloss, L. (1951). *Stratigraphy and sedimentation*. W. H. Freeman and Company, San Francisco, USA.

Lade, P. V., Yamamuro, J. A., and Bopp, P. A. (1996). "Significance of Particle Crushing in Granular Materials." *Journal of Geotechnical Engineering*, 122(4), 309–316.

Massarsch, K. R., and Fellenius, B. H. (2002). "Vibratory compaction of coarse-grained soils." *Canadian Geotechnical Journal*, NRC Research Press Ottawa, Canada, 39(3), 695–709.

Mitchell, J. K., and Soga, K. (2005). *Fundamentals of soil behavior*. John Wiley & Sons.

Mooney, M. A., and Rinehart, R. V. (2007). "Field Monitoring of Roller Vibration during Compaction of Subgrade Soil." *Journal of Geotechnical and Geoenvironmental Engineering*, 133(3), 257–265.

Panayiotopoulos, K. P. (1989). "Packing of Sands - A Review Uniform spheres." 13, 101–121.

Rollings, M. P., and Rollings, R. S. (1996). *Geotechnical materials in construction*. McGraw-Hill.

Salgado, R. (2008). *The engineering of foundations*. McGraw Hill.

Salgado, R., and Yoon, S. (2003). *Dynamic Cone Penetration Test (DCPT) for Subgrade Assessment. JTRP Technical Reports*.

Selig, E. T., and Yoo, T. S. (1977). "Fundamentals of vibratory roller behavior." *Proceedings of the ninth international conference on soil mechanics and foundation engineering*, Tokyo, 375–380.

Simoni, A., and Houlsby, G. T. (2006). "The direct shear strength and dilatancy of sand-gravel mixtures." *Geotechnical and Geological Engineering*, 24(3), 523–549.

Tovar-Valencia, R. D., Asce, S. M., Galvis-Castro, A., Salgado, R., Asce, F., Prezzi, M., and Asce, A. M. (2017). "Effect of Surface Roughness on the Shaft Resistance of Displacement Model Piles in Sand."

Uesugi, M., and Kishida, H. (1986). "Frictional resistance at yield between dry sand and mild steel." *Soils and Foundations*, 26(4), 139–149.

USACE. (1995). *Construction Control for Earth and Rock-fill Dam, U.S. Army Corps of Engineers*.

Wadell, H. (1932). "Volume, shape and roundness of rock particles." *J. Geol.*, 40(5), 443–451.

Wang, J.-J., Zhang, H.-P., and DEN, D.-P. (2014). "Effects of Compaction Effort on Compaction Behavior and Particle Crushing of a Crushed Sandstone-Mudstone Particle Mixture." *Soil Mechanics and Foundation Engineering*, Springer US, 51(2), 67–71.

Wersäll, C., and Larsson, S. (2013). "Small-scale testing of frequency-dependent compaction of sand using a vertically vibrating plate." *Geotechnical Testing Journal*, 36(3).

Wersäll, C., Nordfelt, I., and Larsson, S. (2017). "Soil compaction by vibratory roller with variable frequency." *Géotechnique*, 67(3), 272–278.

Yamada, S., and Sato, K. (2005). "Effects of particle crushing on mechanical behaviour of sand." *Proc. International Conference on Foundations 2005*.

Youd, T. (1973). "Factors Controlling Maximum and Minimum Densities of Sands." *Evaluation of Relative Density and its Role in Geotechnical Projects Involving Cohesionless Soils*, ASTM International, 100 Barr Harbor Drive, PO Box C700, West Conshohocken, PA 19428-2959, 98-98–15.

Youd, T. L. (1972). "Compaction of Sands by Repeated Shear Straining." *Journal of the Soil Mechanics and Foundations Division*, ASCE, 98(7), 709–725.

Zheng, J., and Hryciw, R. D. (2015). "Traditional soil particle sphericity, roundness and surface roughness by computational geometry." *Géotechnique*, Thomas Telford Ltd, 65(6), 494–506.